Modelling, Analysis, Control and Experimental Validation of Electromechanical Valve Actuators in Automotive Systems

Carlos Ildefonso Hoyos Velasco

Tutor:
Prof. Mario di Bernardo

Co-Tutors:
Prof. Stefania Santini
Dr. Alessandro di Gaeta
(Istituto Motori, CNR, Napoli)

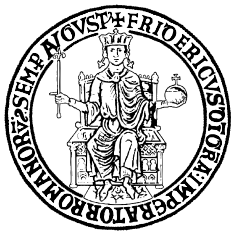

Dissertation submitted in partial fulfillment of the requirements for the degree of Doctor of Philosophy.

Submitted to:

Department of Systems and Computer Engineering
Faculty of Engineering
UNIVERSITY OF NAPLES FEDERICO II
Naples, Italy.
Nov. 2011.

Printed in Italy.
Naples, November 2011.

To the family Hoyos Velasco

ACKNOWLEDGMENTS

To God for giving me the blessings, the grace, the life and other gifts.

I want to express special words of gratitude to all persons, who have contributed to the successful completion of my degree of Doctor of Philosophy. This important achievement would not have been possible without the help, the advice and the support of all them.

First of all, I would like to thank my supervisors, professor Mario di Bernardo, professor Stefania Santini and Dr. Alessandro di Gaeta. This Ph.D. thesis would not exist without their constant scientific and moral support. Moreover, I thank them for all the countless formative and rewarding scientific discussions, that we had during these three years, where the theory, the technique and the beauty behind them were merged in exquisite mathematical formalisms. I learned a lot from their methods to do and guide the scientific research. They made unique my Ph.D. experience and I will take with me all their teachings as a invaluable thesaurus of my life.

I thank Professor Francesco Garofalo for all his help during my Ph.D. course. I thank all colleagues from the SINCRO Group (Piero, David, Alessandro, Lucia, Giovanni and Umberto) for their suggestions to improve my research during our Labmeetings. Umberto deserves special thanks for his help, advices and fruitful cooperation, which have enormously contributed to this thesis. I thank to the SINCRO staff: Dino, Achille, Michelle, Anamaria and Ana; to the Ph.D. students (Francesca, Mariacarla, Fanny, Emmanuela and both Giussepes); to the students (Giuseppe, Francesco and Ylenia); and to the staff of the University of Naples Federico II, for their technical support. Special thanks to Michelle who picked me up periodically each week and to all members of the soccer group, we shared nice emotions playing soccer.

I thank also colleagues and the staff from the Istituto Motori of the National Research Conuncil of Italy. In particular, Mr. Veniero, Mr. Police, Mrs. Rosa, Biagio, Natale, Fabrizio, Ugo, Valerio, Salvina, Francesco, Pablo and Gabriele for their moral and technical support. Furthermore, I thank the Istituto Motori for funding my Ph.D.

and for the infrastructure to do the research.

God allowed me to meet special people in Italy. I shared with them my life in Naples and I learned a lot of the Italian culture through them. I spent with all them a nice time and they made me feel at my home. Indeed, they are my family in Naples. So special thanks to Francesca Magliulo, Natale, Pablo, Antonio and their families, Mrs. Consiglia, Mr. Vittorio, Luigi, Carmen, Oreste, Fabrizio and Roberto. Very special thanks to Marianna for her love and the wonderful time that we shared.

I thank all them for encouragement throughout all my studies. Above all, I would like to thank everyone for the real and deep friendship, kindness and for creating a nice environment to work and live in Italy.

I want to thank also my former professors Fabiola Angulo, Gerard Olivar Tost and Gustavo Osorio for their support and help at the beginning of my studies in Italy. Additionally, I thank them and also to Nicolas Toro, Cesar Arango, Germán Castellanos, Eduardo Cano, Luis Enrique and Armando Ustaríz, professors from National University of Colombia at Manizales, for contributing to my professional carrier, with their methods and opportunities and for showing me the wonder of the automatic control and the applied mathematics to engineering.

Colleagues from Colombia were near me, during short periods along my Ph.D. I acknowledge their support, availability, and I thank the nice moments that we shared in Italy. They are Ricardo, John, Julian and Alejandro.

I am eternally indebted to my parents Juan Bautista and Libia Emitalia for all their support and love. Thanks to my grandmother Irene. Thanks to my brothers Fredy and Laureano and my sisters Anayancy, Alba and Aura Cristina, who inspired me with their way to strive for the excellence. I thank also my nieces Adriana, Tatiana and the small Valentina, and my nephew Jorge Luis.

Carlos Ildefonso Hoyos Velasco

Naples, November 2011

ABSTRACT

This Thesis is concerned with the modelling, analysis and control of novel mechatronic valve actuators for automotive systems, specifically, the control of the mechanical valves to intake and exhaust gases in Internal Combustion Engines (ICE). Scientific studies have shown that significant benefits in terms of engine efficiency and emissions can be obtained through the adoption of variable valve actuation. Current engine technology are based on the use of a mechanical driven camshaft, which is a no flexible device due to its strongly coupling to crankshaft position. Thus, it is not possible to adjust or adapt in real time the valve features according to the engine working conditions. Hence, there is the need of designing innovative mechanisms to actuate the engine valves. In so doing, traditional mechanical cam systems can be removed and a train of single actuated valves is incorporated into the ICE, leading to the development of camless engine technology. Electro-Mechanical Valve Actuators (EMVA) have been considered as one of the most promising technological solutions to develop this novel engine technology. To achieve all the potential benefits of the EMVA systems, two crucial control problems have to be tackled and solved efficiently: the control of the first lift manoeuvre, known as First Catching Control (FCC) problem, and the control of the valve seating velocity, known as Soft Landing Control (SLC) problem. The thesis shows that the analysis and control of the EMVA device can be successfully addressed in the framework of non-smooth dynamical system and nonlinear control theory, furthermore, the tuning of non linear controllers can be successfully done by using closed loop bifurcation diagram analysis. In particular, a non-smooth mathematical model is proposed, estimated and validated experimentally. A novel Key-on controller is proposed to solve the FCC control problem, while a combined feedforward-sliding mode controller is proposed to solve the SLC control problem. The proposed control approaches have been tested numerically and validated on an experimental setup, leading to successful results.

GLOSSARY

Notation	*Description*	*Units*
$h(t)$	Valve position	m
$v(t)$	Valve velocity	m/s
$x(t)$	Valve trajectory	
$h_r(t)$	Reference valve position	m
$v_r(t)$	Reference valve velocity	m/s
$x_r(t)$	Reference valve trajectory	
h_{max}	valve maximum position	mm
h_{eq}	valve middle position	mm
h_{min}	valve minimum position	mm
m	mass	Kg
k	spring stiffness	N/m
$F_f(v)$	Nonlinear friction force model	N
$F_e(h)$	Elastic (spring) force	N
$F_{ext}(t)$	Time variant external force	N
γ	vector of friction parameters	-
$\delta\gamma$	Vector of variations for friction parameters	-
$\hat{\gamma}$	Vector of estimated friction parameters	-
ν	Vector of plant parameters	-
$\delta\nu$	Vector of variations for plant parameters	-
$\hat{\nu}$	Vector of estimated plant parameters	-
u	Control signal	N
u_s	Saturated control signal	N
$u_{max}(h)$	Dynamic upper bound for control action u	N
$u_{min}(h)$	Dynamic lower bound for control action u	N
F_M	Magnetic Force	N
u_M	Magnetic Force computed by reference model	N
μ	Restitution coefficient	-
μ_o	Restitution coefficient for lower impacts	-
μ_c	Restitution coefficient for upper impacts	-

Notation	*Description*	*Units*
w_n	natural angular velocity	rad/s
f_n	natural oscillation frequency	Hz
i_u	Upper coil current	A
i_l	Lower coil current	A
i_{ud}	Upper desired coil current	A
i_{ld}	Lower desired coil current	A
Ω	Target region for Key-on control	-
Ω_{max}	Target region for valve opening	-
Ω_{min}	Target region for valve closing	-
r_h	Radius for target region	mm
r_v	Radius for target region	m/s
T	Key-on time	s
$h(T)$	Position at Key-on time T	mm
$v(T)$	Velocity at Key-on time T	m/s
T_r	Rise time	s
T_{max}	Maximum admissible Key-on time	s
i_{max}	Maximum admissible current	s
$h^c_{\Omega_{max}}$	Center of Ω_{max}	m
$h^c_{\Omega_{min}}$	Center of Ω_{min}	m
$h^{MAX}_{\Omega_{min}} = h_{min} + 2r_h$	Maximum value for Ω_{min}	
$h^{MIN}_{\Omega_{max}} = h_{max} - 2r_h$	Minimum value for Ω_{max}	
T_L	Interval of time to perform SLC.	s
T^{max}_{LT}	Maximum admissible total landing time.	s
S	Subinterval.	
h_d	Desired coordinate for $h(t)$ at SLC.	m
v_i	Impact velocity when $h = h_{min,max}$	m/s
$i_r(t)$	Piecewise smooth current pattern	A
i_s	Saturation current	A
T_{rs}	Time constant	s
$s(e)$	Sliding surface	
β	Constant	N
u_{ff}	Feedforward control action	N
u_{fb}	Feedback control action	N
Δf	Term to describe a general disturbance force	N
F_{nl}	Nonlinear part of friction model	N
u_{ec}	Equivalent control	N
ρ	Scalar to weight nonlinear friction force	-

ACRONYMS

Notación	*Meaning*
ICE	Internal Combustion Engine
VVA	Variable Valve Actuation
VVT	Variable Valve Timing
EMVA	Electro-Mechanical Valve Actuator
FCC	First Catching Control
SLC	Soft-Landing Control
CCC	Coil Current Controller
FTC	Force to Current
Key-on	Controller to solve FCC
VE	Velocity Estimator
SMC	Sliding Mode Control
GA	Genetic Algorithm
OVC	Open Valve Command
EMFs	Electro-Motive Forces
FEM	Finite Element Method
NMSE	Normalized Mean Square Error
SN	Saddle Node bifurcation of cycles
SH	Subcritical Hopf bifurcation

CONTENTS

CHAPTER 1

INTRODUCTION

Ignoranti quem portum petat
nullus suus ventus est.

(Lucio Anneo Séneca, 2 b.C. - 65 a.C.)

1.1. Motivation

This Thesis is concerned with the analysis, modeling and control of mechatronics devices in automotive systems, specifically, the control of mechanical valves to intake and exhaust gases in Internal Combustion (IC) engines. Scientific studies [48, 51, 112, 115, 118] have shown that significant benefits in terms of fuel consumption, emissions, and torque production can be obtained through the adoption of Variable Valve Actuation (VVA) operations [48, 58, 115], in particular cylinder deactivation and Variable Valve Timing (VVT) over all engine operating conditions. It is well known that, current engine technology uses mechanical driven camshaft to perform the opening and closing phase of exhaust and intake valves of the engine. Therefore, the profile of such valves is strongly coupled to crankshaft position. This mechanical solution to drive the valves, provides reliable and accurate valve operation, the degrees of freedom of the valve namely, valve timing, valve lift and anchoring [50, 97] are inherently fixed to the cam profile. Therefore, the valve train is not a flexible device and, once the cam-follower mechanism is designed during the engine

development, it is not possible to adjust or adapt in real time the valve features according to the engine working conditions, over the entire range of speed with the aim of improving engine efficiency and reduce pollutant emissions.

Thus, to meet current and future exhaust gas emission standards, while accomplishing customer expectations, in terms of both fuel reduction and performance, new spark ignition engine technologies are necessary [81]. Hence, there is the need of designing innovative VVA mechanisms allowing VVT operations to improve fuel consumption [45, 118], torque production [97, 115], engine efficiency [8], and emissions reduction [51, 107] thanks to the de-coupling of the valve timing from the piston motion [41]. VVT also allows the reduction of energy losses caused by the pumping action [43] and by the spinning of the mechanical device (pulley and camshaft) used to drive the valves.

Solutions based on mechanically driven camshafts cannot modify, on-line and continuously, the valve operation profiles. Furthermore, it is well known that, for high-speeds, the engine performance is deteriorated and valves do not evolve in a regular periodic motion (see [6] and references there in). As a result, engines evolution is pointing towards promising camless solution [112, 115], where the traditional mechanical cam system is removed and a single actuator is incorporated to drive each valve.

Hence, the development of an effective VVT system strongly relies on innovative valve actuators and over the last years different devices (electro-hydraulic, pneumatic, motor-driven and Electro-Mechanical Valve Actuators (EMVA) [14, 98, 101, 112]) have been proposed to implement VVT. Despite that different technologies could be used, several issues and drawbacks have to be solved for each technological solution in order to make the novel engine concept reliable and efficient. EMVA systems has been considered as the more promising solution to develop this novel engine technology. With this kind of mechatronic device, two main control problems have to be solved for the correct performance of the system. The first one is concerned with the design of a control strategy necessary to move at the key-on of the engine, the valve from its rest central position to the magnetic coil neighborhood. Sometimes this problem is referred as "First Catching Control" (FCC) problem in the literature (see [37, 50]), and this task must be performed in less than 150 (ms). The second control problem, known in technical literature as "Soft Landing Control" (SLC) problem [21, 37, 104, 123, 129, 134], concerns with the avoidance of high speed impacts at valve closing or opening during the engine motion. Specifically in EMVA system, impact velocity less than 0.1 (m/s) is admissible and the control task im-

plemented to avoid high intensity impacts must act on the system in a very short time interval, less than few milliseconds, i.e. 4 (ms) [37, 50], in order to guarantee an adequate load variation ability of the valvetrain.

The strong saturation of power actuators, the high nonlinear coupling between the mechanical and magnetic parts embedded into the valve actuator, and the coupling with the engine make these control tasks cumbersome obstacles to overcome for large low cost production of this camless technology. In particular, a complex and robust control scheme has to be designed and implemented to control each single valve, while other one to synchronize the whole set of valves. Thus, it is required to develop advanced mechatronic devices and control approaches to implement advanced combustion system aimed at meeting stringent emission standards while improving fuel consumption and efficiency.

From a control viewpoint, since friction has a very strong influence on the performance and behaviour of mechanical systems, good representation and estimation of friction phenomena are important [7, 90]. Friction modeling is challenging since such physical phenomena often exhibits highly nonlinear (nonsmooth) dynamics [86]. Friction is also very important for the control engineer, when designing drive systems, where high-precision control is required. Thus, the availability of new precise measurement techniques or prediction methods through models, lead to the proper compensation of friction effects by applying predicted driving force. From the control viewpoint, it is useful to understand well friction in such a way that, through the understanding of its effects on the closed loop system dynamics, suitable control actions can be designed to reduce its effects.

From previous discussion, mathematical modeling, nonlinear control system theory and nonlinear dynamics analysis play a key role when solving such challenge technological control problems of EMVA system in automotive engineering. Indeed, on the basis of a suitable nonlinear mathematical model, it is possible to design robust nonlinear controllers [73, 117]. And by considering the nonlinear dynamics for open and mainly for resultant closed loop system, such nonlinear dynamics can be characterized, while analyzing also how variation of control parameters affect those induced dynamics. Therefore, the analysis, comprehension and characterization of the effects of such induced non linear dynamics lead to the successful understanding of controller effects on the system, while allowing to tune properly the controller parameters.

This thesis was carried out as part of a wider industrial research project entitled

"Study of advanced components for a new generation of internal combustion engines" (L. 297/99, Project no. 8052016, CUR UBN09634, financed by Ministero dell'Istruzione, dell'Università e della Ricerca (MIUR), developed at the Istituto Motori of the National Research Conuncil (IM-CNR) of Italy and commissioned by Dell'Orto S.p.A. The aim is to develop and test a single valve prototype of EMVA system.

1.2. Outline of the thesis

The rest of the Thesis is outlined as follows.

Chapter 2 presents an introduction to EMVA system in Automotive Engineering. In particular, it contains a brief background on Internal Combustion (IC) engine and motivates the application of mechatronic actuators to drive the engine valves and their potential use for future camless engines. After describing the electromechanical valve actuator, this chapter also describes its advantages, disadvantages and the control challenges to be addressed in the Thesis.

The mathematical modelling of the system is discussed in Chapter 3. Since, the control design relies on the knowledge of mathematical model of the EMVA system, in this Chapter, its model is derived. In particular, a non-smooth mathematical model that includes a nonlinear friction force is proposed. Model is identified and validated against experimental data. Furthermore, a sensitivity analysis was done numerically in order to evaluate the prediction capabilities of mathematical model for EMVA, when considering model parameter variations.

Chapter 4 addresses the so-called First Catching Control (FCC) problem, proposing a novel control approach to solve it. In technical literature, feed-forward controllers have been proposed to solve the FCC control problem [16,37] and few attempts to the use of feedback control strategies have led to high values of the coil currents necessary to move the valve, leading to non feasible solutions (see, for example, [37]). The proposed Key-on controller is based on energy control [68] of mechanical systems, and derived by using Lyapunov's direct method [117]. Feasible coil currents are produced with this control approach while satisfying application requirements. The closed loop system was analyzed in the context of bifurcation theory and the analysis of the closed loop bifurcation diagram is used as a tool to tune the controller gains. Induced non-linear dynamics and the performance of Key-on control approach is successfully validated experimentally.

Chapter 5 deals with the problem of closing or opening the valve while avoiding vibrations and impacts (Soft-Landing Control (SLC) problem). This is basically a tracking and stabilization control problem. We propose a control scheme that use a model based trajectory planner to obtain the reference trajectory, while the idea behind the approach is to stabilize the system through the combination of a feedforward and a feedback control action. The feedforward control action is computed using the nominal model of the plant and the feedback control action is obtained by using Sliding Mode Control [131]. Our approach ensures the successful tracking and stabilization of the EMVA. After testing the control efficiency through numerical simulation, with acceptable results, the analysis of robustness against friction parameter variation is performed, leading to a wide range of friction conditions where control still satisfies control specifications.

Chapter 6 summarizes the main contributions of the Thesis.

Further technical and theoretical results are presented in Appendices A and B, respectively, while Appendix C describes other research results obtained on the experimental validation of switched adaptive controllers for Piece-Wise Affine systems, which were obtained in the laboratories from University of Naples Federico II. The results presented in the Thesis have been presented at international scientific conferences and have been submitted for journal publication [30–32, 34, 35, 39, 133].

CHAPTER 2

ELECTRO-MECHANICAL VALVE ACTUATORS IN AUTOMOTIVE ENGINEERING

Itaque etiam non assecutis voluisse, abunde pulchrum atque magnificum est.

(Plinio il Vecchio, 23-79 a.C.)

This chapter presents a background on Internal Combustion Engines (ICE) and motivates the use of mechatronics actuators in automotive systems. In Sec. 2.1 a general introduction to the chapter is presented. In Sec. 2.2 a brief historical background is presented together with a description of the working principles of ICEs and the four-stroke cycle. The implementation of Variable Valve Actuators and its potential benefits in future camless engine is shown in Sec. 2.3, while electro-mechanical valve actuators are introduced in Sec. 2.4. Advantages, disadvantages, control challenges are discussed specifically in subsections 2.4.1 and 2.4.2. A final discussion in Sec. 2.5 ends the Chapter.

2.1. Introduction

To meet current and future exhaust gas emission standards [99], while accomplishing customer expectations in terms of fuel reduction and performance, new spark ignition engines are necessary [42, 58, 105, 115, 125]. In current technology, the intake and exhaust valves which control the flow of gases are mechanically operated by the camshaft. Therefore, the valve train is not a flexible device and, once the cam-follower mechanism is designed during the engine development, it is not possible to adjust or adapt in real time the degree of freedom of the valves (namely, valve timing, opening duration, maximum lift and also anchorage) according to the engine working conditions [50, 97]. On the contrary, by using an active control approach, it would be possible to implement Variable Valve Actuation (VVA) operations, allowing to change on-line all the characteristic features of the valve. Note that VVA operations contribute to improve improve fuel consumption [45, 118], torque production [97, 105, 126], engine efficiency [8, 115] and to reduce emissions [81, 107, 118] thanks to the de-coupling of the valve timing from the piston motion [41] and the reduction of energy losses caused by the pumping action [43, 84].

Despite different technologies could be used to perform VVA operations, several issues and drawbacks have to be solved for each technological choice in order to make the novel engine concept reliable and effectively operative. At the end of the chapter, reader will identify the potentialities of camless engines, advantages and disadvantages of a promising solution based on an electromechanical devices and the control challenges originated from the use of these novel actuators.

2.2. Internal Combustion Engine

Thr internal combustion engine is a device that uses the explosive combustion of fuel to push a piston within a cylinder making it move. The motion of the piston then turns a crankshaft that then turns the car wheels through a drive shaft. The purpose of of IC engine is the production of mechanical power from the chemical energy stored in the fuel. Currently, spark-ignition engine (called Otto or gasoline (petrol) engine) and compression-ignition engine (diesel engine) are widely used in transportation applications (land, sea and air), because of its simplicity, ruggedness and high power/weight ratio.

2.2.1. Brief history

In 1673, the Dutch physicist Christian Huygens designed, but never built, an internal combustion engine that was to be fueled with gunpowder. The very first self-powered road vehicles were powered by steam engines and, based on this device, in 1769 Nicolas Joseph Cugnot built an automobile, that was recognized by the British Royal Automobile Club and the Automobile Club de France to be the first. IC engine design started when commercial drilling and production of petroleum began in the mid-1850s. In 1860 ICE became a practical reality when Belgian-born engineer, Jean JosephÉtienne Lenoir patented a double-acting, electric Spark-Ignition (SI) internal combustion engine fueled by coal gas. Then, in 1863, Lenoir developed the first marketable engine of this type, where gas and air were drawn into the cylinder during the first half of the piston stroke, while the cycle was then completed with the exhaust stroke. Mr. Lenoir attached this improved engine version (using petroleum and a primitive carburetor) to a three-wheeled wagon that managed to complete an historic fifty-mile road trip. Some 5000 of these engines were built between 1860 and 1865 [62]. An atmospheric engine was then developed by Nicolaus A. Otto and Eugen Langen in 1867 and an improved version was proposed by Otto, which consisted on an engine cycle with four piston strokes: an intake stroke, a compression stroke before ignition, an expansion or power stroke and finally an exhaust stroke. This prototype first ran in 1876 and became the breakthrough that founded the IC engine industry. At the same age, in 1862, Alphonse Beau de Rochas, a French civil engineer, patented, but did not build, a four-stroke engine (French patent #52,593, January 16, 1862)[1].

After Otto's engine development, along engine history, several engineers proposed further improvements for the engine. For instance, the German Karl Benz in 1885 successfully designed and built the world's first practical automobile to be powered by an ICE based on two stroke engine concept. Latter in late 1800s, various types of carburetors were developed to vaporize the fuel and mix it with air. In 1892, the German engineer Rudolf Diesel outlined in his patent a new form of ICE, where combustion was obtained by injecting a liquid fuel into air heated solely by compression. In 1902, the first magneto-ignition system embedded in a vehicle; latter in 1913 Bosch developed the first complete electrical system, which consists of the magneto-ignition system with the spark plugs, the starter, the DC generator [54]. It was around the 80s, when the Electronic Control Unit (ECU) started to be used,

[1]The discovery of this unpublished patent led to controversy and doubts about the originality of Otto's patent for this engine concept so that, in Germany it was declared as invalid [62]

that exploited control concepts in order to meet the new strict legislative constraints on efficiency, safety, environmental compatibility and comfort [54]. The electronic fuel injection system was also proposed to replace old carburetors. In particular, the ECU determines automatically the amount of fuel, the ignition timing and other engine parameters, necessary to make the engine run in a desirable way.

It might be thought that after a one and half century of development, the internal combustion engine has reached its top and there are not any potential improvements to be done. However, this is not the case. During the past three decades, new factors for change have become important and significantly affect engine design and operation. Such factors are: the need to control the urban air pollution and the need to achieve significant improvement in fuel consumption and engine efficiency as well. Several studies have shown that the automobile is a major source of hydrocarbon and oxides of nitrogen emissions, and the prime cause of high carbon monoxide levels in urban areas (see [62] and references therein for further details). As a result, new emission standards for automobiles started to be introduced since 1960, becoming more and more restrictive with the years. In particular, it is expected to reach the European Union (EU) objective of 120 (g/km) CO_2 by 2012 (see Fig. 2.1) through the proper engine technological improvements or by using other green sources as bio-fuels (see [99] for further details about legislation standards).

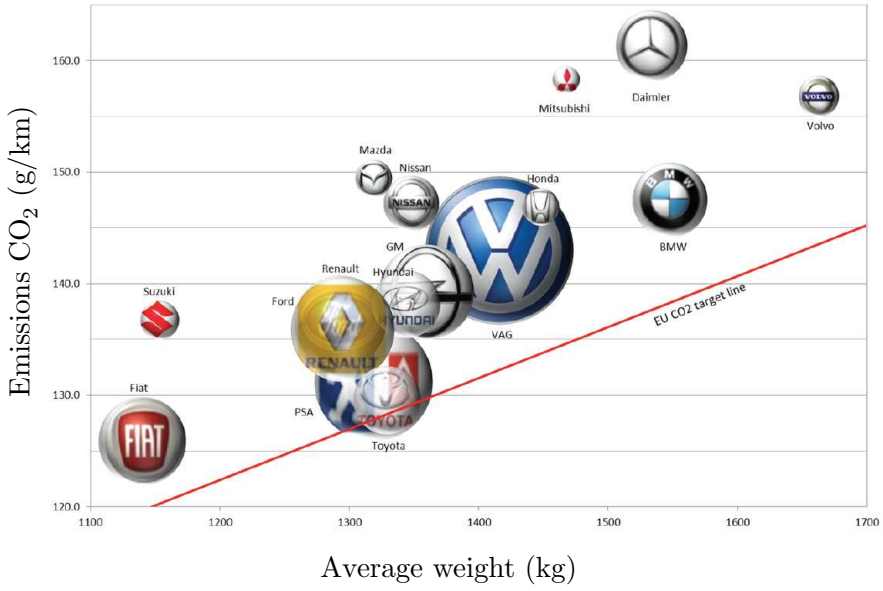

Figure 2.1.: Average CO_2 emissions vs. average weight of cars registered in 2010 ([47]).

2.2.2. Four-stroke engine cycles

In a reciprocating engine, the piston moves back and forth in a cylinder and transmits power through a connecting rod and crank mechanism so to drive a shaft. The steady rotation of the crank produces a cyclical piston motion. The piston comes to rest at the top-center crank position and bottom-center crank position when the cylinder volume is at its minimum or maximum, respectively. Furthermore, one (two) intake valve, located in the top of combustion chamber, is synchronized with the crank angle/piston stroke in order to allow the induction of fresh air or air–fuel mixture into the cylinder. In the same area one(two) exhaust valve, aimed at expelling the gasses from combustion, is also located. Valves present opening and closing events here referred as: Exhaust Valve Opening (EVO), Exhaust Valve Closing (EVC), Intake Valve Opening (IVO) and Intakce Valve Closing (IVC).

The operating cycle consists of a sequence of events occurring in four strokes of the piston during two revolutions of the crankshaft (see Fig. 2.2(a)). Such events are described as follows: *(i)* the first stroke is defined as Induction stroke; it starts with the piston at top dead center (TDC) position and ends with the piston at bottom dead center (BDC) position; *(ii)* the second stroke is defined as Compression stroke, that starts with both valves closed. During this stroke the piston moves from BDC to TDC position, where the trapped mass is compressed to a small fraction of its volume through upward piston movement. Toward the end of this stroke, combustion is initiated and in-cylinder pressure increases rapidly. *(iii)* The third stroke is defined as Power or Expansion stroke, which starts at TDC and ends at BDC. Here, the combustion is completed and in-cylinder pressure reaches its maximum value. In the following expansion phase, gases push the piston down, while transferring work to the piston, forcing the crank to rotate. As the piston approaches BDC the exhaust valve opens (EVO event) to initiate the expulsion of the first portion of the burned gases. *(iv)* The fourth stroke is defined as Exhaust stroke, which starts from BDC and ends at TDC. Here, the piston pushes out the remaining burned gases. As the piston approaches the TDC position, the intake valve opens again and the exhaust one closes (EVC event) just after TDC.

Notice that between the intake valve opening and exhaust valve closing at TDC, there exists a time interval where both valves are partially open, leading to the possible direct transfer of air-fuel mix from intake valve to the atmosphere through the exhaust valve.

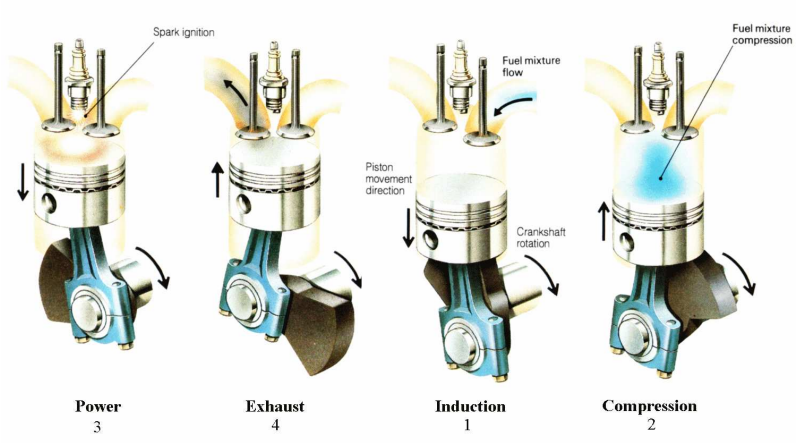

(a)

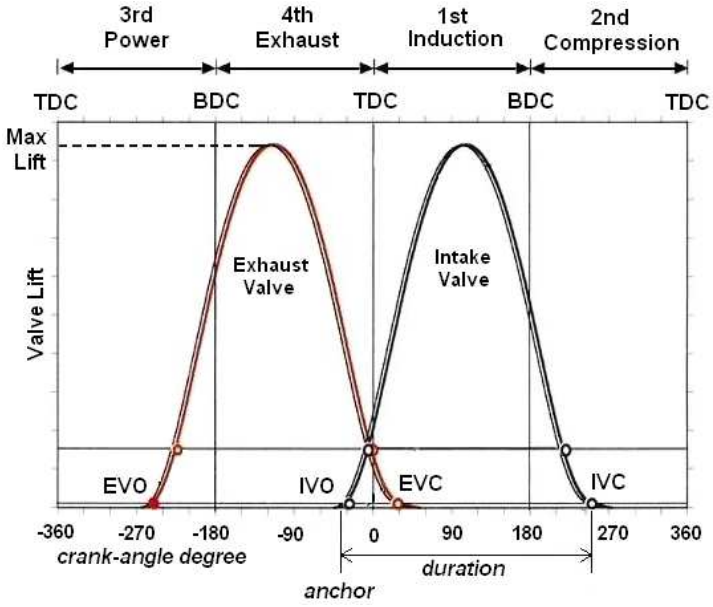

(b)

Figure 2.2.: Four-Stroke Cycle in spark ignition engine and valve events: a) Four-Stroke Cycle ([2]); b) Valve lift profiles ([38]).

2.3. Engine evolution: from Cam to Camless

Currently, the intake and exhaust valves in ICEs are synchronized through a mechanical driven camshaft, by means of pulleys as it is depicted in Fig. 2.3(a). The drawback with this system is that it is a purely mechanical system and therefore the valve events (EVO, EVC, IVO and IVC) cannot be effectively modified on line. Despite cam-system is robust, it must evolve in order to allow VVA operations. Furthermore, as it was remarked before, a lot of the energy used to spin the camshaft should be used better in order to increase the engine torque and efficiency, as well.

More recently it has been proved that emission reduction, fuel consumption [118], engine efficiency and torque [115] can be improved through the adoption of VVA methods [48, 58, 115]. Different solution still based on the use of the mechanical cam shatf have been proposed, which consists on modified cam-follower profiles that can be implemented keeping the traditional and purely mechanical engine structure. However, the main drawback in the case is at high speed values, when the engine performance is deteriorated since the valves do not evolve with a regular periodic motion (see [6] and references therein). Additionally, the use of mechanical driven camshaft increase the energy losses due to the high work required to spin the camshaft and the train of valves through the pulley, and to the presence of additional friction forces acting on mechanical parts. Therefore, engines evolution is pointing towards camless solution [107,112,115]. Furthermore, the rotation of the mechanical cam-shaft is perceived as a significant source of undesired noise and vibrations, originated by the rotating or reciprocating engine components. Note that the legislation aimed at reducing environmental noise [66], born in the 70's, is becoming more and more restrictive in these recent years and drives toward the use of noiseless cam-less solutions.

Different companies and car developers are working in order to produce engines with VVA features. In particular, FEV [110] and Nissan motor [48] have been pioneers in the development of mechanically variable valve-train technologies and cylinder deactivation systems through the modification of the cam-follower [17, 43, 128] or by combining it with other variable camshaft phasing units, as the UniAir system of FIAT [59]. However, all solutions continue to be strongly linked through the mechanically driven camshaft thechnology, which is not able to produce effective VVA operations, for example, in terms of opening duration and VVT (see Figs. 2.4 and 2.5). As it is expected, due to potentialities of camless engine, in last two decades, different car corporations have started to work in the development of some camless prototypes as FEV [16, 55, 106], Nissan [130], Renault [11], GM [121], SIEMENS [93], FORD [26, 82, 92] and Honda [96].

The challenge is to find the right combination of innovation, analysis, testing, integration and calibration. The development of an effective VVT systems strongly relies on innovative valve actuators [65], leading to the removal of the traditional cam system (shown in Fig. 2.3(a)) and the embedding into the ICE, the actuated valve (see Fig. 2.3(b)). Over the last years different devices (electro-hydraulic [14, 27], pneumatic [88, 98, 111, 135], motor-driven [101, 108, 109] and Electro-Mechanical [18, 19, 46, 92, 94, 106, 107, 125]) have been proposed to implement VVT. The key problem is to design and test single variable valve actuators, so to be used in the

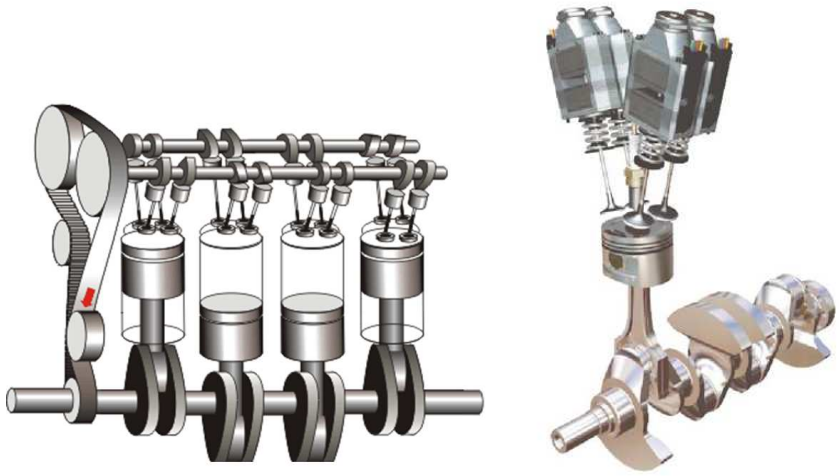

(a) (b)

Figure 2.3.: Two engine concepts: (a) Driven camshaft engine [2]; (b) Camless solution [1].

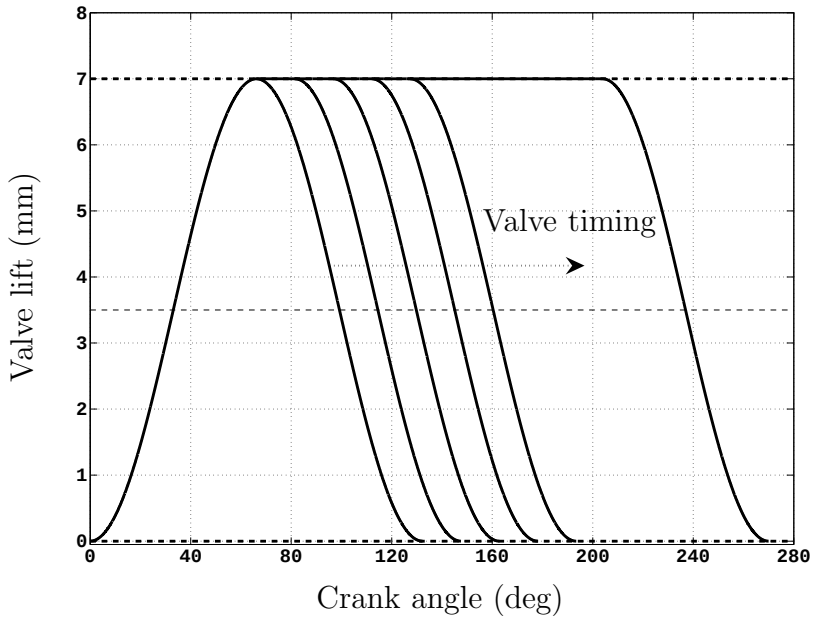

Figure 2.4.: Variation of the mean flow area through valve timing when considering fixed valve lift and variable valve event.

next generation of camless valve-trains.

2.4. Electro-Mechanical Valve Actuators

The development of Electro-Mechanical Valve Actuators (EMVA) strongly funds on the effective control of solenoids. It is crucial since the precision and time re-

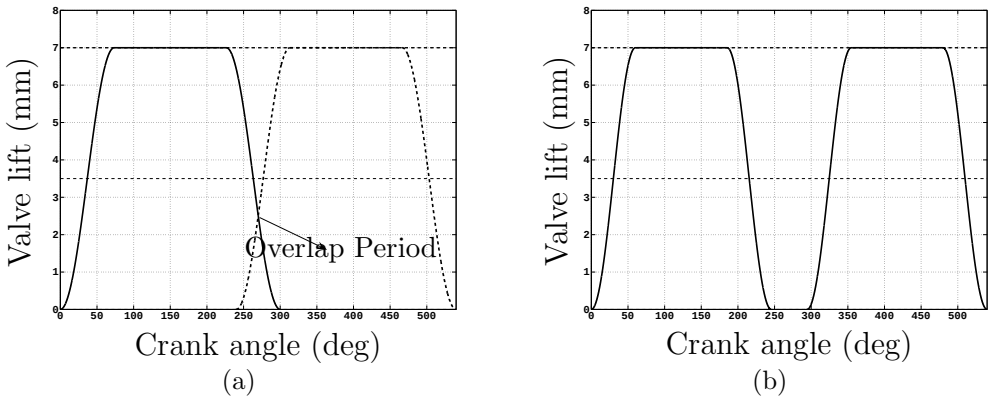

Figure 2.5.: Valve profiles: (a) Phenomena of overlapping; (b) Profile without overlapping with variable valve events.

sponse are limiting factors to realize a reliable camless engine. With the recent rapid progress in permanent-magnet technology, especially through the use of high-energy-density materials, very compact and high-performance electromagnetic linear actuators are now available. This opens to new possibilities for high-force motion control in mechatronics applications.

An innovative actuator for the ICE should be designed to achieve a high level task. It consists on moving a mass of about 0.150 (g), in a time less than few milliseconds ($3-4$ ms), starting from one end stroke with null velocity and reaching the opposite end stroke with low impacting velocity [63]. Note that old, but robust, cam-based mechanisms (camshaft and cams) perform such a complex manoeuvre in a hostile environment, where high temperature and disturbances are presented.

One of the most promising technological solutions, able to accomplish the above mentioned task with a minimum energy consumption, is based on a device that consists of two opposed magnets and two balanced springs working in parallel according to the schematics in Fig. 2.6. Here a ferromagnetic armature, connected to the engine valve by a non-ferromagnetic stem, is placed between the two magnets and moved trough a magnetic force. When the turn-key is in the off position, the armature is held in the intermediate position between the coils by the balanced springs. At engine startup, the upper electromagnet pulls up and holds the armature. In such condition the springs store the mechanical energy and, when the upper magnet is deactivated, the elastic energy is released and the spring-mass system behaves like a harmonic oscillator in free evolution. When engine is running, the motion from open to close condition and vice versa can be easily done by using the energy stored into the springs. The working principle consists on storing potential energy at the end-stroke to make the valve moves to the opposite magnet through the proper

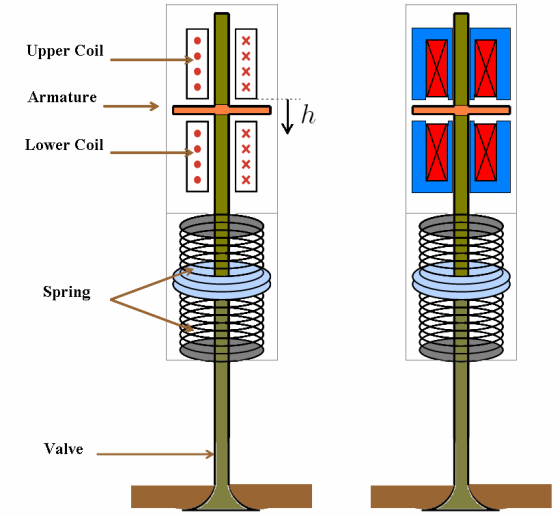

Figure 2.6.: Schematic diagram of an electromagnetic mechanism for engine valve actuation.

compensation of friction and other energy loses.

2.4.1. Advantage and disadvantage

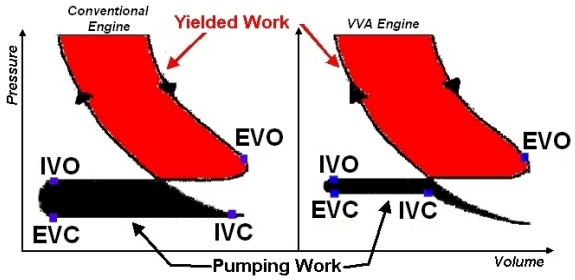

Figure 2.7.: Schematic presure vs. volume diagrams of a conventional engine(left) and one controlled by a VVA system (right)([38])

Following a literature review, among the advantages, we have that EMVA system can lead to a notable improvement in terms of a significant reduction in pumping losses as it is depicted in Fig. 2.7, where the comparison between conventional mechanical driven camshaft as valvetrain (left) and a VVA system (right) is shown. The red area of the plot corresponds to the yielded work during the cycle, while the black area corresponds to the work needed to intake and exhaust gases (i.e., pumping losses). Note that, it is a flexible device and allows to implement valve deactivation, which is a very effective way to reduce cyclic variability at low loads. Furthermore, with the adoption of EMVA systems, the index of NO_x emissions can be reduced more than 60% for loads smaller than 1 (bar) of Break Mean Effective Pressure(BMEP) and 30% for loads higher than 2(bar) of BMEP [51]. EMVA system also allows for an infinite variability of the duration and timing of the open and close

cycles, which promises further improvements in power output, fuel efficiency, and exhaust emissions. Finally, internal friction is significantly reduced since there are fewer moving parts (at low speeds, about 25% of an engine's friction is caused by the valvetrain) leading to further improvements in terms of horsepower, torque and fuel economy. Despite all benefits of EMVA systems, there exists some disadvantages which are related to technological problems when implementing the system in terms of synchronization, control and power availability. For example, considering that a sufficient level of current is required to drive each EMVA and since a full driven camless engine has several valves, i.e 16 valves, there is a significant increase of the electrical power to feed the whole system. Highly performance battery has to be embedded into the automobile electrical system so to provide enough energy to power the system. Furthermore, for a four cylinder engine with four valve per cylinder, the complexity of the overall structure of the system significantly increases and effective schemes must be adopted to control the entire valve train motion. Note that, the deactivation of cylinders should be changed over time according to a well-defined sequence, thus leading to complex synchronization control schemes [51]. Another pressing problem to be addressed is related to the soft landing of the valve, that, if not solved completely, it induces high impacting motion. The presence of impacts leads to the increase of engine noise and the worsening of the comfort of the car passengers.

2.4.2. Control challenges

As already mentioned above, to achieve all the potential benefits of the EMVA systems, two crucial control problems have to be tackled and solved efficiently by car manufactures: the first lift manoeuvre, known as First Catching Control (FCC) problem, and the control of the valve seating velocity, known as Soft Landing Control (SLC) problem. In what follows we provide some further details about these two crucial problems that have been addressed during the Ph.D.

The FCC control problem consists of moving the valve from its resting position (middle equilibrium position) to an end stroke (closed or open valve state) at the engine startup. Taking into account that the magnetic force decreases rapidly and nonlinearly with the air gap and no potential elastic energy is initially stored in the system, the control authority on the armature is low. Hence, the first lift manoeuvre turns to be a complex and arduous task to be accomplished with feasible coil currents. We remark that to implement the effective management of the entire system of valves, power requirements needed to accomplish the first catching play a

crucial role. In [26], in order to provide an effective approach for the initialization of the engine valves, the maximum number of valve that can leave the equilibrium position is computed from the actual power supply capability, which depends on the battery charge state, battery life, as well as the ambient and the engine temperatures. It is apparent that this number could increase if and only if the the energy to complete the first lift per each single valve decreases. Again, in order to reduce the instantaneous power requirements, inventors propose in [26] to initialize engine valves sequentially. As a consequence, the time needed to complete the first lift of each valve becomes crucial to meet customer satisfaction in terms of waiting time at the key-on.

Despite its central role, few attention has been made by the existing automotive literature to solve the problem of the first lift. Some remarkable exceptions can be found in [15,16,37,83,108]. More in detail, simple and viable solutions to address the first lift of the valve at engine startup were patented in [15,16], where armature oscillations are induced by alternatively supplying current pulses to the electromagnets at the mechanical resonant frequency of the system. In [83], permanent magnets are incorporated into the EMVA structure. Obviously, this last solution is expensive and no efficient from an energy viewpoint since, during valve openig/closing, the magnetic field generated by currents through the coils not only has to move the armature, but also has to compensate the magnetic force created by the permanent magnets.

By the other hand, the SLC has as a control goal to close or open the valve, while avoiding impacting phenomena. An acceptable landing velocity should be less than 0.03 (m/s) at 600 (rpm) engine speed and less than 0.3 (m/s) at 6000 (rpm) engine speed [4], although, during the design of the traditional camshaft, the seating velocity is limited below 0.05 (m/s) [123]. This requirement becomes more arduous to accomplish since the valve stroke has to occur in a very short time (about $3-4$ (ms)) to guarantee an adequate load variation ability of the valvetrain [50, 51].

To solve the SLC control problem, different control strategies have been proposed in the technical literature. For example in [44,134], the EMVA system is controlled in open loop via a series of properly tuned voltage levels, and in [37, 57, 83] via current pulses. Since open loop control is sensitive to disturbances and suffers poor repeatability, closed loop strategies have been also extensively used on the basis of different EMVA modeling. For instance, based on a linearized electromagnetic dynamics, in [104], the soft landing of an EMVA actuator is addressed by using a nonlinear feedback strategy, where the control parameters were tuned by a extremum

seeking control. In [125], a Linear-Quadratic Regulator feedback controller was developed to control the actuator for soft seating; in [44], based on a nonlinear force model fitted by a 5-th order polinomial function, a sliding mode sensorless approach has been proposed to track a reference trajectory aimed at the soft-landing. In [94], a sliding surface combined with an adaptive pre-action technique was used to avoid saturation. Moreover, in [123] the quiet seating control is designed in the basis of a linearized model of EMVA, while in [67] a simplified nonlinear model was used to design a control law based on the exact linearization. Finally, observer based, adaptive and iterative cycle-to-cycle controllers have been also proposed as viable solutions [102], [103] and [63, 104, 129].

2.5. Discussion

Thanks to the de-coupling of the valve timing from the piston motion and the reduction of energy losses due the pumping action, the camless technology is a promising solution to improve engine performance.

Advanced control methodologies are necessary to ensure an effective and robust combustion process, that accomplishes the stringent emission standards while reducing fuel consumption.

In this thesis such control problems are addressed in an innovative way contributing significantly to the development of future camless engine.

CHAPTER 3

MATHEMATICAL MODELLING AND EXPERIMENTAL SETUP

> As far as the laws of mathematics refer to reality, they are not certain; and as far as they are certain, they do not refer to reality.
>
> *(Albert Einstein, 1879–1955.)*

This chapter addresses the derivation of a mathematical model for a double magnet Electro Mechanical Valve Actuator (EMVA), and the description of the experimental setup. Also, it expounds the experimental identification method and the model validation for the system. The goal is to study and derive a suitable nonlinear model to represent EMVA dynamics to be used for control design. An introduction to the chapter is presented in Sec. 3.1, the EMVA system with all its subsystems is described in Sec. 3.2, while Sec. 3.3 presents the details of the experimental setup. Then, Sec. 3.4 presents the mathematical modelling for the mechanical and electro-magnetic system, while the model identification and validation procedure is presented in Sec. 3.5. Sec. 3.6 studies the sensitivity of the EMVA model against parameter variations and finally, conclusions are drawn in in Sec. 3.7. The results presented in this chapter have recently appeared in [30].

3.1. Introduction

Given the strict requirements to be satisfied by the EMVA system in order to allow VVA operations, suitable control methodologies have to be designed. The success of the controller design strongly depends on the knowledge of an appropriate mathematical model of the system.

New engine technology requires the reliable control of the valve and, considering that the whole EMVA system involves the interaction of different subsystems, the accurate description of each one of them is necessary. Among different phenomena, the bounded-nonlinear magnetic force and the frictional effects of the mechanical part have to be modeled with the higher possible accuracy. For instance, it is really important to obtain a suitable model to represent the system when velocity is small, mainly to properly account for friction effects when dealing with control tasks that evolve achieving low velocities as part of the control goal, e.g. SLC [21, 85, 104] and FCC [39] controllers.

3.2. EMVA System Description

The EMVA consists of two opposed magnets and two balanced springs working in parallel. Each magnet consists of a coil and a core, where upper and lower magnetic forces are induced by means of appropriate upper and lower coil currents. The mechanical valve coupled through a ferromagnetic armature to the two magnetic coils is driven through a magnetic force produced by upper and lower coil currents. To this aim a commercial 12 (V) car battery feeds an actuation power circuit, which is composed by two closed loop subsystems, each one controlled via double band hysteresis control aimed at tracking a reference current by producing a voltage output (see Fig. 3.1) and [39] for further details).

The armature is placed between the two magnets and a rigid non-ferromagnetic thin stem transfers directly the armature motion to the engine valve. Both bodies are rigidly connected via preloaded springs, yielding a single moving part. Hence, in what follows, we will refer indifferently to valve or armature motion.

During operating conditions, one of the electromagnets holds the valve in one of the two extremal positions, while overcoming spring forces and storing potential energy that can be used later to perform easily a possible successive manoeuvre towards the other extremal position. Thus, in principle, the motion from one extremum to the other can be done by exploiting the stored potential energy and by compensating

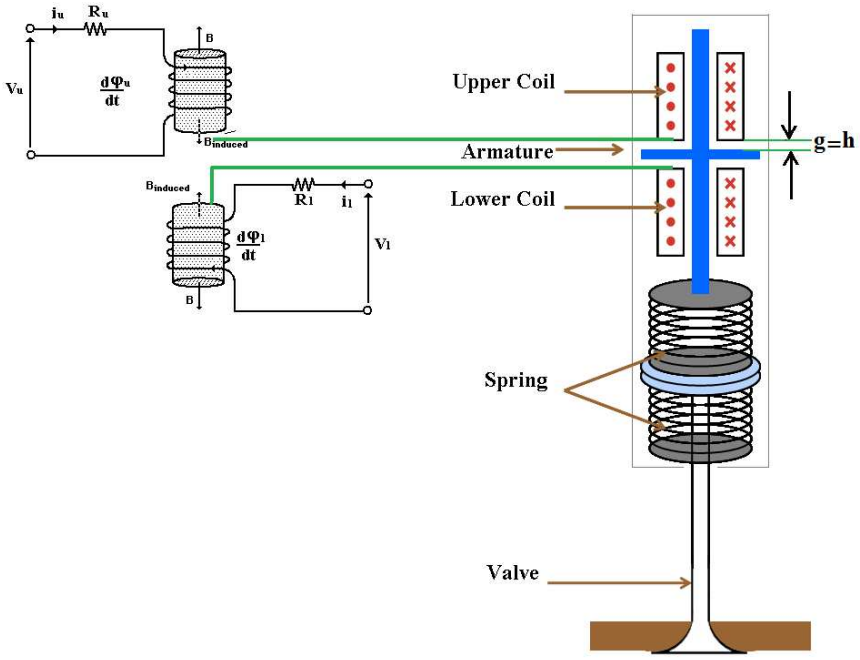

Figure 3.1.: EMVA system description. Schematic depicts the electrical and magnetic system coupled to mechanical one.

properly the friction losses during a valve stroke. For instance, when the valve is closed, the upper magnet pulls up and holds the armature, while both springs store the potential energy. Once the upper magnet is deactivated, the elastic potential energy is released and the valve starts to move in free evolution as an harmonic oscillator. Then, the valve can be captured and held by the lower electromagnet when the armature reaches a threshold distance from it, which could be in the range $0 - 1$ mm (valve open). Note that, in the absence of current, the armature rests at the intermediate position between the two coils due to the presence of two balanced springs.

A similar series of events occurs when the moving part is opened and is released from the lower electromagnet towards the upper magnet that then holds it. In general, electromagnets can exert high forces at low distances, hence, power requirements of the system are quite low in this specific situation, whereas high currents are required to drive the system if the armature is far away from the electromagnet (corresponding to an air gap greater than 1 (mm)). Additionally, the electromagnet can produce only an attractive force, that is, there exists only an accelerating force in one sense.

Despite its apparent simplicity, the behavior of the EMVA is affected by many nonlinear phenomena which can dramatically alter its dynamics. Namely:

- *Friction*, including all friction forces along all the sliding parts.

- *Impacts*, occurring when one of the moving bodies in the system (valve, armature) hits the mechanical constraints. From the application viewpoint, impacts with velocity greater than 0.1 (m/s) are undesirable since they are responsible of mechanic wear and high intensity noise [57, 104, 125] and mainly, they can cause loss of controllability at holding phase (loss of the valve). Possible impacts occur when *(i)* the valve hits the valve seat during closing, *(ii)* the armature, attracted from the lower magnet, impacts with the core of lower coil during an opening valve event (see Fig. 3.2 for details).

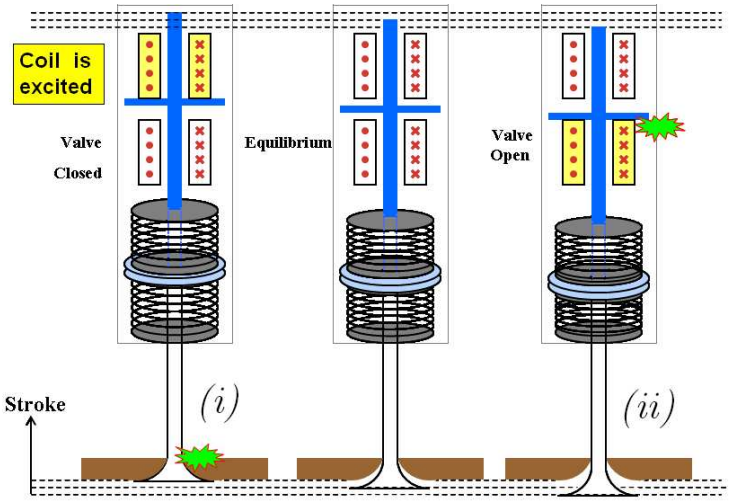

Figure 3.2.: Impact phenomena in EMVA system: Scheme of EMVA system at closed, neutral and open positions. It also shows valve stroke and the activation and deactivation of coils and the possible impact phenomena

- *Nonlinear magnetic force*, depending on both coil currents and air gap through nonlinear relations that can be modeled by different approaches, as, for example, in [38, 44, 83, 125, 134]. Furthermore, if both coils are activated simultaneously, an induced flux appears in each of them due to the presence of the other one. With the aim of avoiding opposite forces that can brake the valve, usually when the upper coil is turned on the lower is turned off, and vice versa. The EMVA prototype of interest is alternatively operated according to this philosophy.

- *Back-electromotive forces*, being induced in magnetic coils when the ferromagnetic armature moves [38, 104, 134].

- *External force.* A further nonlinear effect is due to gas pressure forces acting on the engine valve during the engine motion [21]. Such an external force acts

as a disturbance on the valve motion.

A block scheme for the system in Fig. 3.1 is depicted in Fig. 3.3. Here, the interaction is shown between three main subsystems namely: electrical, magnetic and mechanical parts.

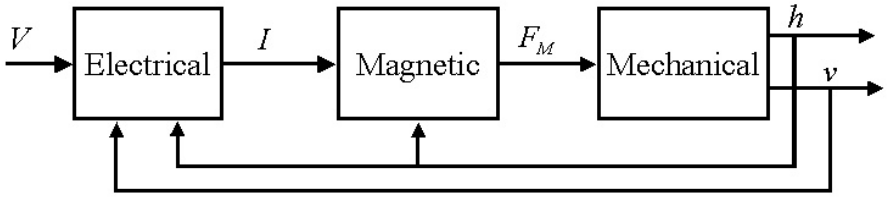

Figure 3.3.: Block diagram for EMVA system. Here, $V = [v_u, v_l]^T$ is a vector, with v_u (V) and v_l (V) being the upper and lower coil voltage, respectively; $I = [i_u, i_l]^T$ is a vector, with i_u(A) and i_l (A) being the upper and lower coil current, respectively; F_M (N) is the magnetic force; h (m) and v (m/s) are the valve position and velocity, respectively.

According to [38] and as it is schematized in Fig. 3.3, the EMVA dynamics are the result the interaction between the electrical, the magnetic and the mechanical subsystems. More in detail the electrical subsystem describes the coil current dynamics, while the mechanical subsystem takes into account armature dynamics. The interaction between the electrical and the mechanical part is due to the magnetic force generated by the coil current through the magnetic block in Fig. 3.3, which is applied directly on the armature.

3.3. Description of experimental set-up

This work relies on the electromechanical valve prototype designed in [36, 50] and developed at the Istituto Motori of the National Research Council of Italy and commissioned by Dell'Orto S.p.A. The valve has standard dimensions so as to be located in a 2 Liter commercial gasoline internal combustion engine. This prototype has been designed and analyzed using Finite Element Methods (FEM) and details on the design process can be found in [38], where a dynamic Lumped Parameter Model was developed evaluating thoroughly all magnetic aspects of the actuator. Particular effort was devoted to model the flux linkage and the magnetic forces that were analyzed using FEM data from simulations of a magneto-static distributed parameter model of the EMVA (see [38] for further details). Note that all non-linear self/mutual inductances and back-ElectroMotive Forces (EMF) terms were analytically expressed and taken into account in the proposed model.

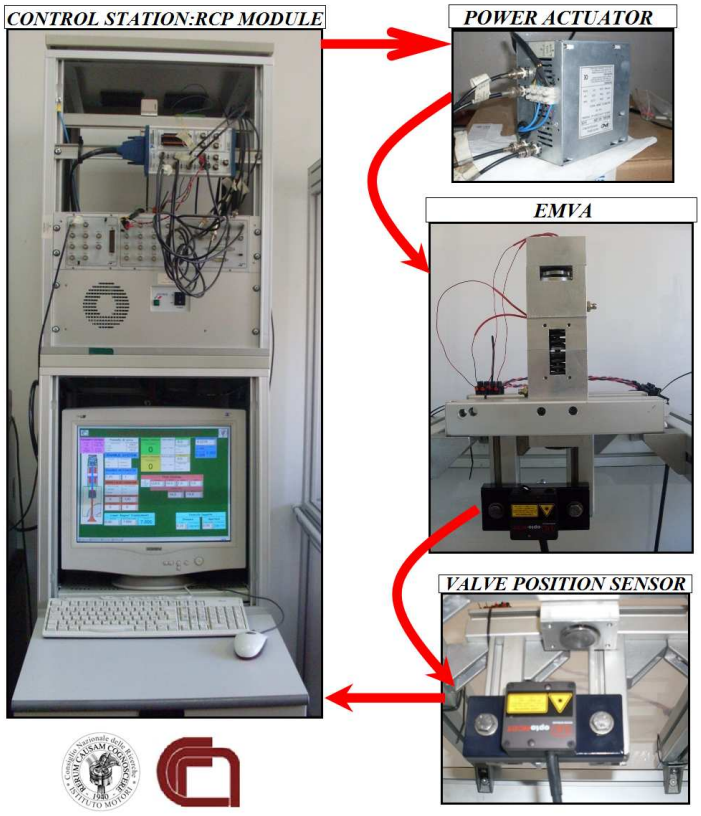

Figure 3.4.: Details on the experimental set up consisting of a Rapid Control Prototype (RCP) station, a power actuator, the EMVA System and a valve position sensor.

A picture of the experimental set-up used in this work, is shown in Fig. 3.4. Since the EMVA needs to be properly controlled during engine valve operations, a Rapid Control Prototype (RCP) system is used for real time testing of different control laws. The RCP station is a dSPACE based system equipped with the DS1005 processor board, an analog I/O board DS2201 and a digital I/O board DS4002. A laser position sensor LD1627 (MICROEPSILON) (working in the range $0-10$ (mm) with cut-off frequency of 37 (kHz)) is used for the on-line measurement of the valve position. The high frequency measurements necessary for the analysis are taken by using the acquisition board NI6123 (National Instrument) that samples at 500 (kHz) per channel. Note that the control input is the magnetic force that must be induced indirectly into the system by means of the electrical power actuator. Hence, given a desired magnetic force to be provided to the system, the RCP station computes on-line the corresponding reference values for the lower and upper coil currents by using the inversion algorithm presented in Appendix A.

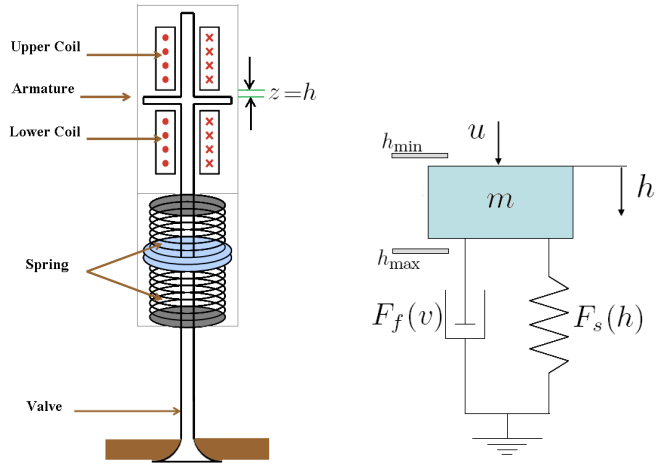

Figure 3.5.: EMVA System: a) schematic of mechanical system; b) block scheme for EMVA as an harmonic oscillator.

3.4. Mathematical model

The EMVA system can be though of as a mechanical oscillator schematically depicted in Fig. 3.5(b). It can be modeled using Newton's law under the single-mass assumption, considering equal preloaded springs and the presence of a nonlinear friction force. Thus, the dynamic behavior of the system can be mathematically described as that of a mechanical oscillator with friction given by:

$$\begin{bmatrix} \dot{h} \\ \dot{v} \end{bmatrix} = \begin{bmatrix} v \\ -\frac{F_e(h)}{m} - \frac{F_f(v)}{m} + \frac{F_{ext}(t)}{m} + \frac{u}{m} \end{bmatrix}, \tag{3.1}$$

where h (m) is the armature position (coinciding with the valve position); v (m/s) is the armature velocity (or valve velocity); m (kg) is the combined mass of the armature and the valve; $F_e(h)$ (N) is the elastic force exerted by springs; $F_f(v)$ (N) is the friction force; $F_{ext}(t)$ (N) describes the external forces affecting the valve dynamics and u (N) is the electromagnetic force assumed to be the system input. Expressions of each of these forces will be given below.

To ensure that the valve is suitably airtight on its seat during the closing phase, the armature position h can only vary in the finite interval $[h_{min}, h_{max}] \subseteq]0, g_{max}]$, being g_{max} the maximum air gap between the armature and one coil core. Note that h_{min} is strictly bigger than 0, since the armature never touches the upper magnet during the closing phase. Furthermore, h_{min} and $(g_{max} - h_{max})$ correspond to residual air gaps occurring between the armature, the valve and the upper and

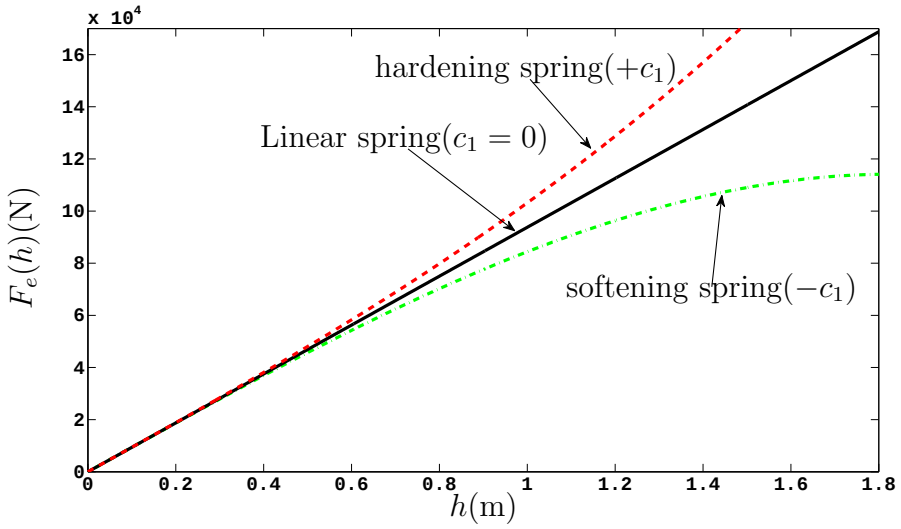

Figure 3.6.: Elastic force in a single degree of freedom spring: linear, soft and hard spring for $j = 2$ and $c_1 = 0.1$.

lower magnets, respectively. Such gaps are carefully specified in the design to deal with possible dilation phenomena (system performs in high temperatures conditions) and the necessity to reduce the magnetic forces in the valve holding conditions [36].

Furthermore, considering a symmetric preloaded system, the middle position, say h_{eq}, can be nominally computed as:

$$h_{eq} := \frac{h_{min} + h_{max}}{2}. \tag{3.2}$$

3.4.1. Spring force

The total elastic force in EMVA system can be given by $F_e(h) = k(h - h_{eq})$, with k (N/m) being the total stiffness, and $h_{eq}\,(m)$ is also the equilibrium position (3.2) of the valve at rest when external forces are absent, whereas the use of nonlinear spring forces as in [73] could be represented by $F_e(h) = k(1 \pm c_1(h - h_{eq})^2)(h - h_{eq})$, with $+c_1$ for the case of hardening springs or $-c_1$ for softening springs (See Fig. 3.6).

3.4.2. Friction force model

Several models of friction are available in the literature [7, 23, 25, 33, 61, 86]. In [21,37,38,63,83,95,104,125,129] mathematical models have been proposed for EMVA system, where the valve is represented as a mechanical oscillator with linear friction to describe the mechanical system. A non linear friction force model is considered

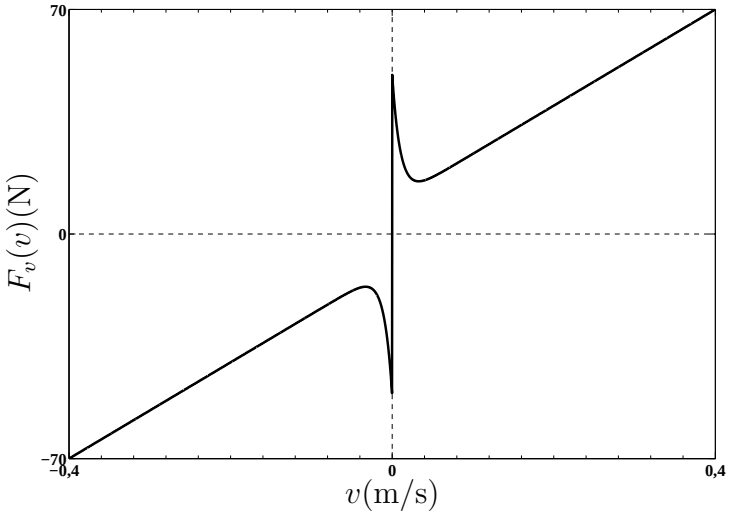

Figure 3.7.: Nonlinear friction force given by model (3.3) for parameters $F_c = 10$ (N), $F_s = 50$ (N), $v_s = 100$ (m/s) and $\sigma = 150$ (N/s).

in [44], which is aimed at modeling dry friction and damping forces and corresponds to a combined model of Coulomb and viscous friction. After careful consideration we chose to model friction in EMVA by using a model that combines classical friction models (viscous and coulomb) [7] and Stribeck friction effect [119]. This model has been also considered by different authors [33, 91].

Simulations of the friction force based on Stribeck curve allows to describe a junction between dry and viscous friction. The friction force model can be formulated as:

$$F_v(v) = (F_c + (F_s - F_c)e^{-(\frac{1}{v_s}|v|)^p})\text{sgn}(v) + \sigma v, \tag{3.3}$$

where v (m/s) is the sliding speed, F_c (N) is the Coulomb sliding friction force, F_s (N) is the stiction force, v_s (m/s) the sliding speed coefficient, p an exponent and σ (N/s) the viscous friction coefficient. Fig. 3.7 depicts the shape of nonlinear friction model (3.3).

3.4.3. Control Input

We assume that both actuators work as a hybrid or switched system, that is, when the upper coil is turned on, the lower is off, and viceversa.

Since there is a maximum upper bound for the magnitude of the current that flows into the coils, say i_{max} (A), the effective electromagnetic force u is bounded. Hence, under the hypothesis of symmetry in the behavior of the valve actuator, we can

assume that the signal u must belong to the following set:

$$\mathbb{U} = \{u \in \mathbb{R} \mid -F_M(i_{max}, h) \leq u \leq F_M(i_{max}, g_{max} - h)\}, \tag{3.4}$$

where i_{max} (A) is the maximum admissible current, g_{max} (mm) is the maximum air gap and the magnetic force in a given coil $F_M(i, z)$ is assumed to be a known nonlinear function of the current i (upper bounded by i_{max}) in the coil and the air gap z. Such a function derived from a FEM approach in [38], is:

$$F_M(i, z) = m_F(z)i + \frac{2}{\pi} n_F(z) \arctan\left(\frac{\pi}{2}\left(s_{0_F}(z) + s_{1_F}(z)i\right) i\right), \tag{3.5}$$

where $m_F(z)$, $n_F(z)$, $s_{0_F}(z)$ and $s_{1_F}(z)$ are some shape coefficients (see [38] for further details). Different approaches to describe the electromagnetic force neglecting higher order effects of flux saturation and leakage can be also found in [104, 125].

For different values of the coil current $i = i_{max}$, Fig. 3.8 depicts the nonlinear magnetic force $F_M(i, z)$ produced by upper magnet (air gap $z = h$) with $i = i_u$, where i_u (A) is the upper current, or by lower magnet ($z = g_{max} - h$) with $i = i_l$, where i_l (A) is the lower current.

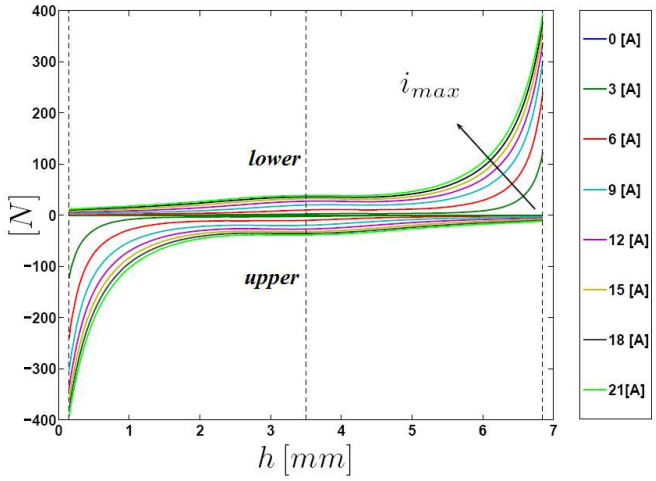

Figure 3.8.: Nonlinear behavior of the magnetic force as a function of the air gap (h or ($g_{max} - h$)) for different values of the maximum admissible current i_{max}.

3.4.4. Impact modeling

To model possible impacts between the armature and the mechanical constraints depicted in Fig. 3.2, a collision rule can be added to (3.1). In particular, letting t_k be the generic time instant when a generic impact occurs, one common approach

found in the scientific literature aimed at modeling impact phenomena is that of using the non conservative Newton restitution law given by:

$$v(t_k^+) = -\mu v(t_k^-), \quad \mu \in [0,1], \tag{3.6}$$

where t_k^- and t_k^+ are the time instants just before and after impact occurs, μ is a dimensionless factor named restitution coefficient, which gives information about how elastic a collision is, e.g. $\mu = 0$ and $\mu = 1$ describe the case of inelastic and elastic collisions, respectively.

Usually this coefficient is considered to be constant, however in general it is a function itself of the impact velocity [6]. Thus, the relationship between velocities during an impact phenomena can be modeled as:

$$v(t_k^+) = -\mu(v(t_k^-))v(t_k^-), \quad 0 \leq \mu \leq 1, \tag{3.7}$$

For the sake of simplicity and since the goal is to avoid impacts occurring in the EMVA, in this work the simplest approach is considered, where $\mu \in]0,1[$ is assumed to be a constant factor. Furthermore, since the valve operates in a bounded space with two physical constraints, impact phenomena can happen when the valve body reaches these boundaries. Considering a different collision law, the impact law can be defined as:

$$v(t_k^+) = \begin{cases} -\mu_c v(t_k^-), & \text{if } h(t_k) = h_{min}, \\ -\mu_o v(t_k^-), & \text{if } h(t_k) = h_{max}, \end{cases} \tag{3.8}$$

where μ_c and μ_o are the restitution coefficients to model impacts during closing and opening events respectively. These coefficients have to be derived from experimental data analysis.

From a control viewpoint, the existence of impacts in EMVA system becomes one of the main problem to be addressed. Impacts can cause loss of controllability at catching state, leading to the loss of the valve (see Fig. 3.2) and even its destruction. Notice also, that from engine performance viewpoint, impacting phenomena can generate loud noise and wear the physical structures.

Additionally, besides impacting motion, backlash phenomena [60] could also be present. They are due to impact phenomena over lower coil structure and the structure of the mechanical system, which is not a rigid body, and it is possible to obtain

a separation of the valve bodies, as it is depicted in Fig. 3.9. This phenomena could be present due to the fact that the armature movement is constrained because of the lower barrier imposed by magnet surface. Thus, when the valve is being opened with high force and armature impacts lower magnetic coil, the valve should continue moving due to its kinetic energy, leading to a separation from the armature; after that instant, the valve must return to join again the stem, generating new impacts or the loss of the valve, by forcing the detachment of the armature from the lower magnet.

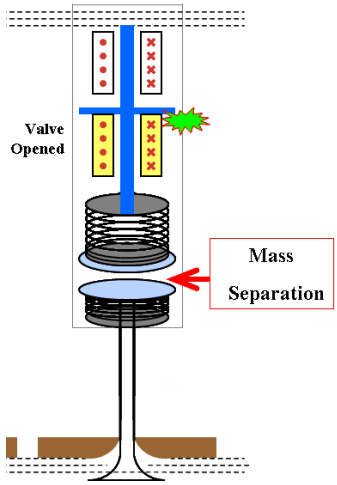

Figure 3.9.: Possible backlash phenomena in EMVA system when rigid body assumption is not considered

It is admissible to neglect backlash effects in the system if springs with high stiffness are used to construct the valve. Thus, it is reasonable to assume that the entire system behaves as a rigid body, with the valve position coinciding with the armature gap.

3.5. System identification

To estimate parameters for EMVA, we can formulate a nonlinear programming problem (NLP) with differential-algebraic constraints. In particular, the problem becomes that of solving the following optimization problem:

$$\min_{\gamma} J(y(\gamma), y_{exp}), \tag{3.9}$$

subject to the constraints:

$$\begin{aligned} \dot{x} &= f(x, u_{exp}; \gamma), \\ y(\gamma) &= w(x, u_{exp}; \gamma), \\ x_0 &= y_{\exp}(t_0), \\ H(\gamma, x) &\leq 0, \end{aligned} \tag{3.10}$$

where J is a chosen cost function to be minimized; $\gamma \in \mathbb{R}^p$ is the vector of parameters to be identified; $y(\gamma)$ is the output of system computed through mathematical model; $x \in \mathbb{R}^n$ is state vector; $f : \mathbb{R}^n \times \mathbb{R}^m \rightarrow \mathbb{R}^n$ is the system vector field; y_{exp} is the measure of the system output, while $u_{exp} \in \mathbb{R}^m$ is the measure of system input; $H(\gamma)$ is the system restriction equation set, that includes system constraints and bounds.

The identification problem is to find the optimal solution γ^* in the parameter space that minimizes cost function J, while satisfying system constraints $H(\gamma, x)$.

3.5.1. Parameter identification for EMVA system

For the case of EMVA, by assuming known the magnetic force model and electromagnetic dynamics, the mathematical model for mechanical part (3.1) has to be estimated. To this aim, the derivation for equations (3.9) and (3.10) is done based on the physical (experimental) knowledge of the system parameters and physical constraints. Thus, the cost function J is written in terms of the estimation error:

$$e_s = y(\gamma; u_{exp}, t) - y_{\exp}(u_{exp}, t), \tag{3.11}$$

where $y_{\exp}$ is the experimental trajectory obtained for the system, for an input $u_{exp} \in \mathbb{R}^2$, which corresponds to upper and lower coil currents (i_{uexp} and i_{lexp}) applied to the real system, and y is the the valve position predicted by the mathematical model for a given parameter set γ and for the measured input u_{exp}(currents)[1].

Model (3.1) is identified and validated by using a training set of experimental data, acquired during free oscillations of the valve starting from the closed position to the release state. Specifically, the parameters to be estimated in EMVA system are:

$$\gamma = \{F_s, F_c, v_s, \sigma\}. \tag{3.12}$$

[1] In order to apply those currents (i_{uexp} and i_{lexp}) into system dynamics, they are transformed from current to magnetic force at each position through the use of existent numerical model for magnetic force (see Appendix A and [37] for further details).

Specifically, the behavior predicted by the model (3.1) is compared to the experimental data and the parameter values are adjusted in order to minimize the disagreement between the two signals (estimated and measured) in terms of the Normalized Mean Square Error (NMSE):

$$J(\gamma) := \sqrt{\frac{1}{\bar{t}} \int_0^{\bar{t}} \left(\frac{y(\gamma; t) - y_{\text{exp}}(t)}{y_N} \right)^2 dt}, \tag{3.13}$$

where y_N is a normalization factor chosen equal to the maximum valve position h_{max} and $\bar{t}$ is a time instant large enough for the valve to reach its equilibrium position, i.e. $y = h_{eq}$, $v = 0$. Note that, all other parameter values were derived from direct knowledge of the experimental prototype or on the basis of straightforward geometrical and physical considerations. The metric $J(\gamma)$ is commonly referred as a cost function, and for this case it is built in the basis of the representation error (3.11) and when dealing with nonlinear systems, the cost function $J(\gamma)$ usually displays a large number of local optima. Furthermore, variable measurements are always strongly affected by noise. Hence, a Genetic Algorithm (GA) [24] is used to select the near-optimal region, while a non-linear least squares method based on the Levenberg-Marquardt algorithm [89] is then used to seek the optima locally.

Regarding the impact law, impact model is derived for both manoeuvres, opening (o) and closing (c), by using a training set from data base with experimental registers including impacting phenomena. The detection is done through numerical analysis of temporal response, where slopes are computed for both cases pre and post impact instant, allowing to obtain the velocities $v(t_k^-)$ and $v(t_k^+)$ respectively. Based on computed pre and post impact velocities, for different impact events in the same manoeuvre (closing (c) or opening (o)), it is possible to obtain at each impacting instant the ratio $\mu_i = v_i^+ / v_i^-, i = \{1, ...n\}$.

3.5.2. Experimental model validation

The effectiveness of the identification procedure is shown in Fig. 3.10, where the evolution of the model is compared to one obtained experimentally. Thus, it is evident that model (3.1) is able to capture the system behavior not only during transients, but also during steady-state conditions, when the velocity tends to zero. By comparing this result with the obtained by [44], where a dry friction model was used, it is clear that the use of combined friction model (viscous, Coulomb and Stribeck effect) yields better results during both transient and steady state response. Finally, the identified and measured values of the system parameters are summarized

Table 3.1.: Parameter values of the EMVA model

Symbol	Description	Value	Unit
m	Mass	0.144	kg
k	Spring stiffness	93773	N/m
h_{eq}	Equilibrium position	$3.5 \cdot 10^{-3}$	m
F_c	Coulomb sliding friction force constant	2.5267	N
F_s	Maximum static friction force constant	13.9	N
v_s	Inverse sliding velocity coefficient	17.315	s/m
p	scalar	1	
σ	Viscous friction coefficient	7.5153	Ns/m
h_{max}	Maximum stroke	$6.85 \cdot 10^{-3}$	m
h_{min}	Minimum stroke	$0.15 \cdot 10^{-3}$	m
g_{max}	Maximum air gap	$7 \cdot 10^{-3}$	m
μ_c	Coefficient of restitution for closing	0.292	-
μ_o	Coefficient of restitution for opening	0.254	-
r_u	upper coil resistance	0.625	Ω
r_l	lower coil resistance	0.625	Ω

in Table 3.1.

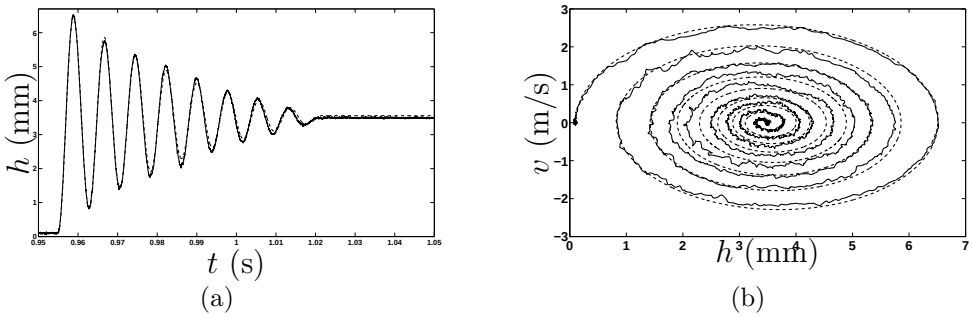

(a) (b)

Figure 3.10.: Validation results. Experimental data (solid line) *v.s.* model predictions (dashed line): a) time history of the valve position h (mm); b) phase portrait.

3.6. Sensitivity analysis for EMVA mathematical model

Since friction force is the term that could present major changes when EMVA is running due to the variable temperature and different lubrication condition, it is important to evaluate the sensitivity of the obtained mathematical model against those possible friction variations. In particular, the variation of friction parameters (for a given range around nominal parameter values $\gamma^* = \{F_s^*, F_c^*, v_s^*, \sigma^*\}$) can cause a variation in the magnitude and shape of static nonlinear friction force model, as depicted in Figs. 3.11 and 3.12 for single and joint variation of parameters γ, respectively. Since no explicit solution for EMVA mathematical model exists, the parameter variation effects and sensitivity analysis are carried out through numerical analysis. By doing so, the effects caused by the variation of nonlinear friction force

parameters on the functional NMSE (3.13) are shown in Fig. 3.13(a). From the shape of functional NMSE, it is clear that it presents different local minima, with the global minimum equivalent to zero at $\gamma = \gamma^*$. Such local minima are more frequent for parameters σ and F_c. In particular, from the picture it is clear that for small variations of the parameters, say within $\pm 10\%$, small variations in the system trajectories are observed with errors that never exceed $\pm 2\%$. Finally, the maximum error, for a simultaneous variations of all parameters of interest in our analysis, never exceed 4%.

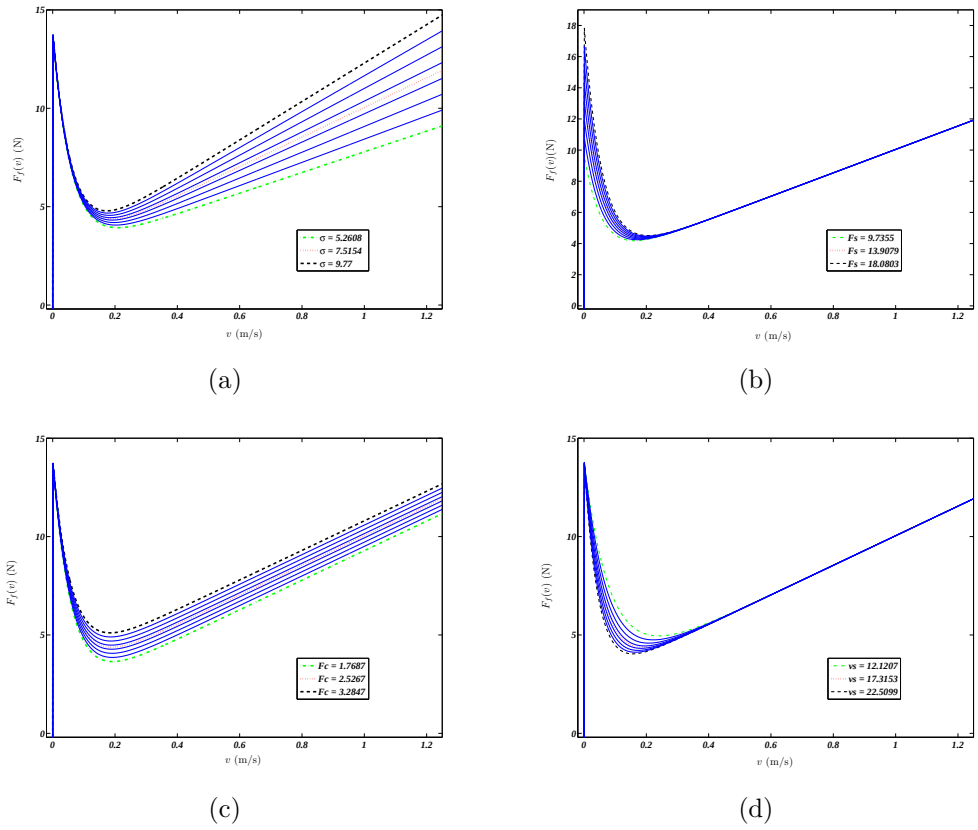

Figure 3.11.: Single parameter variation of friction force model parameters in a range of $\pm 30\%$ and their effect on friction force nonlinearity $F_f(v)$: a) σ; b) F_s; c) F_c; d) v_s.

The effect of a simultaneous parameter variation, both on steady state and transient behavior is also evident from the time history of the perturbed trajectory reported in Fig. 3.14. Here, in particular it is evident the effect of viscous friction parameter σ in the time evolution response, where the damping effect is clear for greater values of this parameter, while the effect of coulomb force parameter F_c is not so evident.

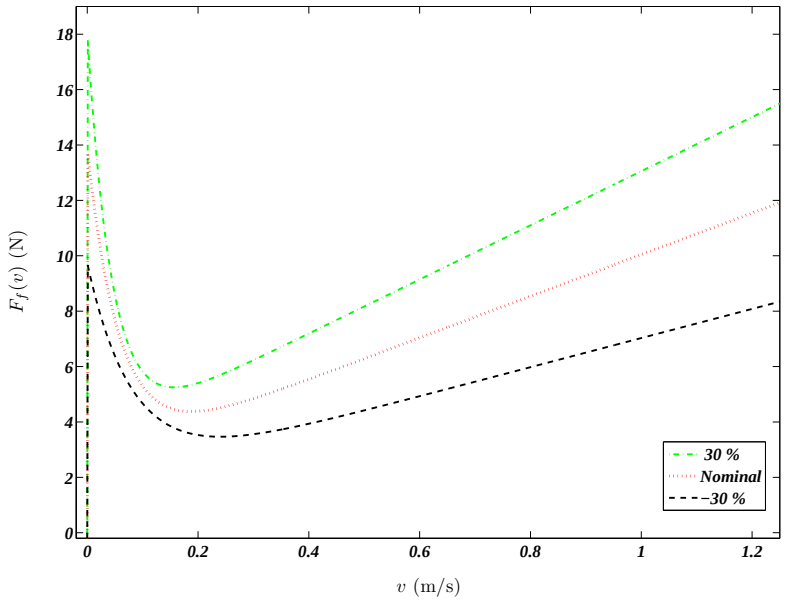

Figure 3.12.: Shape for friction force model $F_f(v)$ when a join parameter variation is considered in a range of $\pm 30\%$.

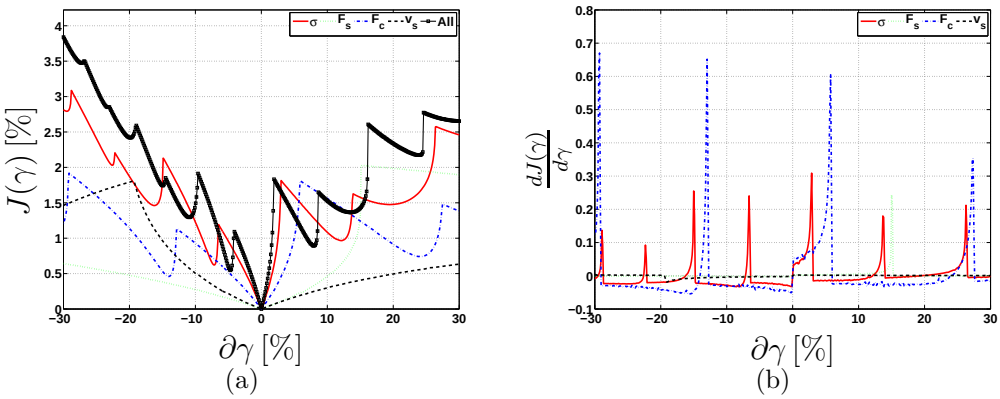

Figure 3.13.: Variation of cost function (3.13) for different single variation of friction parameters around nominal values γ^*: a) $J(\gamma)$; b) Variational ratio $\frac{\partial J(\gamma)}{\partial \gamma}$

3.7. Discussion

In this chapter we have proposed a mathematical model to represent the EMVA dynamics. EMVA system consists of different subsystems. The power electronics system to performing the electrical coil current controller and the electromagnetic dynamics, and the inclusion of all those dynamics into a mathematical model leads to a complex system. Thus, in order to avoid complexity, a simplified model is obtained through the consideration of some physical assumptions. Spring forces

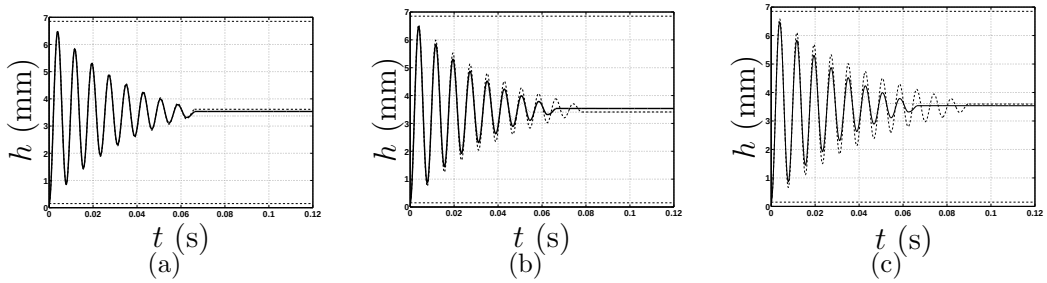

Figure 3.14.: Time history of the valve position for a joint variation of all the friction model parameters: a) $\delta\gamma = \pm 3\%$; b) $\delta\gamma = \pm 20\%$; c)$\delta\gamma = \pm 30\%$

have been supposed to be linear, while the total mass of the system was estimated for equivalent single rigid body and considering the spring as a distributed mass body. Particular effort was devoted to describe the nonlinear properties of friction force, leading to a static nonlinear friction model that includes viscous, Coulomb and Stribeck effect.

The model parameters were estimated based on experimental measures and through the use of nonlinear optimization numerical tools. It has been shown that the chosen model is able to reproduce observed experimental dynamics.

In the next chapters different control techniques are designed based on the mathematical model presented in this section.

CHAPTER 4

KEY-ON CONTROL

> He who loves practice without theory is like the sailor who boards ship without a rudder and compass and never knows where he may go.
>
> *(Leonardo Da Vinci (1452-1519))*

This chapter addresses the Key-On control problem for the double magnet Electro Mechanical Valve Actuator (EMVA) described in Sec. 2. Specifically, Sec. 4.1 introduces the Key-on control problem, which is formally stated in Sec. 4.2, while Sec. 4.3 presents a nonlinear control approach based on energy methods to solve the control problem. The performance of the controller is analyzed numerically in Sec. 4.4 by obtaining a closed loop bifurcation diagram. The results of the bifurcation analysis are also used to tune the controller gain as shown in Sec. 4.5. The control robustness respect to parameter variation is studied in Sec. 4.6. The implementation of the controller is described in Sec. 4.7, while the experimental validation of both closed loop nonlinear dynamics and control performance are presented in Sec. 4.8. A discussing section is in Sec. 4.9. The results presented in this chapter have recently appeared in [30, 31].

4.1. Introduction

In order to make EMVA a reliable solution to perform VVA operations in Camless engines, an extremely delicate stage to be addressed is the Key-On control at engine start-up, when friction phenomena strongly dominate the system dynamics, particularly at low velocities. The task has to be designed in order to move the valve from its rest position (the middle of the stroke) to one end of the stroke (depending if one wants to close or open the valve at start) while satisfying low energy consumption requirements and avoiding high intensity impacts (impacting velocity less than 0.1(m/s)) [104].

This first maneuver is critical since the armature starts at the central position and the magnetic force is strongly nonlinear with respect to air gaps and currents as it is shown in Fig. 3.8. Hence, high power is required to initiate the valve motion and this makes the first lift hard to be accomplished with feasible coil currents provided by automotive electrical power circuits [22, 39]. To overcome this problem different technological solutions have been adopted, based on a special design of the EMVA itself or on the addition of further actuation to attain the first lift maneuver with admissible coil currents. For example, the use of Permanent Magnets (PM) has been proposed in [5, 69]. Alternatively, in [101, 108] an electrical motor, driven by an open-loop control input, is added to operate the device. Obviously, with this kind of solutions, the complexity of the overall system increases. Recently, the first catching problem has been tackled in [37, 39] by exploiting the mechanical resonance of EMVA to drive the system during first lift. In this case, the model-based control law requires good knowledge of the system resonance frequency and suffers from parameter uncertainties mainly due to the friction variations. Note that, in this scenario, an effective solution of the first catching problem can help the industry to overcome obstacles for a low-cost mass production of camless technology, recently announced by automotive components industry [105].

Here, a controller is designed, analyzed and tuned with the aim of solving the Key-on control problem while satisfying the practical constraints for the possible application in a commercial engine. In particular a nonlinear controller based on energy methods is proposed, tuned through a bifurcation diagram and validated experimentally.

4.2. Key-on control problem statement

During key-on, the armature must be driven from its rest position $x(0) = [h_{eq}\, 0]^T$ to a sufficiently small neighborhood of one of the extremal positions with a sufficiently small velocity (less than 0.1 (m/s)) in order to avoid impacts [37, 44, 104, 125] (first catching maneuver). Once the armature is near the magnetic coil boundary, a different control strategy must be used to catch the armature.

4.2.1. Problem statement and specifications

Consider the EMVA nonlinear model (3.1) with initial conditions $[h_{eq}\, 0]^T$. Let

$$\Omega := \{x \in \mathbb{R}^2 \mid \left(\frac{h - h_c}{r_h}\right)^2 + \left(\frac{v - v_c}{r_v}\right)^2 < 1\}, \tag{4.1}$$

be the target region in state space we wish the valve dynamics to enter, where $x = [h\ v]^T$ is the state vector, r_h (m) and r_v (m/s) are the radius of the ellipsoids centered in $x_c = [h_c\ v_c]^T$. Note that in general $v_c = 0$, while h_c can be set alternatively to $(h_{min} + r_h)$ or $(h_{max} - r_h)$ depending on whether we want to open or close the valve at start. The target regions, respectively close to the valve open or closed position, are named as Ω_{min} and Ω_{max} (see also Fig. 4.1 and Tab. 4.1 for the parameter values).

Once the target Ω region has been selected, the time instant, say $T > 0$, when the trajectory first enters that region is defined as key-on time and $h_T = h(T)$ and $v_T = v(T)$ are the values assumed by the armature position and velocity respectively at that time instant.

The *Key-on control problem* is to find a feedback control law $u = u(h, v, t)$ aimed at destabilizing the stable rest equilibrium $x(0) = [h_{eq}, 0]^T$ and driving the valve towards the desired phase-space region Ω in a finite time T, so that $[h(T)\ v(T)]^T \in \Omega$, while it holds:

$$\begin{aligned} &h_{min} < h(t) < h_{max}, \qquad \forall\, t \in [0, T], \\ &T_r < T < T_{max}, \\ &i_j \in [0, i_{max}], \qquad j = \{u, l\}, \end{aligned} \tag{4.2}$$

where T_r corresponds to the natural rise time of the EMVA system, T_{max} is the maximum admissible bound on the key-on time T, i_u and i_l are the upper and lower coil currents, respectively, and i_{max} is the maximum admissible value of coil currents provided by the actuators.

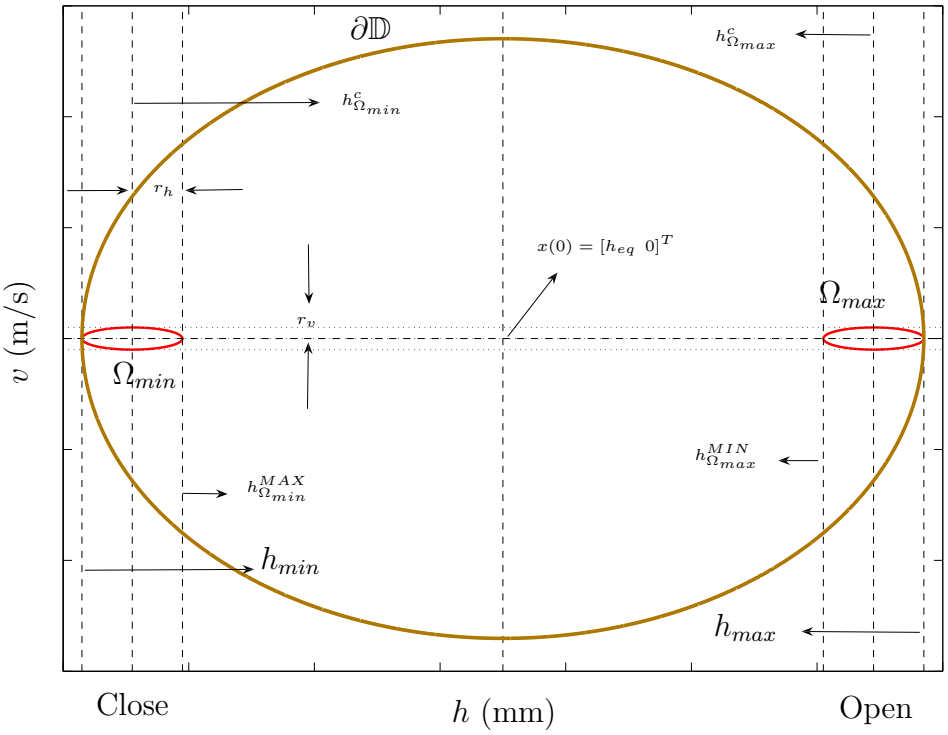

Figure 4.1.: Schematic representation of the admissible target regions (Ω_{min} and Ω_{max}) in state-space. Here $h^c_{\Omega_{min}} = h_{min} + r_h$; $h^{MAX}_{\Omega_{min}} = h_{min} + 2r_h$; $h^c_{\Omega_{max}} = h_{max} - r_h$; $h^{MIN}_{\Omega_{max}} = h_{max} - 2r_h$.

Table 4.1.: Target region parameters

Symbol	Description	Value	Unit
r_h	Ellipse radio on position edge	$0.4 \cdot 10^{-3}$	m
r_v	Ellipse radio on velocity edge	0.1	m/s
$h^c_{\Omega_{max}}$	Center of Ω_{max}	$6.45 \cdot 10^{-3}$	m
$h^c_{\Omega_{min}}$	Center of Ω_{min}	$0.55 \cdot 10^{-3}$	m
T_{max}	Maximum key-on time	$100 \cdot 10^{-3}$	s
T_r	Rise time	$3.9 \cdot 10^{-3}$	s

4.3. Energy based Key-on control

Energy based control law is based on the energy control approach presented in [9,10,56,114,127]. This technique originates from the pioneering work in [68], where the classical problem of the swinging up an inverted pendulum was addressed. More recently, this control technique has been shown to be effective even in the presence of friction losses and gravity [100].

The controller is designed by using a nonlinear model of the dynamic behavior of the EMVA system and in the basis of Lyapunov direct method. Control explicitly takes into account the effects of friction on the valve motion and the magnetic

force modeled as in [38]. The resulting control strategy is itself nonsmooth. The closed-loop dynamics is then studied on the basis of nonlinear system theory and the bifurcation analysis [28, 120]. The closed loop bifurcation diagram is validated experimentally and used as a tool to tune the controller gain. The experimental analysis and validation are in good agreement.

4.3.1. Key-on control design

The key idea behind the approach is to control the overall mechanical energy of the EMVA mechanical system (3.1), defined as:

$$E = K + U = \frac{mv^2}{2} + \frac{k(h - h_{eq})^2}{2}, \tag{4.3}$$

where K and U are the kinetic and the potential energy, respectively.

Differentiating (4.3), the overall energy rate is given by:

$$\frac{dE}{dt} = mv\dot{v} + k(h - h_{eq})\dot{h}. \tag{4.4}$$

Substituting (3.1) into (4.4), we then obtain:

$$\frac{dE}{dt} = v(-F_f(v) + u). \tag{4.5}$$

The above expression for the total energy rate clearly confirms that the energy can be directly controlled by means of the electromagnetic force u being fed to the system. To destabilize the stable equilibrium position and then drive the armature to the selected target region Ω, the control action u must provide the EMVA with a quantity of force that is at least enough to compensate all the dissipative effects due to friction $F_f(v)$.

To proceed with the control design, here we use the candidate Lyapunov function:

$$V = \frac{1}{2}(E - E_0)^2, \tag{4.6}$$

where E is expressed as in (4.3) and E_0 is the energy evaluated when the valve is at its closing or opening position, namely $E_0 = \frac{k}{2}(h_{min} - h_{eq})^2$ or $E_0 = \frac{k}{2}(h_{max} - h_{eq})^2$, respectively. Here we assume that $|h_{min} - h_{eq}| = |h_{max} - h_{eq}| := \Delta h$.

Clearly, V is continuous and differentiable. Moreover $V \geq 0$ for all h,v with $V(h, v) = 0 \Leftrightarrow E = E_0$ as it is shown in Fig. 4.2(a). Hence, we have that $V > 0$ in

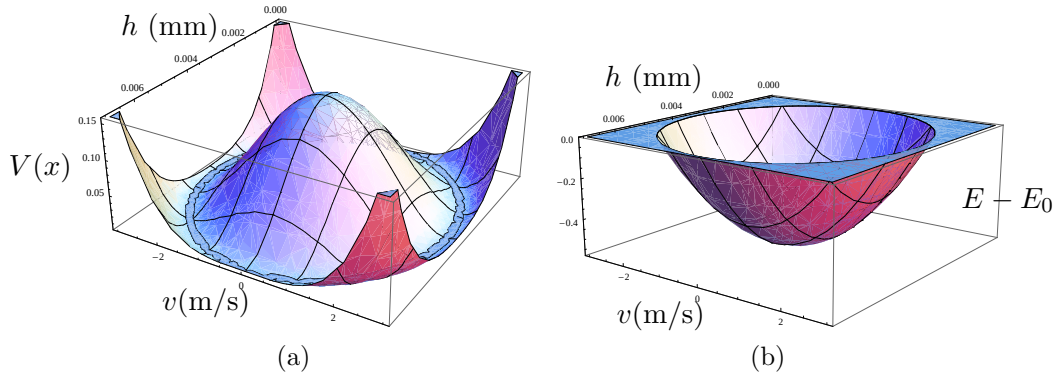

Figure 4.2.: Candidate like-Lyapunov function: a) $V(x)$; b) Shape for term: $E - E_0$.

the domain:

$$\mathbb{D} := \{(h, v) \in \mathbb{R}^2 : \frac{1}{2}(mv^2) + \frac{k}{2}(h - h_{eq})^2 < \frac{k}{2}(\Delta h)^2\}. \tag{4.7}$$

(The boundary for subset $\mathbb{D}$ denoted by $\partial\mathbb{D}$ is shown in figure 4.1).

Differentiating expression (4.6) and then using equation (4.5), after simple algebraic manipulations, we get:

$$\dot{V} = (E - E_0)(-F_f(v) + u)v. \tag{4.8}$$

To destabilize system (3.1), we need $\dot{V}$ in (4.8) to be negative in $\mathbb{D}$ [73, 117]. Since the term $(E - E_0)$ in (4.8) is always negative in $\mathbb{D}$ (see Fig. 4.2(b)), the control signal $u(t)$ must be chosen according to the sign of $v(t)$ so that:

$$\begin{cases} u > F_f(v), & \text{if } v > 0; \\ u < -F_f(v), & \text{if } v < 0. \end{cases} \tag{4.9}$$

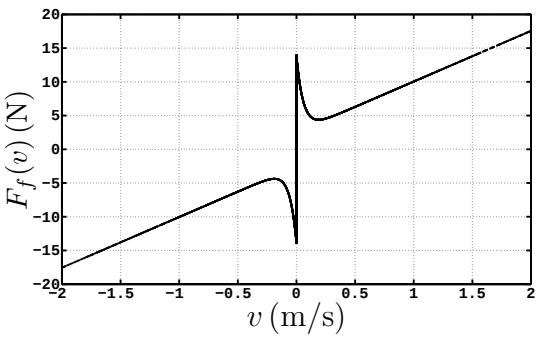

Figure 4.3.: Nonlinear friction force as a function of the valve velocity v.

Note that, as always happens in physical devices, the valve velocity v is bounded to a certain maximum admissible value, say v_η. Thus, according with the friction model in (3.3), the nonlinear friction force $F_f(v)$ turns to be bounded too. Hence, the controller (4.9) is chosen as:

$$u = \alpha \text{sgn}(v), \qquad \alpha \in \mathbb{R}^+, \tag{4.10}$$

where α is the absolute value of the control signal to be chosen appropriately to compensate the nonlinear friction effect. With a slight abuse of terminology, in what follows we will refer to α as the control gain.

Note that due to the presence of limits on the maximum admissible current, the effective control action, say u_s to the plant will be saturated as follows:

$$u_s = \begin{cases} u_{max}, & \text{if } u \geq u_{max}; \\ u, & \text{if } u_{min} < u < u_{max}; \\ u_{min}, & \text{if } u \leq u_{min}. \end{cases} \tag{4.11}$$

where $u_{max} = F_M(i_{max}, g_{max} - h)$ and $u_{min} = -F_M(i_{max}, h)$ according to expression (3.4). The bounds u_{max} and u_{min} are dynamic, as they strongly depend on the actual valve position h. Thus, they have to be computed on-line by using the model of the magnetic force (3.5).

4.4. Closed loop dynamics analysis

In this section, bifurcation analysis is used to analyze the closed loop nonlinear dynamics for energy based controller, when considering the control gain α in (4.10) as a bifurcation parameter). In particular, bifurcation analysis is then used as a tool to tune such a control gain α. Note that, if the maximum friction force and other undesired disturbances to be compensated were perfectly known, it would be possible, at least theoretically, to compute exactly the amount of energy necessary to compensate them and, consequently, to select the minimum additional control effort able to destabilize the system. However, there can be large mismatches and uncertainties in the friction estimate and thus, in practice, an acceptable tuning cannot be achieved via a simple model based design. Conversely, the design of the control action via bifurcation analysis provides a robust way to calibrate such an action against all possible model uncertainties/mismatches. Furthermore, it provides an insight into both the performance of the tuned system and the nonlinear dynamics

of the closed-loop process for a wide range of values of the control gain α.

4.4.1. Closed loop bifurcation diagram

Closed loop dynamics induced in system (3.1) by Key-on controller (4.10) is analyzed numerically through a continuation method, where system parameters are set to nominal values (See Tab. 3.1) and control gain α is continued in the range $[0, 30]$. Such a range is chosen from friction force curve Fig. 4.3, in order to cover all possible cases to be compensated. Fig. 4.4 shows the closed-loop bifurcation diagram of the EMVA system with respect to variations of the control gain α, while the maximum value of the admissible current is fixed according to the physical actuator constraints ($i_{max} = 18$ (A)).

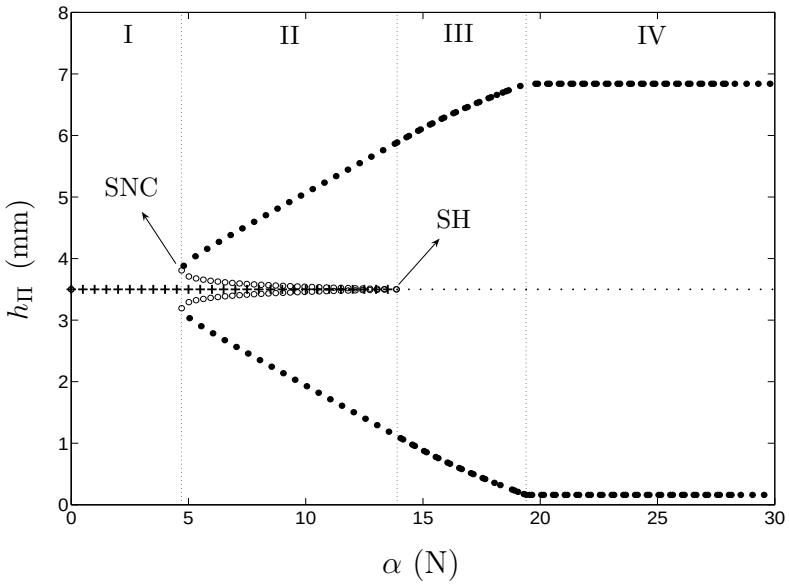

Figure 4.4.: Numerical bifurcation diagram of the closed-loop system. Empty-circles branches correspond to unstable limit cycle, solid-circles branches to stable limit cycles, crosses-branch to stable equilibrium set and dotted-branch to unstable equilibrium set.

A Poincaré section defined by $\Pi := \{v \in \mathbb{R}, h \in [h_{min}, h_{max}] \mid v(t) = 0,\ h(t) = h_{max} \text{ or } h(t) = h_{min}\}$ was used to capture the asymptotic solutions of the system, considering also possible impacting behavior. For each value of the control gain the last 40 samples of the armature motion $h(t)$ were stored. The diagram was derived in two stages: firstly α was varied from zero (corresponding to an open-loop condition) to 30 (N) obtaining the forward bifurcation diagram. A second numerical bifurcation diagram was then derived with α being decreased from 30 (N) to 0 (N) (backward diagram). The complete bifurcation diagram was then obtained by overlapping the

forward and backward diagrams, so as to highlight hysteretic phenomena. The location of the unstable limit cycle was obtained using an approximate technique based on a describing function analysis [31], which is described in Appendix B.

The numerical bifurcation diagram in Fig. 4.4 shows that the closed-loop EMVA exhibits coexisting solutions and several bifurcations. The diagram is characterized by four regions of different qualitative behavior, which is associated with different values of α. In what follows, we study each of these scenarios in greater detail, complementing the bifurcation diagram with time-series and phase plane portraits at the most significant values of the control gain.

Region I. For $\alpha \in [0,\ 4.7]$, friction losses are not compensated by the control action and the asymptotic behavior of the system is characterized by a stable equilibrium set (see the branch marked with the symbol "+" in the bifurcation diagram). This phenomenon depends on the nonsmooth set-valued nature of friction and the equilibrium set corresponds to a stationary mode for which the friction elements are sticking. Numerical evidence for the presence of the equilibrium set is provided in Fig. 4.5, where it is shown that, for a given value of α, trajectories originating from different initial conditions are attracted towards different points on the equilibrium set. The analytical characterization of this phenomenon using Filippov analysis for the system is reported in Appendix B. A more general description of friction-induced equilibrium sets and their attractivity has been studied in the case of multi-degree of freedom mechanical systems in [80, 132].

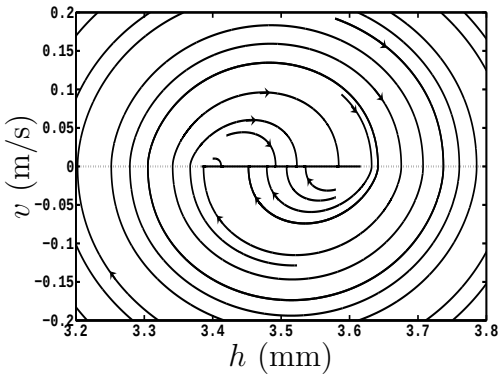

Figure 4.5.: Region I. Equilibrium set: Phase space plot for $\alpha = 3$.

When $\alpha = 4.7$, the Key-on control action starts to weakly compensate the friction force and a *Saddle-Node bifurcation of Cycles* (SNC) is observed to occur, with two limit cycles one stable, the other unstable being formed. Notice that the origin remains stable throughout and it is not involved in this bifurcation scenario. The half stable limit cycle divides the phase space into two regions (referred as external and

internal). Valve motion converges to the stable limit cycle when the initial condition belongs to the external region, while it is attracted towards the equilibrium set, when it starts from an initial condition belonging to the internal region as shown in Fig. 4.6.

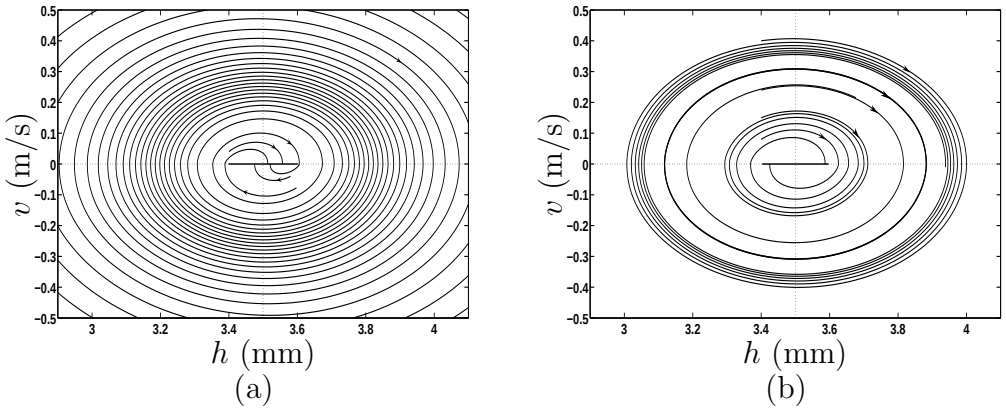

Figure 4.6.: Numerical evidence of the saddle-node bifurcation of limit cycles. Phase portrait: (a) $\alpha = 4.4$ (N); (b) $\alpha = 4.8$ (N).

Region II. For $\alpha \in]4.7, 13.9]$, the system shows a more complex dynamic behavior characterized by the coexistence of two attractors and one repeller. Namely, one unstable and one stable limit cycle coexist with the equilibrium set. In this region, as α increases, the equilibrium set shrinks to the fixed point $[h_{eq}, 0]^T$ (for $\alpha = 13.9$ (N)). This behavior is shown in Figs. 4.7 and 4.8 (See Appendix B for further details on the analysis of the equilibrium set). Simultaneously, the stable and unstable limit cycles tend to respectively increase and decrease their amplitude (see Fig. 4.9). The unstable solution is characterized through describing function method in Appendix B.

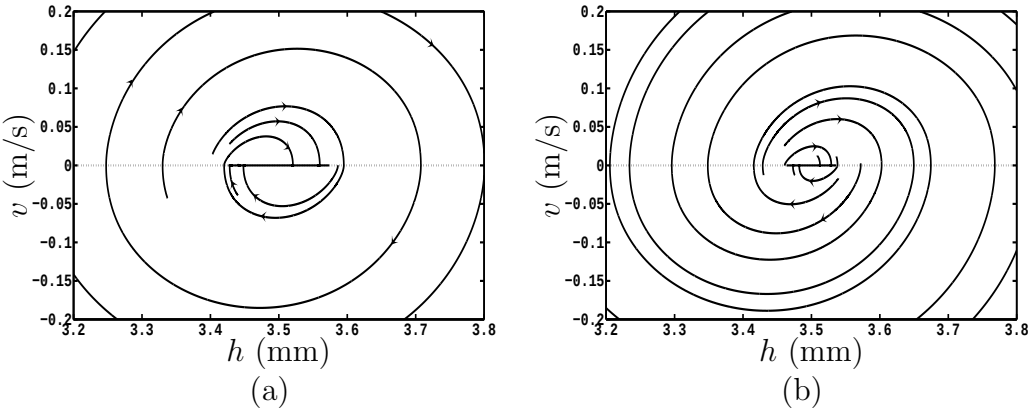

Figure 4.7.: Equilibrium set. Phase plot: (a) $\alpha = 7$ (N); (b) $\alpha = 10.5$ (N) . Increasing α the equilibrium set tends to be shrunk. The different trajectories are originated from different perturbed initial conditions.

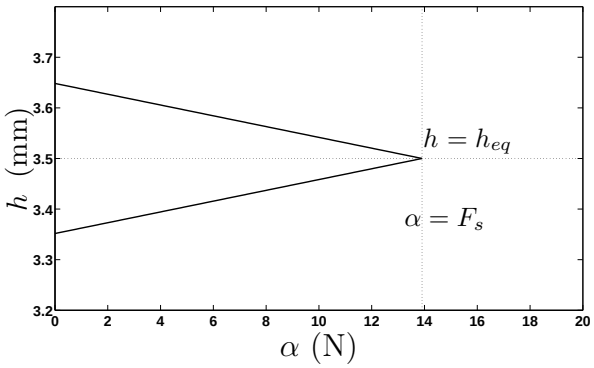

Figure 4.8.: Variation of equilibrium set as a function of control parameter α for $\alpha \in [0\,; Fs]$ (N). For $\alpha = Fs = 13.9$ (N) the system shows a fixed point $[h_{eq},\, 0]^T$.

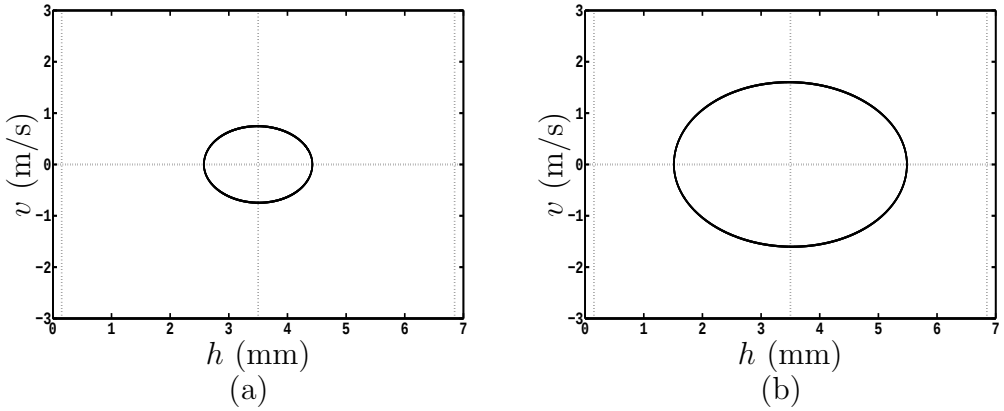

Figure 4.9.: Examples of the dynamic behavior of the valve for two different representative values of α in Region II. Phase portrait: (a) $\alpha = 7$ (N) ; (b) $\alpha = 12$ (N)

For $\alpha = 13.9$ (N) a *Subcritical Hopf (SH) bifurcation* [120] occurs. The unstable limit cycle shrinks to zero amplitude and engulfs the stable fixed point $[h_{eq}\ 0]^T$ rendering it unstable (see Fig. 4.10). Note that the critical point is reached when the control gain assumes a value that coincides with the maximum static friction force $\alpha = F_s = 13.9$ (N) according to the estimated value reported in Tab. 3.1. Specifically, in this condition the Key-on control action is able to compensate the static friction force so that even a small disturbance is enough to take the valve out from its equilibrium state. It turns out that in this situation, it is easy for the Key-on control to move the valve from its release state to a regime of stable oscillations.

Region III. For $\alpha \in]13.9, 19.45]$ (N) in Fig. 4.4, the unstable fixed point (dotted line) stemming from the *SH bifurcation* is surrounded by a stable limit cycle (solid circle line). As the value of α increases, the amplitude of the limit cycle grows until it grazes one of the physical constraints limiting the armature motion. The

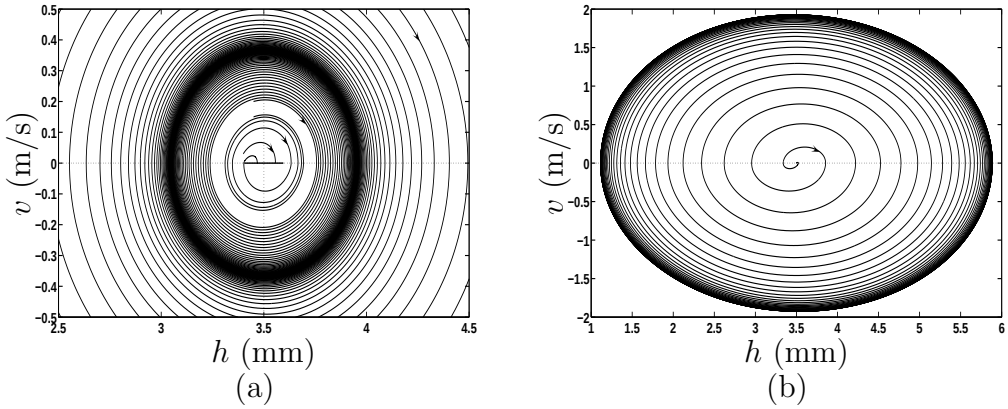

Figure 4.10.: Numerical evidence of the subcritical Hopf bifurcation. Phase portrait: (a) $\alpha < F_s$ (N); (b) $\alpha > F_s$ (N).

grazing bifurcation occurs when the valve touches the boundaries ($h(t) = h_{mim}$ or $h(t) = h_{max}$) with zero velocity for $\alpha = 19.45$ (N) as shown in Fig. 4.11.

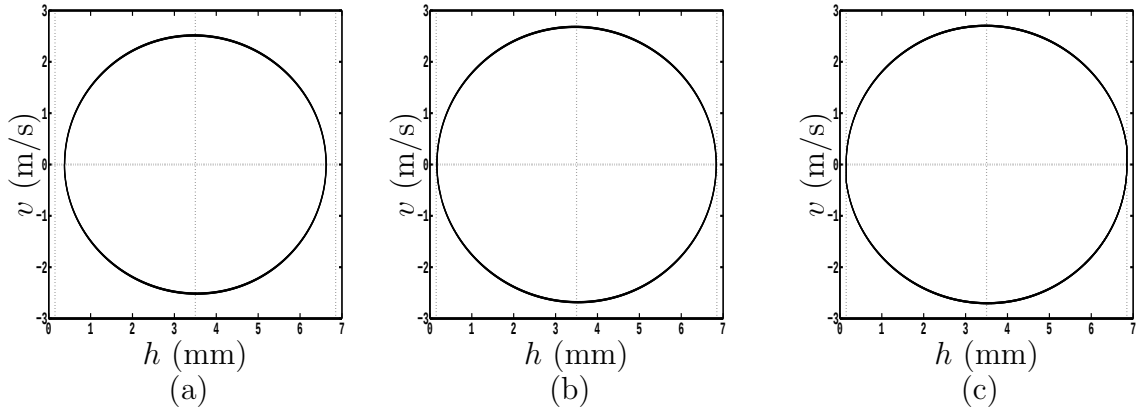

Figure 4.11.: Numerical evidence of the grazing bifurcation. Phase portrait. (a): $\alpha = 18$ (N); (b): $\alpha = 19.45$ (N); (c): $\alpha = 21$ (N).

Region IV. For $\alpha > 19.45$ (N) there is evidence of a multi-impacting behavior (see Fig. 4.12) coexisting with the unstable equilibrium set (respectively, solid-circle line and dotted line in the bifurcation diagram in Fig. 4.4). Obviously, increasing α, impacts become more energetic, hence region IV is not acceptable for the operation of the electromechanical system.

4.5. Controller tuning through Bifurcation diagram

Here we use bifurcation analysis to tune the gain of the control action so as to achieve the specifications summarized in the definition of the target region Ω (see Section

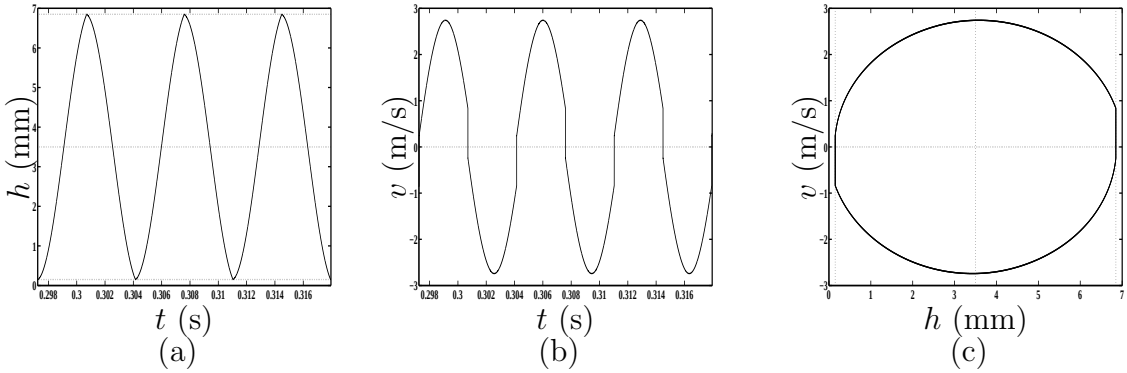

Figure 4.12.: Example of the valve motion in the impacting region IV. $\alpha = 30$ (N). (a): Time series of the valve position h. (b): Time series of the valve velocity v. (c): Phase portrait.

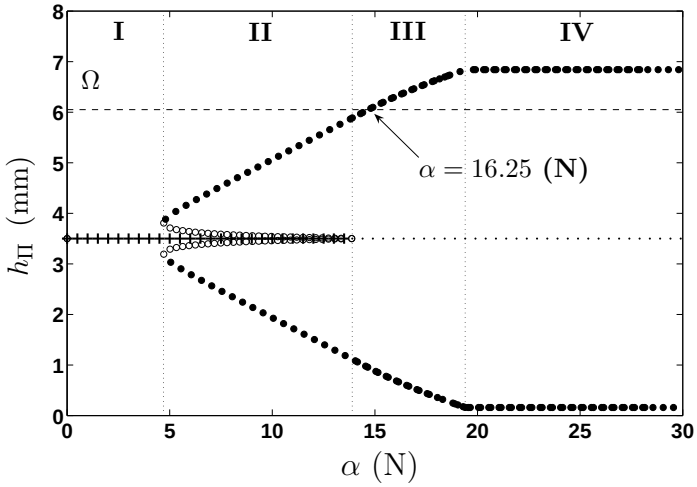

Figure 4.13.: Controller tuning through Bifurcation diagram. The dashed-line refers to the minimum value of $h(T)$ within the target region Ω_{max}.

4.2 and Tab. 4.1). According to the EMVA working principle, once the valve moves from its rest position in the middle of the stroke, it can be easily transferred to the open (close) condition by exploiting all the energy stored in the spring and then feeding into the system with a small amount of energy, just enough to compensate friction losses. Here we locate the target ellipsoid region of the state space Ω close to the open position of the valve, *i.e.* we set $h_c = (h_{max} - r_h) = 6.45$ (mm) ($\Omega = \Omega_{max}$).

Referring to the numerical bifurcation diagram for $i_{max} = 18$ (A) in Fig. 4.13, the minimum value of α at which trajectory enters the region Ω is 16.25 N, for steady state valve position $h(T) = h_{max} - 2r_h = 6.05$ (mm) (dashed line in the bifurcation diagram) and velocity $v(T) \simeq 0$ (m/s).

Since control specifications impose an additional constraint on the maximum key-

on time T (less than 100 [ms]), further numerical investigations showed that this requirement cannot be satisfied in the range $\alpha \in [16.25, 17.6]$. Hence, the admissible control gain should be greater than 17.6 (N) and belong to regions III and IV of the bifurcation diagram. Note that, although big values of α, around 30 (N), are theoretically possible, they must be discarded so as to reduce the control effort and avoid the high energy impacting zone.

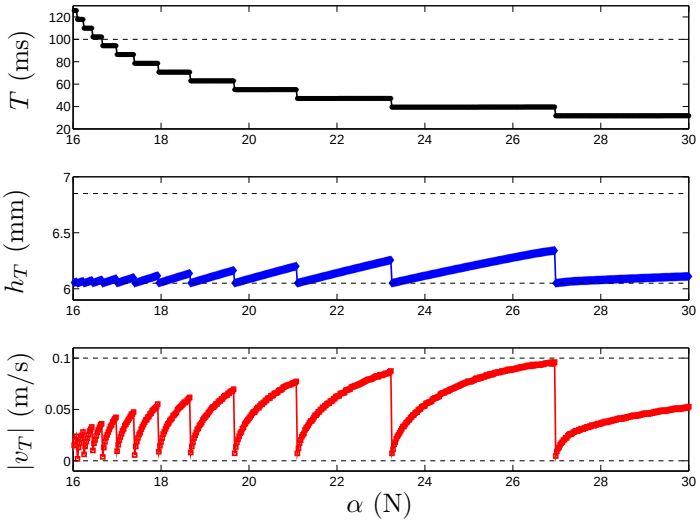

(a)

Figure 4.14.: Key-on controller performance in terms of T, h_T and v_T

Furthermore, in order to evaluate the fulfillment of Key-on control requirements, we test the control performance in terms of the performance parameters v_T, h_T and mainly the key on time T (see section 4.2) in the range $\alpha \in [16.25, 30]$. Such a performance of the Key-on controller is shown in Fig. 4.14(a), where by increasing α, controller fulfills the requirement in T, and a kind of repeated tendency is observed in the parameters performance v_T and h_T, when the value of parameter α is varied. Notice also from Fig. 4.14(a), that T is diminished as well as α increases. This pattern is caused by the way that trajectory $x(t)$ enters the target ellipsoid region Ω, leading to the reduction of one oscillation (swing) in the valve motion at each value of α where the trajectory $x(t)$ reduce one oscillation. Additionally, this evolution produces a reduction of Key-on time T by steps as well as the the number of oscillations. Despite, low key on time T is desired for the application, there exists a trade off between this feature and the final velocity v_T, in order to avoid impacts of high intensity. In particular for $i_{max} = 18$ (A), we found the range of admissible values to be $\alpha \in [17.6, 19.45]$. Similar analysis is carried out for other values of i_{max}, yielding the admissible ranges given in Tab. 4.2.

From the results summarized in Tab. 4.2, the control action has been set so as to be sufficiently high to satisfy control specifications for all values of i_{max} above 12 (A). Hence, the control gain has been set in the range $[19, 22]$ (N), so that, the target region is surely reached with $T < 100$ ms for all values of $i_{max} > 9$A.

Table 4.2.: Control ranges

i_{max} (A)	Target region Ω	$T < 100$ [ms]
18	$\alpha \in [16.25, 30]$	$\alpha \in [17.6, 30]$
15	$\alpha \in [16.81, 30]$	$\alpha \in [18.2, 30]$
12	$\alpha \in [17.97, 30]$	$\alpha \in [18.97, 30]$
9	$\alpha \in [18.22, 30]$	$\alpha \in [19.01, 30]$

4.6. Key-on control robustness

Note that during engine operation, high and varying temperatures can produce important variations in the parameters of the EMVA, that can affect strongly the controller performance. Therefore, the study of such parameters variation and their effect on system behaviour becomes a key point during controller design in order to tune the controller and increase the robustness range where the system performance is acceptable.

Finally, the robustness of the key-on controller against system parameter variations is investigated via numerical simulations. Here, as an example, we show that introducing an uncertainty of $\pm 20\%$ in the friction parameters with respect to the nominal values in Tab. 3.1 (as shown in Fig. 4.15(a)) and for $i_{max} = 12A$, the control algorithm is still able to guarantee the required specifications. Note that, as reported in Fig. 4.15(b), where the trajectory of the closed-loop system still enters the Ω region, for greater values of T, but still within the admissible control region.

4.7. Key-on control implementation

The experimental implementation of the Key-on controller over the real EMVA prototype requires the use of different subsystems, all of them aimed at conditioning the signals yielding a complete and performing functional block. The block diagram for Key-on controller on EMVA system is shown in Fig. 4.16. Here, some key components are:

- VE. Subsystem to estimate the valve velocity v from measures of position h.
- Key-on controller. Subsystem to compute control action u.

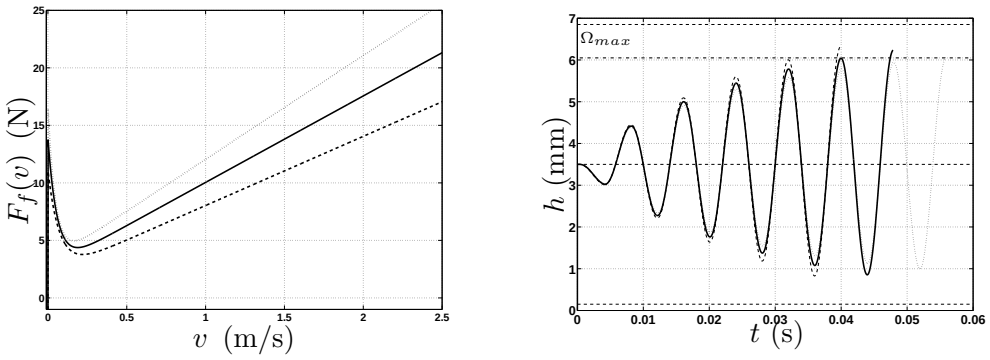

(a) (b)

Figure 4.15.: Simultaneous variation of ±20% in the friction parameters values (namely, σ, F_c, F_s, v_s). A variation of +20% corresponds to the dotted line, −20% to the dashed line, while the solid line corresponds to the nominal values. (a): Representation of the friction force $F_v(v)$. (b): Closed-loop valve trajectory when $\alpha = 22$ and $i_{max} = 12$ (A).

- Saturation block. Subsystem aimed at producing a saturated control action, based on the application of dynamics upper and lower limits according to (3.4).
- Force to Current inversion algorithm. Subsystem to obtain both upper and lower desirable coil currents i_{udes} and i_{ldes}.
- Electrical power actuator. It is an external subsystem conformed by two electrical power converters, whose load is a magnetic coil respectively. This subsystem is named Current Controller Circuit (CCC), regarding that its main task is to track both reference currents, feeding on coils the equivalent coil current to reproduce accurately the desired magnetic force, to then exert it on EMVA ferromagnetic armature.
- EMVA plant. Mechanical part of EMVA system.

Based on the hardware described in Sec. 3.2, the Key-on controller described in Sec. 4.3 is implemented digitally by using the functional block schemes shown in Fig. 4.16, while the sampling time of control task is set to 70 (μs).

Key-on control law requires the use of both state variables, and since the velocity of the armature is not available a proper Velocity Estimator (VE) system has to be used to reconstruct the velocity signal. Since there exists only measures of the position signal h, a velocity estimator (block VE) is proposed to estimate the valve velocity $\hat{v}$ from position h. Velocity estimator plays one important role on system performance and it must provide a good representation of real valve velocity v. It

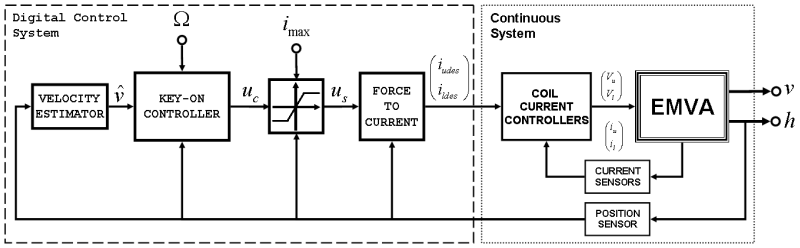

(a)

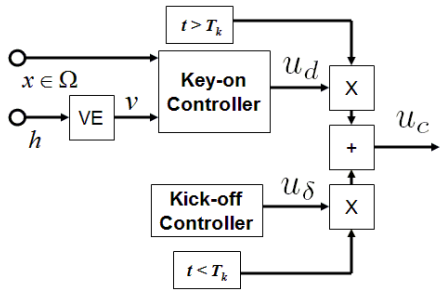

(b)

Figure 4.16.: Schematics of Key-on control implementation: a) Key-on controller scheme; b) Further details.

could be implemented by the simple difference between samples [77]:

$$\hat{v} \cong v_i \simeq= \frac{h_{i+1} - h_i}{T_s}, \tag{4.12}$$

with T_s being the sample time and i the i-th sample. However, due to the presence of noise in position signal, this simple method is a catastrophic solution. Well, regarding the frequency response, the goal is to obtain the frequency response equivalent to derivative operator $\frac{d}{dt} \rightarrow s = jw$. To this aim, a filter to estimate velocity is proposed, where its magnitude response must be linear at least for the frequency range of interest, with a phase response in the neighborhood around 90 degrees. Then, velocity filter is given by:

$$\begin{aligned} G(s) &= \frac{s}{\prod_{i=1}^{n} (1+s\tau_i)} \\ \tau_1 &= \frac{1}{2\pi f_c} \quad \tau_i = a_i \tau_1 \text{ for } i = 2 \dots n \end{aligned} \tag{4.13}$$

where:

$a_i \in]0; 1]$ is a factor to weight the main pole of the filter, $a_i = 0.25$ and $n = 4$ is the order of the filter; $f_c = 1000[Hz]$ is the cut frequency, chosen under the consideration of bandwidth of EMVA dynamic is around $BW \simeq 128[Hz]$. The frequency response (Amplitude and phase) for velocity filter is shown in Fig. 4.17, where dotted line

corresponds to the response of continuous time transfer function $G(s)$ and solid line to the discrete one, say $G(z)$, which is obtained via Tustin approach with $T_s = 70\mu s$ as sample time.

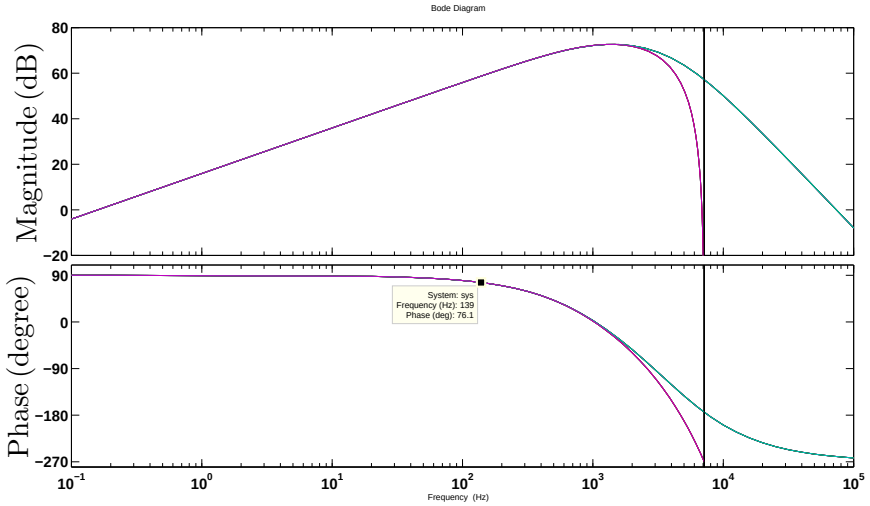

Figure 4.17.: Frequency response for filter to estimate velocity.

Unfortunately, this approach to estimate the valve velocity, introduces an undesirable effect, that is, the estimated velocity $\hat{v}$ is not totally in a phase of 90^o degree with respect to the actual valve position. For instance, given the free oscillation of EMVA system, an estimate of its velocity using versions (continuous and discrete) of the proposed filter is shown in Fig. 4.18. Hence, the estimated velocity $\hat{v}$ presents a delay of 0.5160(ms) respect to actual one v, yielding an uncertainty in the velocity value. The effect of filter is shown in Fig. 4.18. Assuming that $\hat{v} \cong v$, in what follows, valve velocity is referred with v.

Due to the use of VE filter, there exists unavoidable noise and delays, which are introduced in the closed-loop system along the velocity channel. There exists a trade-off between rejected noise band width and delay in the signal. Obviously, different approaches, like for example the use of a linear (non-linear) state observer, are also possible, and here in order to keep the control structure as simple as possible, velocity filter is used. Experimental results confirm that this simple filtering choice does not affect the overall performance of the controller.

Note that the presence of the 'sgn' function in the control law (4.10) introduces high switching frequency due to the unavoidable presence of noise in the estimate of the velocity signal. To reduce high frequency switching, the control law has been implemented through a predetermined dead zone function, f_{dz}, instead of the signum

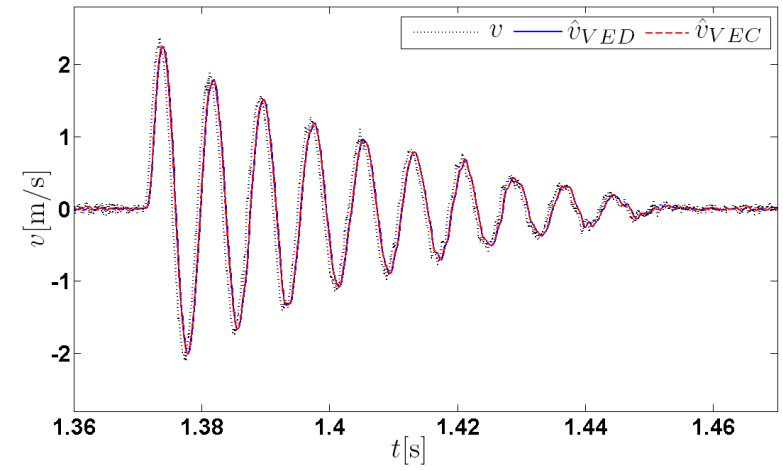

(a)

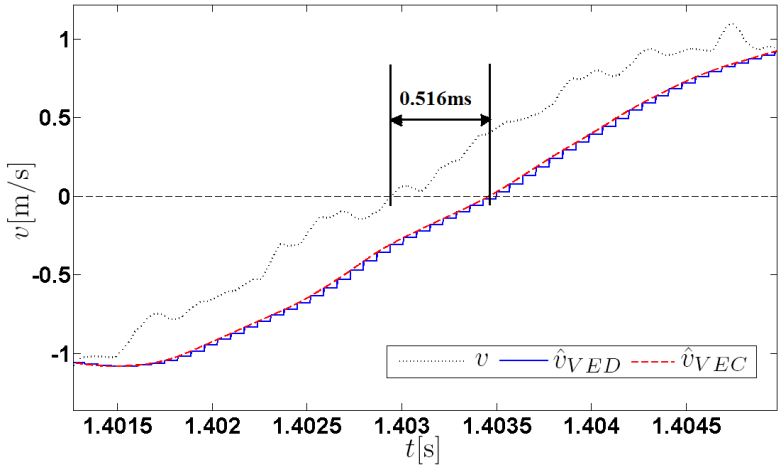

(b)

Figure 4.18.: Comparison of velocity estimators, media filter (Anticausal filter)(v), continuous ($\hat{v}_{VEC}$) and discrete ($\hat{v}_{VED}$) versions of filter (4.13): a) Velocity estimators time response; b) Enlarged zone to evaluate delay effect on estimated velocity.

nonlinearity, i.e.

$$u_d(v, \alpha, v_n) = \alpha f_{dz}(v, v_n), \tag{4.14}$$

with

$$f_{dz}(v, v_n) = \begin{cases} -1 & \text{if } v < -v_n, \\ 0 & \text{if } |v| < v_n, \\ 1 & \text{if } v > v_n, \end{cases} \tag{4.15}$$

where the amplitude of the dead zone, $v_n = 0.09$ (m/s), has been set according to the experimental evaluation of the level of noise in the velocity signal around the zero value.

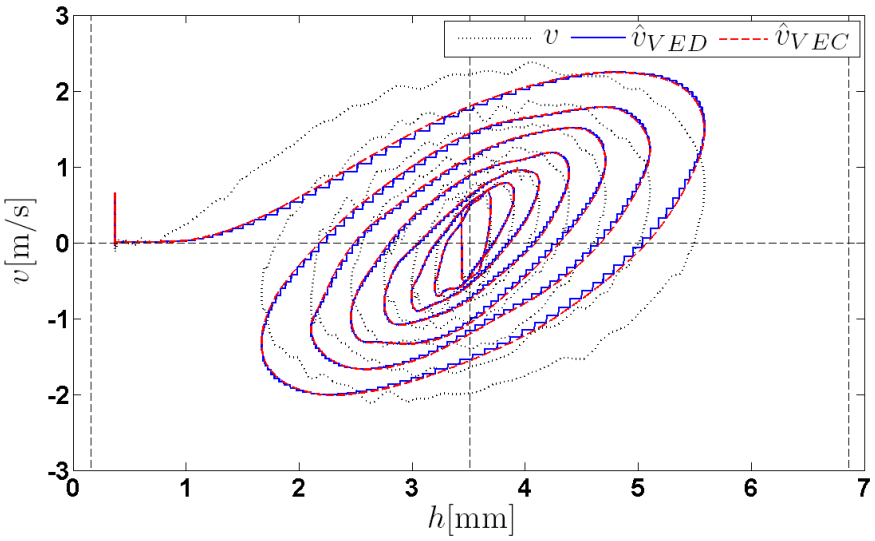

Figure 4.19.: Velocity estimator, a comparison Media filter (Anticausal filter)(v), Continuous ($\hat{v}_{VEC}$) and discrete ($\hat{v}_{VED}$) versions of filter (4.13) Phase portrait effect.

Given that valve motion starts from its rest position ($x(0) = [h_{eq}\ 0]^T$), where $v \in [-v_n, v_n]$, the use of a dead-zone (4.14) requires an additional action to reach a velocity value greater than v_n. In practice, to solve this problem, a "kick-off" control action $u_\delta(t)$ defined by

$$u_\delta(t) = \begin{cases} -F_M(i_{max}, h(t)), & \text{if } 0 \le t \le \frac{T_\delta}{2}, \\ F_M(i_{max}, g_{max} - h(t)), & \text{if } \frac{T_\delta}{2} < t \le T_\delta, \\ 0, & \text{if } t > T_\delta \end{cases} \tag{4.16}$$

is added to the control variable u so as to activate the upper and lower coils only during a short time T_δ, with T_δ being appropriately selected according to the experimental behavior of the system so as to be sufficient for the activation of EMVA at key-on. Note that, in our experiments, kick-off control was performed over an interval $T_\delta = 8$ (ms).

4.8. Key-on: Experimental results

The experimental validation is split in two parts. Where the first experimental stage aims at validating the closed loop dynamics for EMVA system, which were revealed by the numerically closed loop bifurcation diagram, then the second stage consists on the experimental test and validation of the Key-on controller performance.

4.8.1. Experimental closed loop bifurcation diagram

Since in our approach the controller design strongly relies on the bifurcation diagram, in this section we experimentally validate our bifurcation analysis. Comparison results are reported in Fig. 4.20, where it is apparent that agreement between the numerical and the experimental bifurcations diagrams is remarkable despite the unavoidable presence of unmodelled dynamics (such as dissipative effects) or the influence of specific experimental conditions (for example, environment temperature). Specifically, the numerical and experimental diagram show the same qualitative dynamics, such as for example the coexistence of different solutions, with the experimental detection of all main bifurcations events.

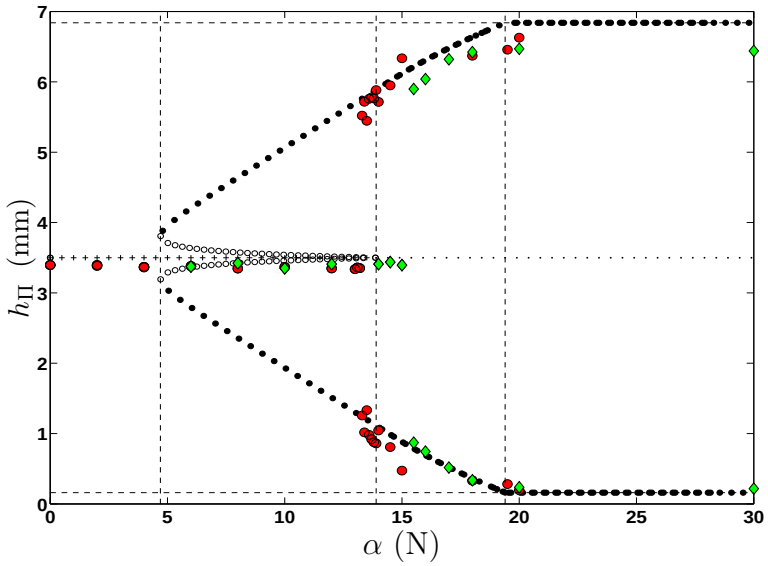

Figure 4.20.: Experimental validation of closed loop bifurcation diagram. Green markers refer to experimental results obtained varying α forward, from 0 N till 30 N and starting from the release state, while the red ones correspond to the case when valve starts near the close position ($h(0) = 1$ (mm) and $v(0) < 0$ (m/s)) and α was varied backward from 30 N till 0N.

Note that experiments necessary to build the bifurcations diagram were performed starting the valve from different initial conditions, namely from the release state ($h \simeq h_{eq}$) or around valve closing ($h \simeq 1$ (mm)). The steady state position of the armature has been measured for different values of α and samples have been plotted on the numerical diagram to compare the experimental behavior of the device with the model predictions. In so doing the different stable solutions, characterized by different basins of attraction, have been experimentally detected. Specifically, the

comparison between the experimental closed-loop bifurcation diagram and model prediction one is shown in Fig. 4.20.

4.8.2. Experimental Equilibrium Set

To complement the bifurcation analysis, some representative experimental trajectories are reported here for the sake of completeness. Namely, in Fig. 4.21 it is shown that for a value of α belonging to Region I, i.e. $\alpha = 2$N, the valve converges to the equilibrium set as predicted from the numerical analysis. The augmented plot of the steady state behavior in Fig. 4.21(b) allows to clearly observe the different equilibrium values attained experimentally by the valve when it starts from different initial conditions.

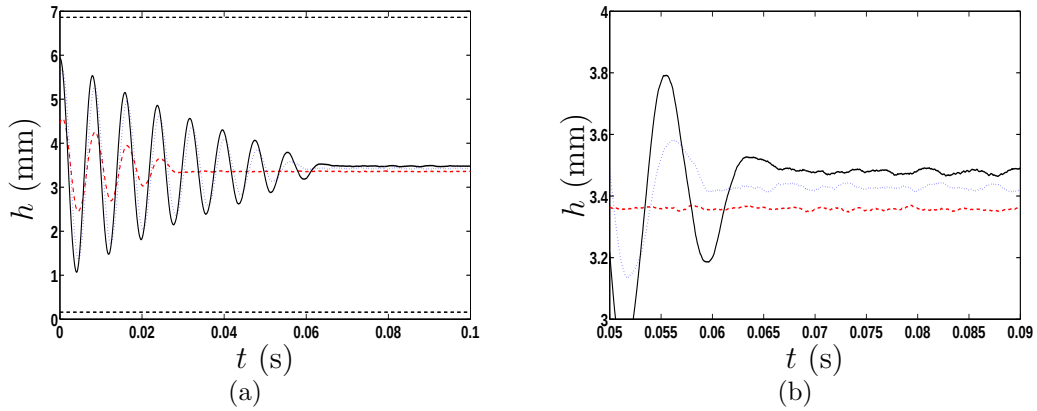

Figure 4.21.: Experimental evidence of the equilibrium set for $\alpha = 2$ (N). (a): time history of the valve position; (b): detail of the steady state.

4.8.3. Limit cycles

Fig. 4.22 shows examples of the experimental behavior of the valve position when the control parameter α belongs to Regions II and III of the bifurcation diagram. In particular, as predicted by the numerical analysis, it is evident that the amplitude of the stable limit cycle grows as α increases (see Figs. 4.22(a)-4.22(c) and 4.22(b)-4.22(d)).

For a greater value of α a grazing bifurcation is experimentally detected and reported in Figs. 4.22(e)-4.22(f). Here the orbit grazes the lower constraint ($h = h_{min}$) with a zero velocity. (Note that experimentally this velocity value is almost zero, due to the unavoidable presence of noise in the velocity signal estimated on line from position measurements.

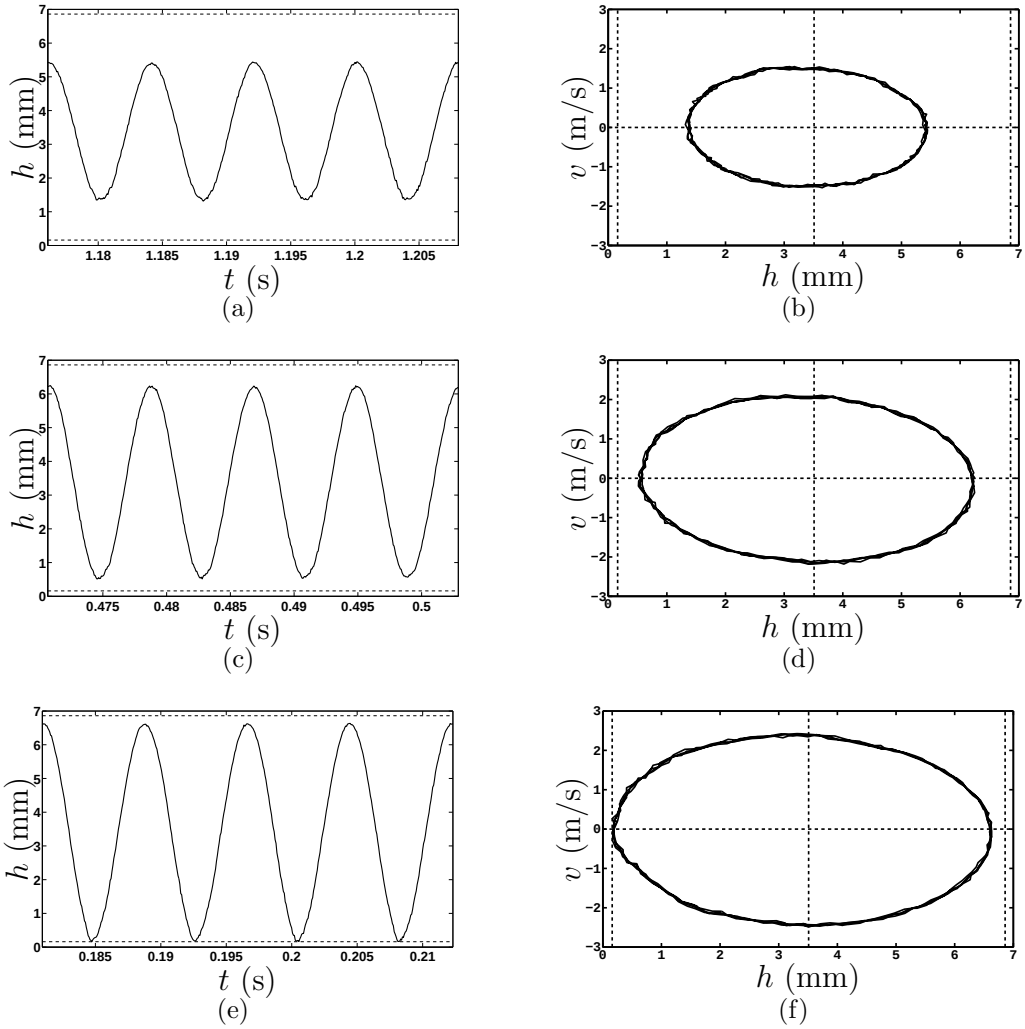

Figure 4.22.: Experimental results in region II and III. Time history of the valve position and phase portrait: a)-b) $\alpha = 13.5$ (N); c)-d) $\alpha = 15$ (N); e)-f): $\alpha = 20$ (N).

Although it is not possible to detect experimentally the presence of unstable solutions, the coexistence of the stable limit cycle, the unstable limit cycle and the equilibrium set can be validated when control gain α is fixed and system is started from different initial conditions. An example is shown in Fig. 4.23 where α is chosen equal to 14 (N) (Region II). Here the trajectory rooted at $x_0 = [2.5173\,(\text{mm}), -0.26888\,(\text{m/s})]^T$ (red solid line) converges to the fixed point, while the motion corresponding to the initial condition $x_0 = [2.4148(mm),\ -0.7182(m/s)]^T$ (black solid line) converges to the stable limit cycle. The unstable limit cycle exists in the white region shown in Fig. 4.23, which separates the basins of attraction of the equilibrium set and that one of the stable limit cycle.

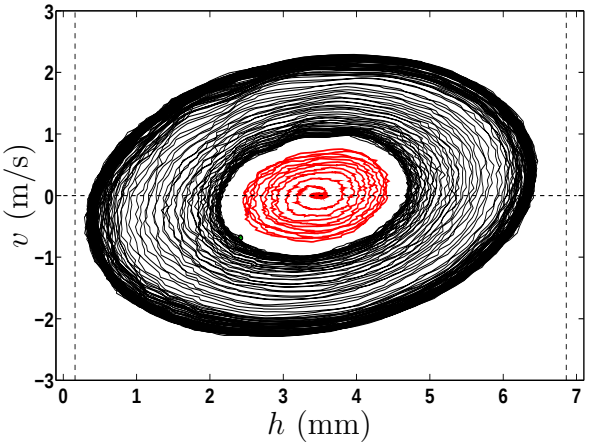

Figure 4.23.: Region II. $\alpha = 14$ (N). Experimental evidence of the coexistence of equilibrium set, stable and unstable limit cycle.

4.8.4. Validation of Key-on control performance

Despite chosen range for controller was set to be $\alpha \in [19, 22]$, different experiments were done in the tuned range $\alpha \in [16.25, 30]$ (see section 4.5). These experiments allow to validate the Key-on controller performance as Fig. 4.24 shows. From picture, it is clear that experimentally EMVA reaches the target region fulfillment the requirement on key-on control time T, for $\alpha > 18.75[N]$. Fig. 4.24 shows besides experimental data, the predicted Key-on time for different current values according with table 4.2, and note that data trend is between the level curve for $i_{max} = 18$A and $i_{max} = 9$A. Furthermore, according with numerical predictions as well as α is increased, the time T is reduced, allowing to reach the target region faster in less number of oscillations.

Conversely, the closed-loop experiments aimed at performing the catching manoeuver are carried out in the chosen control range through the use of bifurcation diagram as a tool to tune the controller. Indeed for $\alpha \in [19, 22]$, EMVA presents a proper performance according with numerical predictions. The motion of the valve is shown in Fig. 4.25 when $\alpha = 22$ (N). Here, the closed loop valve trajectory under the action of the Key-on control strategy is shown to effectively reach the desired Ω_{max} region (with $h_c = h^c_{max} = h_{max} - r_h$). Once the target region is reached (as it is also apparent from the experimental phase portrait depicted in Fig. 4.25(b)), the Key-on control is deactivated and a simple feed forward action is activated that switches on the upper coil while the lower coil is switched off in order to catch the valve. The Ω region, located near the open position ($h_c = 6.05$ (mm)), is reached for $T = 66.2$ms, being $x(T) = [6.17\,(\text{mm}), 0.07\,(\text{m/s})]^T$, while the overall valve closing is performed

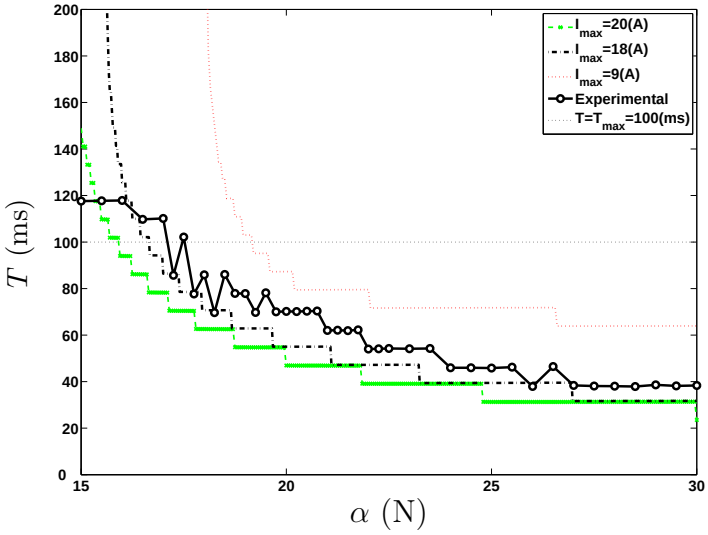

Figure 4.24.: Validation of key-on control performance. The experimental key-on time T (dotted samples) is validated with numerical one computed by simulations, when using different maximum admissible currents i_{max}

in 70.2 ms, within the control specifications as picture 4.25(a) shows.

The time evolution of upper and lower currents can be found in Figs. 4.26(b) and 4.26(a) respectively. Here the dotted line corresponds to the desirable current predicted by simulations, while the continuous line is the current effectively produced by power actuators. It is apparent that, as time increases, the actuator capacity to deliver power is reduced, but, despite this, the control action still guarantees the required performance.

The overall control effort is represented in Fig. 4.27, where the dotted line refers to the upper and lower dynamic bounds u_{max} and u_{min} respectively, for control signal u (see Eqs. (4.10) and (3.4)), while the solid line is the actual u.

It is worth mentioning here that, the experimental key-on control seems to be robust and fulfills the control specifications guaranteeing a closed-loop dynamic behavior that remarkably agrees with the one predicted by the numerical analysis. This is achieved despite the presence of dynamic saturations of the control actuator (considered ideal during the design), the unmodelled dynamics (such as the ones of the dynamic filter used to reconstruct the velocity from the position information), the presence of non smooth nonlinearities (the dead zone necessary for the implementation of the control action, as detailed in Sec. 4.7), and the presence of both noise and parameter uncertainties.

We remark that, for a choice of α which is out of the tuning range with $i_{max} = 18$ (A),

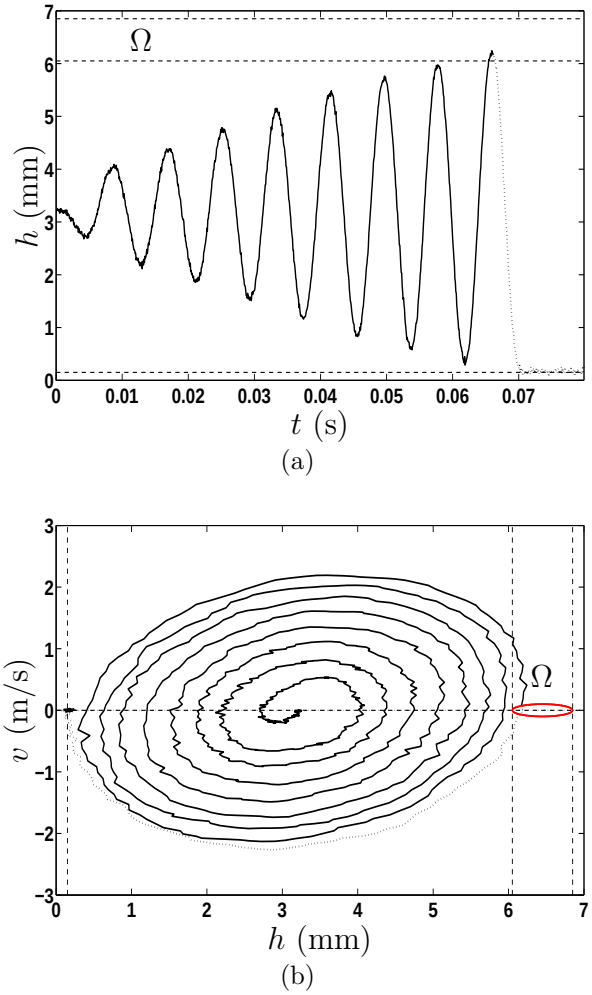

Figure 4.25.: Experimental validation of the key on control when $\alpha = 22$ (N). (a): Time history of the valve position; (b): phase portrait

the key-on problem is again, as expected, successfully solved and the first catching is guaranteed, but for greater values of the key-on and catching time interval that do not fulfill the control specifications. For example, for $\alpha = 17$ (N) the key-on time is $T = 114$ [ms] with an overall catching time of 117.7 [ms].

4.9. Discussion

This chapter has presented the analysis and design of the Key-on controller to solve the first lift manoeuvre in a double magnet EMVA system.

The proposed nonlinear controller was designed based on Lyapunov 's direct method, it makes destabilize EMVA system allowing perform the first lift operation in a robust way by pumping energy into the system through the proper compensation of

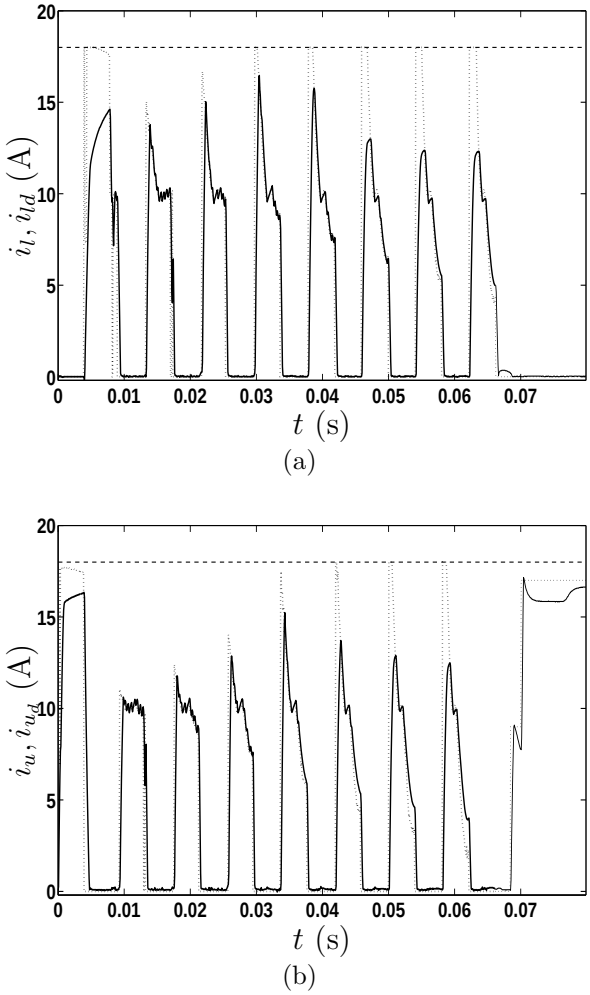

Figure 4.26.: Experimental validation of the key on control when $\alpha = 22(N)$: (a) time history of the lower current (solid line: actual current; dotted line: reference current); (b) time history of the upper current (solid line: actual current: dotted line reference current). Here, the dashed line refers to $i = i_{max} = 18$ (A).

energy losses due to friction.

The analysis of closed-loop nonlinear dynamics and induced bifurcation phenomena were characterized analytically, numerically and moreover tested experimentally. Saddle Node bifurcation of Cycles and Subcritical Hopf bifurcation have been characterized by means of a describing function analysis for a nonlinearity of the type Stribeck. Furthermore, the existence of the induced equilibrium set was characterized in the context of Fillipov systems.

Bifurcation analysis was used as a tool to tune the key-on controller, whose effectiveness and performance was verified directly in the experimental prototype. In the

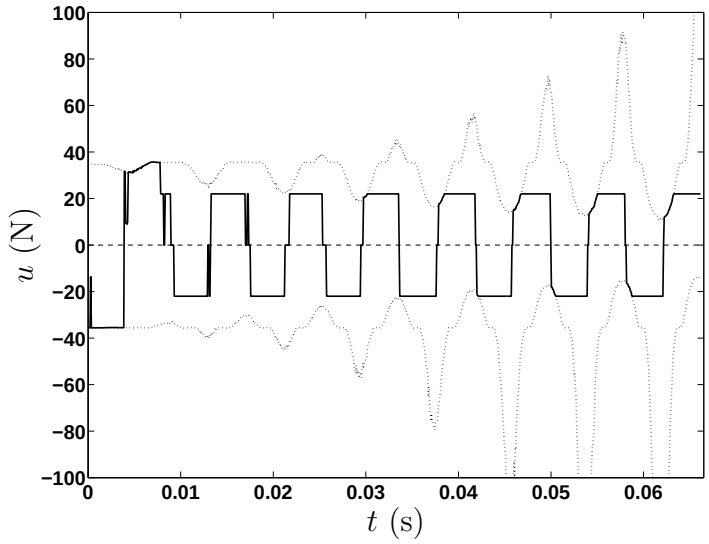

Figure 4.27.: Experimental validation of the key on control when $\alpha = 22$ (N). Time history of the control signal. Dotted line: upper and lower dynamic bounds u_{max} and u_{min} respectively. Solid line: the saturated control signal u_s.

chosen range, say $\alpha \in [19, 22]$, the Key-on controller was tested experimentally in a good agreement with theoretical predictions and the more important reaching the control goal while satisfying application requirements.

We wish to remark that despite undesirable effects of real scenarios such as: measure uncertainty and noise; lack of velocity sensor to make a good representation of valve velocity, which yields loss of information due to unmodelled dynamics of filter to estimate velocity; dead-zone used to avoid high switching frequency due to noise; tracking error of electrical power actuator to provide the desirable currents; parameter variation of friction force model, effects that we did not consider during simulation process and based on the good accuracy of numerical model for electromagnetic actuator, we can observe that the experimental behaviour of EMVA controlled by the proposed key on control agrees acceptable with theoretical and numerical analysis, allowing drive the valve within specifications.

CHAPTER 5

SOFT LANDING CONTROL

> Quanto più ci innalziamo,
> tanto più piccoli sembriamo a
> quelli che non possono volare.
>
> *(Nietzsche (1844-1900))*

This chapter deals with the Soft Landing Control (SLC) problem for the double magnet Electro Mechanical Valve Actuator (EMVA) described in Sec. 2. An introduction to SLC is presented in Sec. 5.1, while Sec. 5.2 defines the SLC control problem and states the control goal. Control design is based on the tracking of a model based reference trajectory, whose derivation is described in Sec. 5.3. Sec. 5.4 proposes a robust nonlinear control scheme to track the reference trajectory while solving the SLC control problem. Numerical results are shown in Sec. 5.5, while a robustness analysis against bounded disturbances are studied numerically in Sec. 5.6. A discussion is in Sec. 5.7.

5.1. Introduction

The EMVA system is considered as an essential actuator for future camless engines [112], and it was shown in Chapter 2 that soft-landing is a cumbersome problem to be solved in order to render robust this actuator, while reducing impacts (see Sec. 2.4.2). In general, several mechanical systems require to perform soft landing opera-

tions in constrained scenarios, where possible and undesirable impacting behaviour can occur due to the existence of bounds in valve motion. Representative examples are: aircraft landing during take off [20, 70–72]; clutch system [40, 49, 53, 64, 87]; moon lander system [76, 85]; container crane [12, 74, 113] and autonomous flight of unmanned helicopter [75, 116].

As it was shown in Chapters 2 and 3, EMVA system motion is constrained between two magnets and the aim of this actuator is to open and close the valve in a reliable, safety and robust manner, and for that purpose a Soft Landing Control (SLC) law is necessary to drive and catch the armature. However, strong impacts can, in general, occur at the end-stroke during opening and closing operations. Thus, it is necessary to seat the valve softly, that is, the valve velocity has to be reduced to a minimum just before it contacts the face of the electromagnet. This operation is necessary mainly to ensure a proper closing and opening of the valve while guaranteeing reliable functionality and a longer component life [21, 37, 44, 84, 94, 129]. Further benefits of SLC are noise reduction and the avoidance of wear and fatigue of components.

Considering the EMVA working principle, in the absence of external forces, the system initially rests at the nominal middle position (3.2), and during engine running the motion from open to close condition and viceversa can be easily imparted by using the stored energy in the springs. Thus, enough acceleration has to be applied through the magnetic force in order to drive the valve in the proper way, so as to reduce the impacting velocity, while ensuring the valve capture. In so doing, the key control actions consist in accelerating and/or braking the system.

First attempts to solve SLC are described in [50, 125, 134], where the system is controlled in open loop via a series of properly tuned current patterns. Since open loop control is sensitive to disturbances and suffers from poor repeatability, closed loop strategies have been also extensively used on the basis of different EMVA modeling, where SLC manoeuvre is developed in two phases, namely approaching and tracking. In so doing, the control action only starts after a position threshold has been reached by the valve. In [124, 125] a feedforward and Linear-Quadratic Regulator feedback controller was developed to control the system for soft seating, while Flatness-Based tracking method is adopted in [21] in order to perform SLC while ensuring the compensation of the combustion gas force disturbances, affecting the exhaust valve solenoid actuators. In [44], based on nonlinear force model reproduced via proper tuned polynomials, a sensorless sliding mode control strategy was used to track a reference trajectory designed for the soft-landing, whereas in [123] the quiet seating control is designed based on a linearized model of EMVA and through

a robust controller via H_∞ loop shaping method for stabilizing the actuator. In [67], a simplified nonlinear model was used to design an exact linearization based control law. In the same way, in [37] the control task was solved via a model-based decoupling control strategies and by using also a full cancelation of vector field components (feedforward controller) based on a linear mechanical model, furthermore, a PD controller was used to make the system track a reference trajectory, which was described through a third order system.

Different control strategies aimed at enhancing the SLC performance have been presented in technical literature [63, 104, 129], where the improvement mechanism is based on Iterative Learning Controller (ILC). In particular, in [63] a tracking controller that consists of a linear feedback and a nonsquare ILC was presented, where the ILC methodology was used to update the feedforward signal of the feedback controller every cycle based on the error between the actual valve position and the desired position; in [104], the SLC is addressed using a nonlinear feedback strategy, where control parameters were tuned by means of an extremum seeking method; while recently in [129], a cycle adaptive feedforward approach was used to solve the control problem.

In [52], different control approaches are shown aimed at controlling systems with input and output constraints, where common constraints from real industrial process are addressed. In the same context, in [94] a heuristic technique is proposed to compute the coil current to soft-land the valve, while avoiding saturation. The control law is based on a cyclic adaptive current preaction combined with a sliding surface.

Despite efforts done by researchers, there are still challenging open problems to be addressed during SLC manoeuvre, whose solution is presented in this Chapter. Here a force control law is designed to track a model based optimal reference trajectory and is based on a combined feedforward and Sliding Mode Controller. The control objective is to render the system robust and reliable so as to be used in the next generation of engines (Camless engines).

5.2. SLC Problem statement

Although the EMVA system is a small mechanical device, in order to satisfy engine performance specifications at high speed, i.e. 6000 (rpm), the closing and opening manoeuvres must be done in a short total landing time, say $T_{TL} < 4$ (ms) [50]. Considering the system structure, by applying a magnetic force (coil current), both

end stroke points are located in the basin of attraction of an attractive point located at the boundary, where the valve velocity grows as well as the valve approaches the boundary, leading to the acceleration of the valve, while increasing its impact velocity. Furthermore, due to the bounded nonlinear magnetic force interacting with the high elastic force, there exists a repulsive point (close to the boundary) between two equilibria (located at the boundary and near to middle position, respectively). Then, the two ending points have to be transformed into attractive equilibria through the proper regulation of the magnetic force.

One of the main control issues of EMVA system lies on the nonlinear response and weak capability of magnetic actuator, that can fail to overcome the increasing and strong elastic force exerted by the springs, as the valve approaches the magnetic coil. This interaction leads to execute a landing manoeuver around an unstable point, where valve can easily point towards the middle position instead of the boundary (loss of the valve without his capture). Indeed, the controllability of the valve can be seriously affected by impacting phenomena, where an acceptable final velocity reported in literature is less than 0.1(m/s). It is important to remark that even the presence of low intensity impacts, could transfer the valve from the attractive to the repulsive zone, causing the loss of the valve. Finally, besides nonlinearity effects, in order to ensure the proper valve opening and closure, the controller must properly take into account that system can strongly be affected by time variant nonlinear friction and external forces. Therefore, the controller must be designed seeking a robust performance with respect to possible system disturbances, model uncertainties, and friction (parameters) variation in general.

The SLC manoeuver involving a nonlinear system subject to a set of constraints, where control must be designed for low energy consumption while satisfying a soft landing operation with low impact velocities within a desired range $[0,v_d]$, i.e. $v_d = 0.1$ (m/s), while taking into account the existence of strong nonlinearities and bounds on actuators authority. Further issues involve the special case where no full state measures are available and external disturbances are present (i.e. gas pressure external force).

5.2.1. Problem definition

The EMVA model (3.1) with initial conditions $[h_0\ v_0]^T$ and the bounds for control input (3.4) can be written in the form:

$$m\ddot{h} + F_e(h;k,h_{eq}) + F_f(v;\gamma) + F_{ext}(t) = u, \quad h(0) = h_0, \dot{h}(0) = v_0, t \in T_L, \quad (5.1)$$

where u is the bounded control variable available to designers, i.e. for opening $0 \leq u \leq u_{max}(g_{max} - h)$ and for closing $-u_{max}(h) \leq u \leq 0$, with $u_{max}(z) = F_M(i_{max}, z)$; $h_0 \neq 0$ and v_0 are the initial condition; $T_L = [t_s, t_i]$ is the interval of time to carry out the landing manoeuver, with t_s and t_i being the starting and ending time, respectively. Let $\nu = \{m, k, h_{eq}, \sigma, F_s, F_c, v_s\}$ be the set of all plant parameters and $\gamma = \{\sigma, F_s, F_c, v_s\}$ be the parameters of the friction force model (3.3).

Furthermore, let $x := [h\ v]^T$ be the state vector and $x_0 := [h_0\ v_0]^T \in \mathbb{R}^2$ the initial state. Moreover, define $S := \{(x_1, x_2) \in R^2 | x_1 = h_d, x_2 \in [a, b]\}$, and let x_d be a generic point in S. Additionally, let t_c be the time instant when the control is switched off, i.e the valve position has reached a constant position threshold, say h_c. Now, let's $x_c = [h_c\ v_c]^T = x(t_c)$ be the state at time t_c, with $v_c \triangleq v(t_c)$ being the final control velocity. Define also $v_i \triangleq v(t_i)$ as the impacting velocity, where t_i is the time instant at which the impacting event occurs. Without loss of generality, we assume $t_s < t_c < t_i$. Finally, let $T_{LT} = t_i - t_s$ be the total landing time and T_{LT}^{max} be the maximum admissible total landing time.

The softlanding control problem is to find a feedback control law $u(t) = u(x, x_0, t)$ *for system* (5.1)*, that starting at* x_0 *yields*

$$x(t) \in \mathfrak{I}(x_d) \qquad as \qquad t \to t_i, \tag{5.2}$$

with $\mathfrak{I}(x_d)$ *being a sufficient small neighborhood of* x_d*, subject to:*

$$\begin{aligned} &h_{min} < h(t) < h_{max}, && \forall\, t \in T_L, \\ &|v_i| \leq 0.1 (m/s), \\ &T_{LT} < T_{LT}^{max}, \\ &i_j \in [0, i_{max}], && j = \{u, l\}, \end{aligned} \tag{5.3}$$

where i_u *and* i_l *are the upper and lower coil currents, respectively, and* i_{max} *is the maximum admissible value of coil currents provided by the actuators.*

The complete SLC manoeuver is developed in three different control stages namely:

i : RELEASE phase. Control action $u = 0$, yielding null lower (upper) coil current, thus system evolves in free oscillation pulled by springs due to the potential energy stored in them.

ii : SLC phase. By using the decoupling approach [37], the control signal u, desired force in (N), is computed through a SLC force control, so that the equivalent upper coil current i_u is computed via an inversion force model, that is, $i_u =$

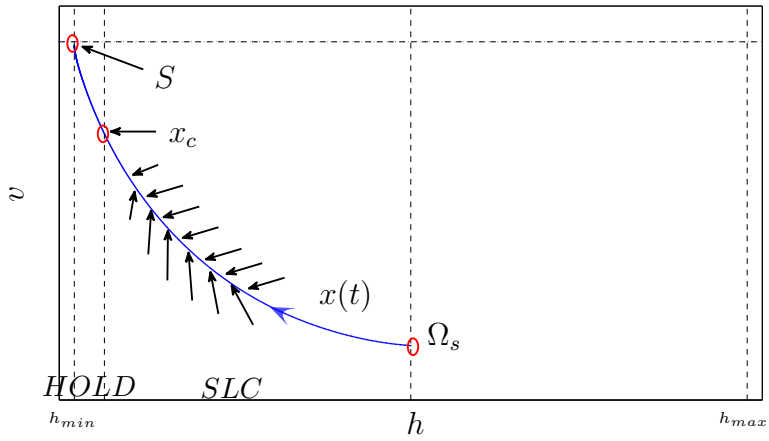

(a)

Figure 5.1.: Schematics for SLC control problem.

$F_M^{-1}(h, u, i_{max})$, where F_M^{-1} denotes the inversion force model for (3.5).

iii : HOLD phase: Once the system overcome certain threshold, say h_c upper current i_u is hold to a holding current value, say i_{uhold}, where system is accelerated and caught by electromagnet to close definitely the valve.

5.3. Model-based trajectory planning

Softlanding control for EMVA system has to be performed in a constrained space where dynamics are strongly nonlinear with bounded control authority and the manoeuver must be carried out in a short interval of time, i.e. $3-4$ (ms) [50, 104], due to engine operation requirements. The soft landing operation cannot be executed solely by using feedback or adaptive control schemes. As a result, we decided to use a feedforward control action computed on the basis of an accurate mathematical model of the system together with a feedback stabilizing controller.

Reference trajectory planning has been designed and utilized to land the valve by different authors [37, 44, 63, 104, 123, 124, 136], where the aim is to obtain a reference trajectory characterized by being a smooth continuation of the natural valve motion. In the case of the EMVA, reference model must include both mechanical and magneto dynamics, in order to take into account also the nonlinear magnetic force features. The advantage of using the EMVA nominal model as a trajectory planner lies in the possibility of designing an ad hoc trajectory taking into account the natural evolution of the model and the actuator nonlinearities. We seek to obtain an optimal current

pattern, so that the trajectory generator produces an optimal trajectory that fulfills SLC requirements in both time and state constraints. Here, a nominal model of the mechanical system and for magnetic force is used in order to calculate a suitable reference trajectory.

The optimal trajectory planning consists in optimizing the current pattern as shown in Fig. 5.2(a), while trajectory satisfies predefined specifications. This current pattern is predefined considering physical constraint of electrical power actuator, that is, ensuring continuous current that starts from zero. This requirement is imposed because, if there exists a discontinuity on current, in the real experiment cannot be performed. The idea behind this current pattern is to energize the coil (inductor) starting from zero and growing with a constant slope until a certain optimal saturation value say i_s, is reached. The current level is then kept constant at this value for $t > T_{rs}$ (see Fig. 5.2(a)).

With the aim of considering the nonlinear magnetic force (3.5) and mechanical dynamics (3.1) in the trajectory planner, the reference system is given by:

$$\begin{aligned} &\dot{h}_r = v_r, \\ &\dot{v}_r = \tfrac{1}{\hat{m}}\left(-\hat{k}(h_r - \hat{h}_{eq}) - F_f(v_r;\hat{\gamma}) + u_M(i_r(t), h_r)\right), \end{aligned} \quad h_r(0) = \hat{h}_{eq}, v_r(0) = v_{eq}, \tag{5.4}$$

where h_r(m) is the reference position and v_r(m/s) is the reference velocity; $\hat{m}$ is the nominal mass of the system, $\hat{k}$ is the nominal spring stiffness, $\hat{h}_{eq}$ is the central position of valve stroke, $\hat{\gamma}$ is the nominal parameter vector of the friction force model (3.3); $h_r(0) = \hat{h}_{eq}$ and $v_r(0) = v_{eq}$ are the initial conditions for position and velocity respectively, with $v_{eq} = v(t_s)$ being the valve velocity, evaluated when valve reaches h_{eq} when it starts from opening or closing valve condition, i.e. $h = h_{max,min}$; $u_M(i, z)$ is the magnetic force model (3.5), with z(m) being the air gap and i(A) the coil current. Furthermore, let us define the reference state vector $x_r = [h_r\, v_r]^T$.

The current $i_r(t)$ is a piecewise smooth current pattern shown in Fig. 5.2(a) and described by:

$$i_r(t; i_s, T_{rs}) = \begin{cases} \frac{i_s}{T_{rs}}t, & \text{if } t \in [0, T_{rs}], \\ i_s, & \text{if } t > T_{rs}, \end{cases} \qquad 0 < T_{rs} < T_{LT}, \tag{5.5}$$

where i_s (A) is the saturation current and T_{rs}(s) is a prefixed time value at which reference current $i_r(t)$ is saturated at value i_s. The block diagram for the proposed trajectory planner is shown in Fig. 5.2(b).

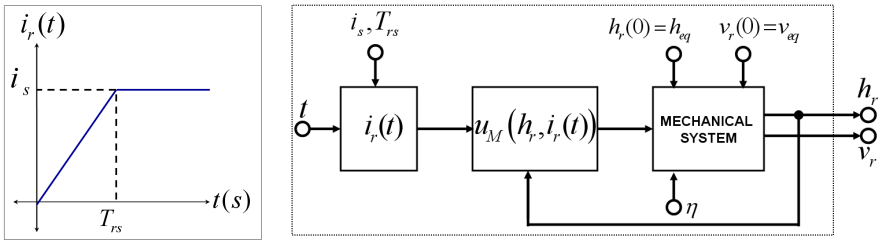

(a) (b)

Figure 5.2.: Trajectory planner for EMVA system: a) current pattern to be optimized by means of parameter i_s; b) schematics for model based reference trajectory planner

The optimal trajectory can be computed via an optimization routine aimed at obtaining the optimal value $i_s^\star$ for current $i_r(t)$ (5.5). Let us define h_{rd} (m) and v_{rd} (m/s) as the desired position and velocity threshold, respectively, t_f as the final time, and the index

$$J(i_s) = \int_0^{t_f} i_r(t; i_s, T_{rs})^2 dt, \tag{5.6}$$

as cost function, with parameter T_{rs} set as: $T_{rs} = 0.5 \cdot 10^{-3}$(s).

The optimal trajectory planning problem is to find

$$\overset{\star}{i_s} = \arg \min_{i_s} J(i_s), \tag{5.7}$$

subject to the system equations (5.4) are satisfied and

$$\begin{aligned} &h_{min} < h_r(t_f) < h_{eq}, \\ &-v_{rd} < v_r(t_f) < 0, \\ &0 < i_s < i_{max}, \\ &T_{rs} < t_f < t_{fmax}. \end{aligned} \tag{5.8}$$

The idea behind this cost function is to obtain a trajectory computed by using the nominal system dynamics, with initial conditions corresponding properly to the nominal model in free oscillation, when trajectory reaches the middle position h_{eq}, starting from end stroke, i.e at $h(0) = h_{max}$. Terminal state of optimal trajectory are expected to be around a desired coordinate $[h_{rd} v_{rd}]^T$ and the optimization problem is solved through numerical simulations by considering it as a nonlinear programming problem.

When the reference system is evaluated with values shown in Table 5.1 and i_s is

varied in the range $i_s \in [3, 11]$ (A), resultant reference trajectories are depicted in Fig. 5.3(b)-5.3(c). From results, it is clear that system can reach an equilibrium point in a levitation condition for low values less than 7, in particular for that condition, elastic force is equal to the applied magnetic force. Then, by increasing i_s, trajectories start to achieve a desired point with low velocities, and for bigger values of parameter i_s impact intensity starts to become stronger. Current pattern, time position evolution and phase portrait trajectories are shown in Fig. 5.3. Notice that all trajectories start at the same initial condition and as parameter i_s is varied terminal condition reaches different values. Considering nominal friction conditions, the optimal reference trajectory is obtained for $\overset{\star}{i}_s = 7.12(\text{A})$.

Table 5.1.: Nominal parameter values for EMVA reference model.

Symbol	Description	Value	Unit
$\hat{m}$	Mass	0.144	kg
$\hat{k}$	Spring stiffness	93773	N/m
$\hat{h}_{eq}$	Valve equilibrium	$3.5 \cdot 10^{-3}$	m
$\hat{\sigma}$	Viscous friction coefficient	7.5153	Ns/m
$\hat{F}_c$	Coulomb sliding friction force constant	2.5267	N
$\hat{F}_s$	Maximum static friction force constant	13.9	N
$\hat{v}_s$	Sliding velocity coefficient	17.315	m/s
$i_s^\star$	Optimal value for saturation current i_s	7.12	A
T_{rs}	ramp time	$0.5 \cdot 10^{-3}$	s
v_{rd}	Desired reference velocity	0.05	m/s
h_{rd}	Desired reference position	h_{min}	m

The resultant trajectory for nominal system (branch of friction is depicted in Fig. 5.4(a)), evolving in time is shown in Fig. 5.4(b). Furthermore, the magnetic force necessary to obtain that reference trajectory is shown in Fig. 5.4(c), this predicted force can serve as a feedforward control signal. The phase portrait for reference trajectory starting at $x_r(0)$ is depicted in Fig. 5.4(d).

We remark, that trajectory planning also aims at computing a feedforward control action in order to compensate the system dynamics under nominal operation conditions(see Fig. 5.4(c)). However, under perturbed dynamics conditions, this control is insufficient to compensate them and a feedforward control action has to provide the necessary control correction aimed at rejecting disturbances.

5.4. SLC Control Design

SLC controller is designed to produce a desired magnetic force u in (5.1) in order to control of EMVA system, and then a force to current transformation [37] is applied in order to obtain the final corresponding (desired) coil currents. Controller is designed

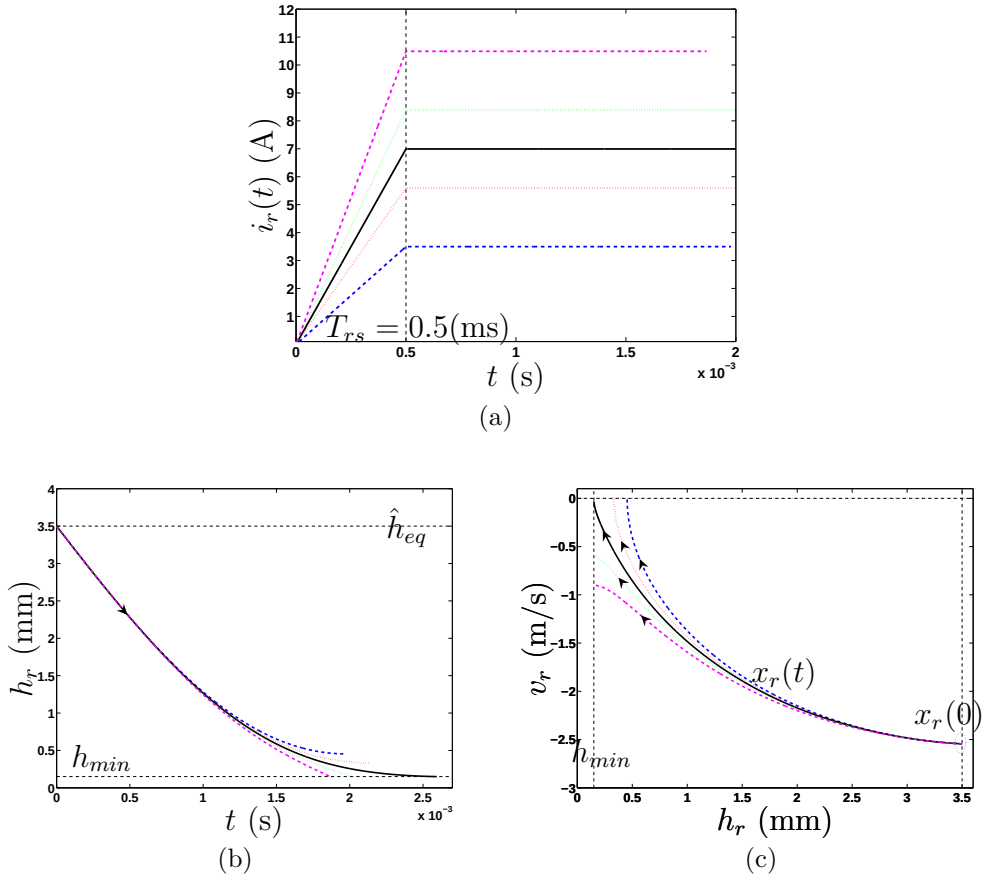

Figure 5.3.: Effect of parameter i_s on reference trajectory when nominal model parameters are used: a) current patterns for different values of i_s; b) time evolution for position in resultant trajectories; c) phase portrait for reference trajectories for each value of i_s.

and evaluated for closing stage (easily extended for opening as well), whose aim is to track the optimal trajectory (5.4).

Given the EMVA system (5.1), by defining the tracking error $e := x - x_r$ between system and reference trajectory obtained by (5.4) with nominal parameters $\hat{\nu}$, and by considering the time invariant surface:

$$s(e) := \dot{e} + \lambda e, \quad \lambda > 0, \tag{5.9}$$

a nonlinear control action u that satisfies SLC control specifications (5.8) can be derived as:

$$u(t) = u_M(i_r^\star(t), h_r(t); \hat{\nu}) + \hat{k}e + (\hat{\sigma} - \hat{m}\lambda)\dot{e} - \beta \mathrm{sgn}(s), \tag{5.10}$$

where $u_M(i_r^\star(t), h_r(t); \hat{\nu})$ in equation (5.4) is the model based magnetic force for

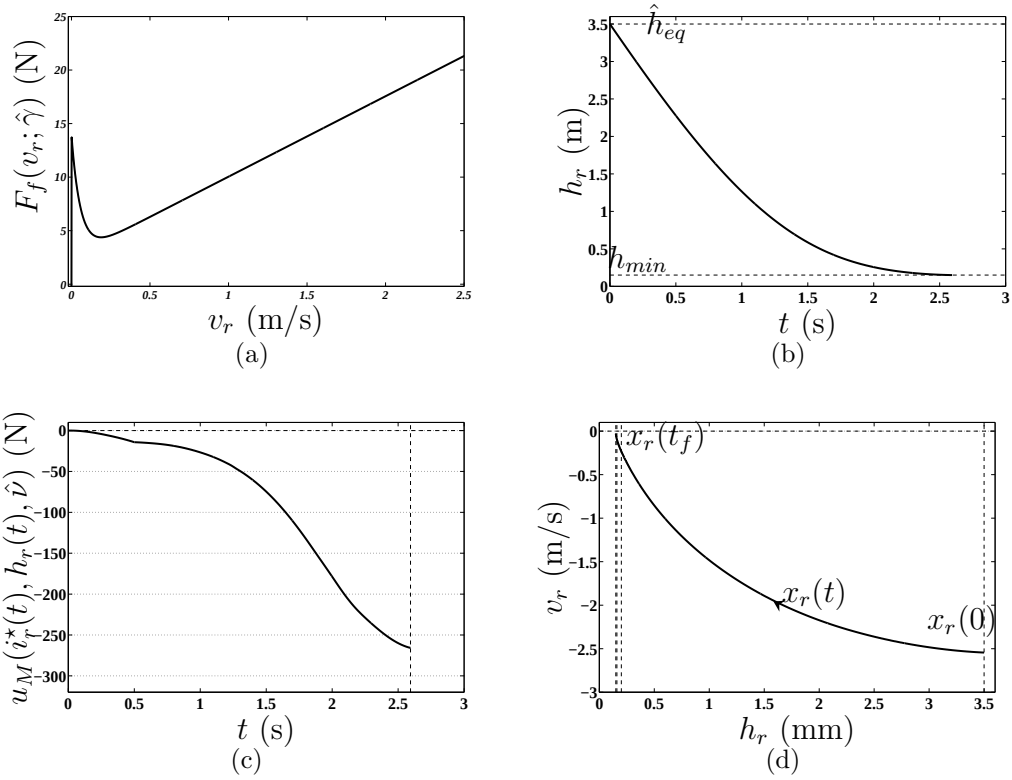

Figure 5.4.: Model based trajectory planning: a) friction force for $v_r > 0$ used to compute reference trajectory; b) time response for position of reference trajectory; c) magnetic force; d) phase portrait.

$i_s = i_s^\star$, used here as feedforward control action, and the remaining part is the feedback control law based on Sliding Mode Control approach [117, 131], with β being a large enough constant.

5.4.1. Control derivation

By rewriting the system (5.1) in the form:

$$m\ddot{h} + F_e(h; k, h_{eq}) + F_f(v; \gamma) + F_{ext}(t) = u_{ff}(t) + u_{fb}(t), \tag{5.11}$$

where u_{ff} and u_{fb} are assumed to be a feedforward and a feedback control actions, respectively.

By choosing as a feedforward control action u_{ff} the magnetic force required for the valve to evolve according to the optimal reference trajectory given by (5.4), we have that:

$$u_{ff}(t) = u_M(i_r^\star(t), h_r(t); \hat{\nu}). \tag{5.12}$$

where $i_r^\star(t)$ is the current profile (5.5) for $i_s = i_s^\star$.

Now, under the assumption that there exists some parameter uncertainties given by:

$$\nu = \hat{\nu} + \delta\nu,$$

where ν is the vector of parameters described in Sec. 5.2.1, and the $\delta\nu = \{\delta m, \delta k, \delta h_{eq}, \delta\sigma, \delta F_s, \delta F_c,$ is the set that collects all parameter uncertainties. By replacing (5.12) into (5.11) and considering the error $e = x - x_r$, and the error of initial conditions $e(0) = h(0) - h_r(0)$, $\dot{e}(0) = v(0) - v_r(0)$, error dynamics for EMVA system becomes:

$$m\ddot{e} + \sigma\dot{e} + ke - \Delta f(e, \dot{e}; \hat{\nu}, \delta\nu) = u_{fb}, \quad |\Delta f| < C, \tag{5.13}$$

where $\Delta f(e, \dot{e}; \hat{\nu}, \delta\nu) = -\delta m\ddot{h}_r(\hat{\nu}) - \delta\sigma\dot{h}_r(\hat{\nu}) - \delta k h_r(\hat{\nu}) + k\delta h_{eq} + \delta k\hat{h}_{eq} - F_{nl}(\dot{e} + \dot{h}_r(\hat{\nu}), \hat{\gamma} + \delta\gamma) + F_{nl}(\dot{h}_r(\hat{\nu}), \hat{\gamma}) - F_{ext}(t)$, with F_{nl} being the nonlinear part of friction force (3.3). Since Δf depends also on the error of the system and due to the nonlinear structure of some of its terms, there exists a coupling with the error dynamics, which can affect strongly the stability of entire system. In general, Δf can include different parameter disturbances, unmodeled dynamics and external disturbances, and for control design purposes, it is assumed to be bounded by certain constant C.

In so doing, the use of this control approach transforms the tracking control problem into a regulation control problem. By considering the sliding surface (5.9) and by defining

$$V(e) = \frac{1}{2}s^2, \quad V(0) = 0, V(e) > 0 \,\forall e \in R^2 - \{0\}, \tag{5.14}$$

as a Lyapunov like function for the closed loop system, whose derivative is:

$$\dot{V}(e) = \frac{1}{2}\frac{\partial}{\partial t}s^2 = s\dot{s}. \tag{5.15}$$

The best approximation for an equivalent continuous control action, namely u_{ec}, that allows to achieve $\dot{s} = 0$, is given by solving $\dot{s} = 0$ in (5.15). Indeed, under the assumption that system 's dynamics are known, that is, $\Delta f = 0$ in (5.13), and by replacing in:

$$\dot{s} = 0 \rightarrow \ddot{e} + \lambda\dot{e} = 0, \tag{5.16}$$

the equivalent control u_{ec} becomes:

$$u_{ec} = \hat{k}e + (\hat{\sigma} - \hat{m}\lambda)\dot{e}. \tag{5.17}$$

Generally speaking, dynamics of system are not exactly known, thus, there exists

an estimation error represented by the term Δf in the estimate of the model, which is assumed to be bounded

$$|\Delta f| < C. \tag{5.18}$$

Therefore, a discontinuous term is added to u_{ec} across the surface $s = 0$, so that:

$$u = u_{ec} - \beta \text{sgn}(s), \tag{5.19}$$

where *sgn* is the sign function:

$$\text{sgn}(s) = \begin{cases} +1, & \text{if } s > 0; \\ -1, & \text{if } s < 0. \end{cases} \tag{5.20}$$

Now, by choosing β in (5.19) to be large enough, and by combining equations (5.13), (5.19) and (5.9), it is possible to compute the derivative of the Lyapunov function (5.14), so that:

$$s\dot{s} = m^{-1}(\Delta f - \beta \text{sgn}(s))s = m^{-1}(\Delta f s - \beta |s|). \tag{5.21}$$

Now, by assuming $\beta = C + p$,

$$s\dot{s} = m^{-1}(\Delta f s - C|s| - p|s|) \leq m^{-1}(-p|s|), \tag{5.22}$$

Since $s\dot{s}$ (5.22) is definite negative from Lyapunov theory, it is possible to conclude that the origin $e = 0$ is a global stable equilibrium point and then the trajectory of the system tracks the trajectories of the reference model, towards surface $s(e)$.

The surface $s(e)$ becomes an invariant set, while allowing some disturbances or dynamic uncertainties, that can be tolerated due to excellent robustness properties of the sliding mode control, without destroying the invariant set properties of the surface (5.9).

5.4.2. Schematics of SLC controller

Control architecture based on feedforward and sliding mode control is depicted in Fig. 5.5, where it is assumed a perfect knowledge of state x of the system to implement the control scheme.

Note that dynamics of Coil Current Controller (CCC) subsystem (see Appendix A) are not taking into account during trajectory design in Sec. 5.3. As a result, such

Parameter	Value
λ	$4.5 \cdot 10^3$
β	35
ε	$5 \cdot 10^{-2}$

Table 5.2.: Parameters values for sliding mode controller

actuator dynamics becomes the first source of disturbance to be compensated by feedback controller.

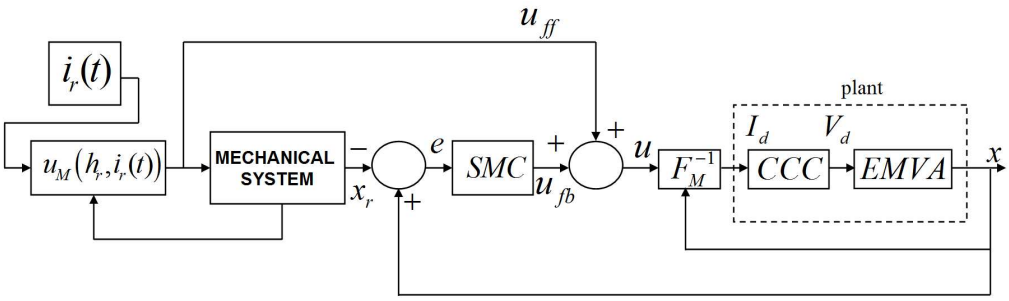

Figure 5.5.: Schematics of the Soft Landing Controller for EMVA system through model based Feedforward combined with Sliding Mode Control.

The discontinuous term in control u (5.10) can yield high switching frequency of actuators. This behaviour is not feasible during control implementation. Thus, in order to avoid such a high switching frequency, function $\text{sgn}(s)$ in (5.10) can be replaced by the function $\text{Sat}(\frac{s}{\varepsilon})$, defined by:

$$\text{Sat}(\frac{s}{\varepsilon}) = \begin{cases} \frac{s}{\varepsilon}, & \text{if } |s| < \varepsilon; \\ \text{sgn}(\frac{s}{\varepsilon}), & \text{if } |s| \geq \varepsilon, \end{cases} \tag{5.23}$$

where ε is a positive constant.

5.5. Results

The controller is tuned for nominal operation condition. Control parameter are given in Table 5.2.

As we referred previously, feedforward control action does not consider internal dynamics of subsystem CCC (electrical power actuator in Fig. (5.5)). Therefore it becomes the first source of uncertainty and it is worth to report that when only feedforward control is used, SLC fails. However, by applying the sliding mode feedback controller for nominal condition, valve is closed and the time evolution of the

valve state is depicted in Fig. 5.6, while control action and upper coil current are shown in Fig. 5.7.

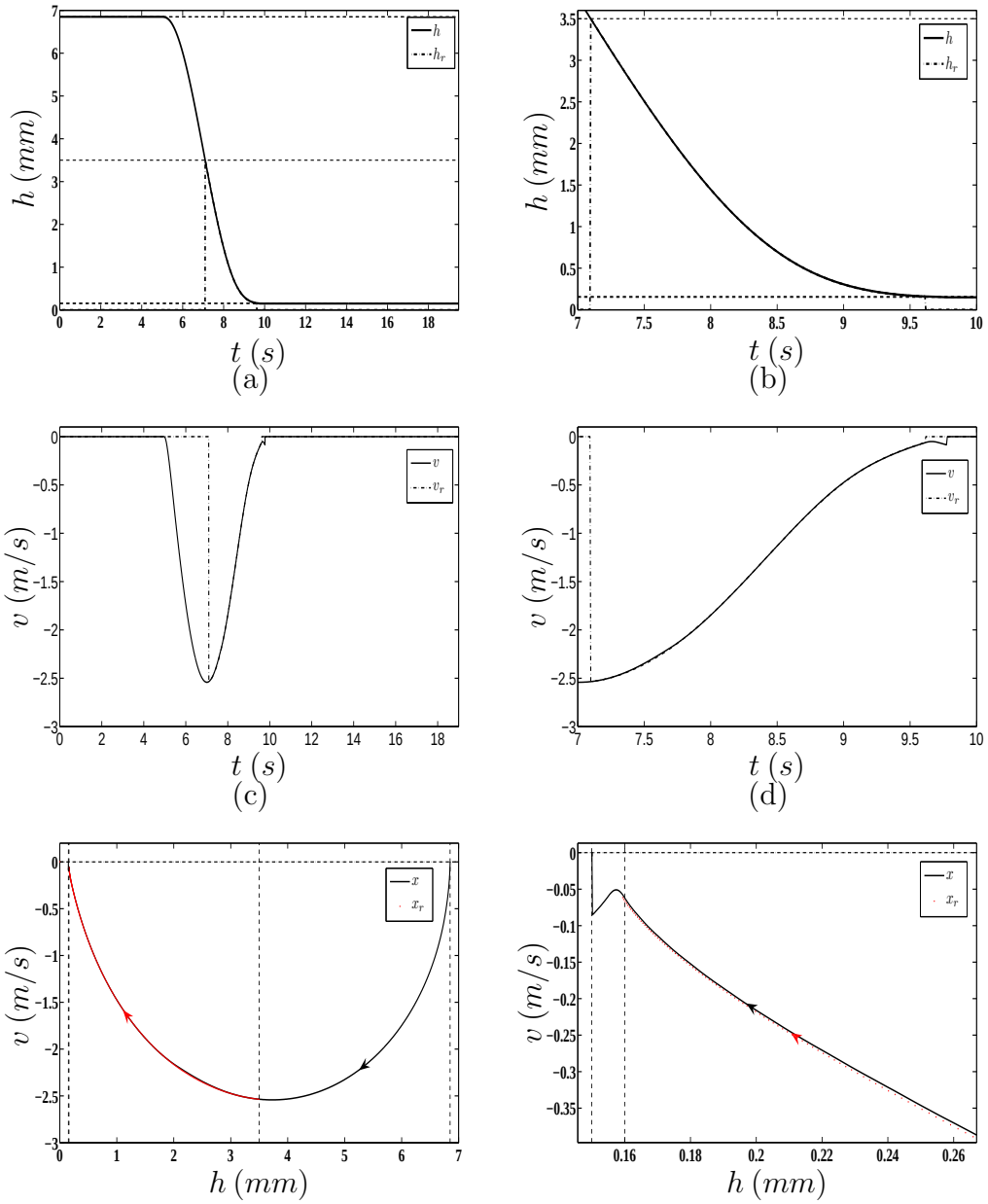

Figure 5.6.: Soft landing control in EMVA system via feedforward and SMC controller: (a-b) valve position; (c-d) valve velocity; (e-f) phase portrait.

Fig. 5.8 presents the application of the proposed controller to perform both, opening and closing maneuvers in EMVA system. In particular, Fig. 5.8(a) depicts the actual valve position h and the reference position h_r. Similarly, Fig. 5.8(b) shows the time evolution for actual v and reference v_r valve velocity. The phase portraits of the trajectories for the closed loop system and reference model are depicted in Fig. 5.8(c). From these results, it is clear the effectiveness of SLC control to close and open the valve, while satisfying the application requirements.

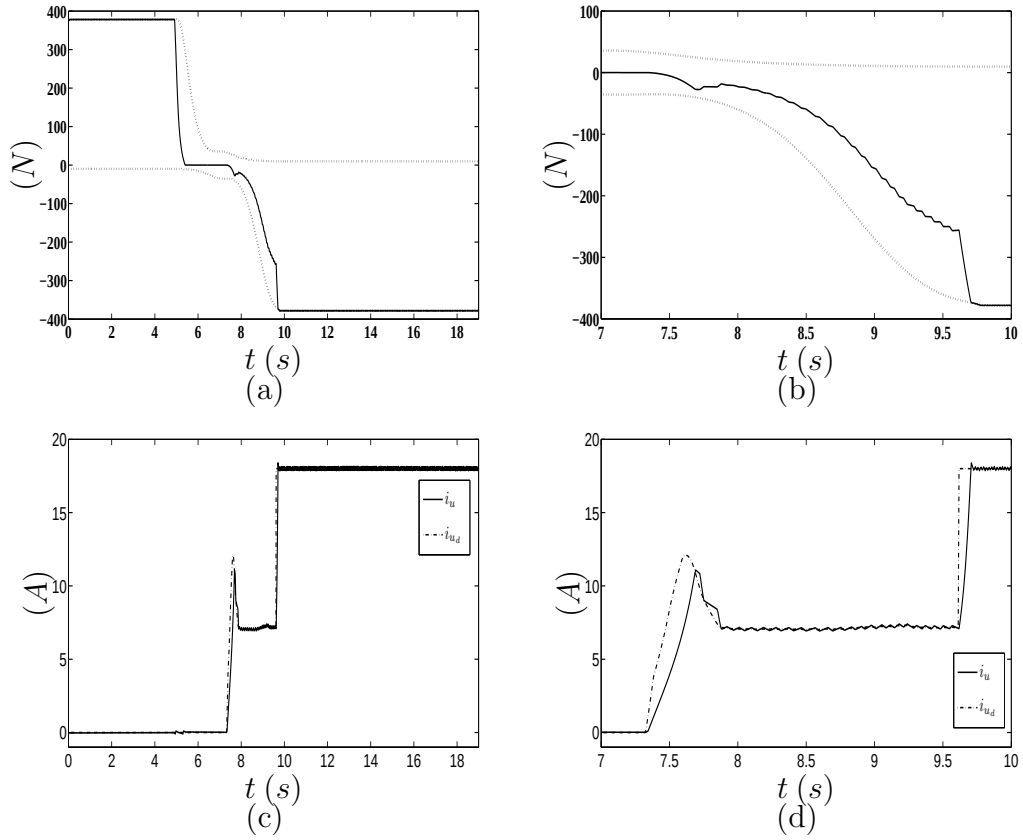

Figure 5.7.: Soft landing control in EMVA system via feedforward and SMC based feedback controller: (a-b) control action; (c-d) upper current.

The overall control effort is plotted in Fig. 5.9, where the dotted lines refer to the upper and lower dynamic bounds, u_{max} and u_{min} respectively, for control signal u (see Eqs. (4.10) and (3.4)), while the solid line is the actual saturated control action u.

5.6. Robustness analysis

In this section, robustness analysis is carried out for the control action. Analysis is done by studying numerically the control performance when considering a variation of the friction force $F_f(v)$ in the plant equations (3.1). To this aim, we consider a scale parameter $\rho > 0$ to affect nominal friction force as $\rho F_f(v; \hat{\gamma})$.

For low friction condition, that is it $\rho < 0.3$, high impacts are observed. Then, this combined control action allows system to perform well in the range $\rho \in [0.3, 1.56]$. For values in parameter $\rho > 1.56$, the valve is lost.

For $\rho > 1.4$ a long tail starts to appear before the valve is caught, which implies that

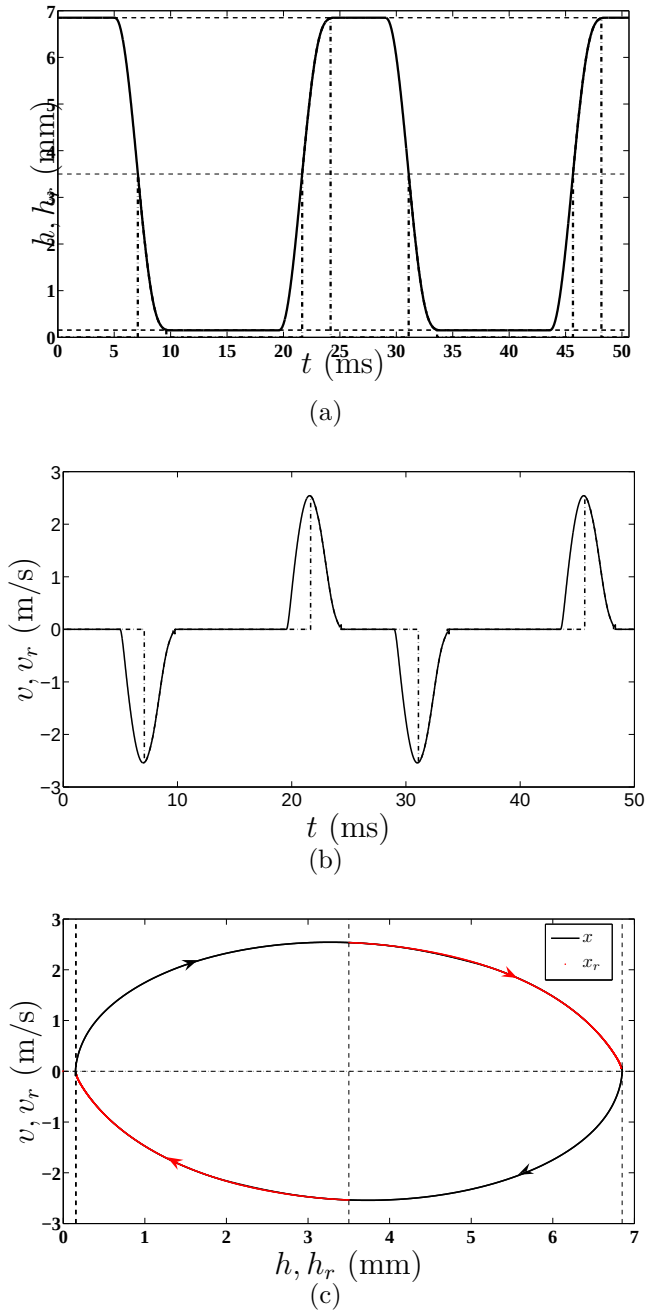

Figure 5.8.: Opening and closing of the valve through SLC controller: a) Valve position; b) Valve velocity; c) Phase portrait.

controller is not able to produce a good tracking performance. Similar phenomena were also observed by [122, 123].

From results of control performance, high impacts are observed for low friction condition, that is it $\rho < 0.5$. Thus, system evolution for $\rho = 0.2$ is depicted in Fig. 5.11. For friction conditions greater than nominal one, long tail takes place in valve trajectory, as it is depicted in Fig. 5.12 for $\rho = 1.5$. Proposed control algorithm

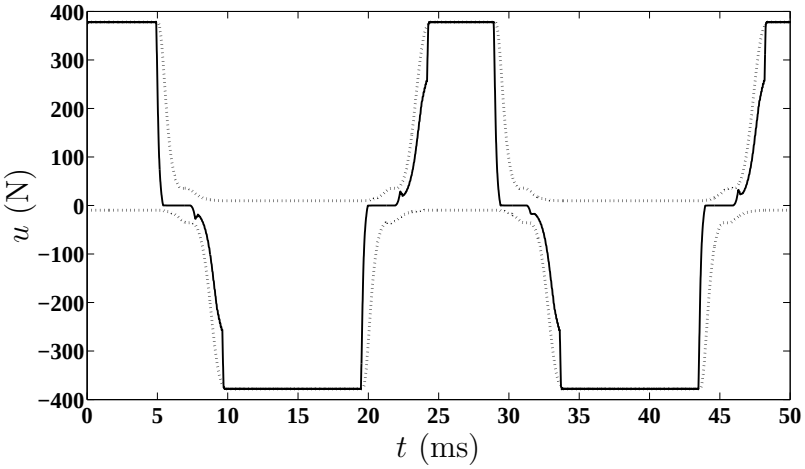

Figure 5.9.: Opening and closing of the valve through SLC controller: Time history of the control signal. Dotted line: upper and lower dynamic bounds u_{max} and u_{min} respectively. Solid line: the actual control signal u.

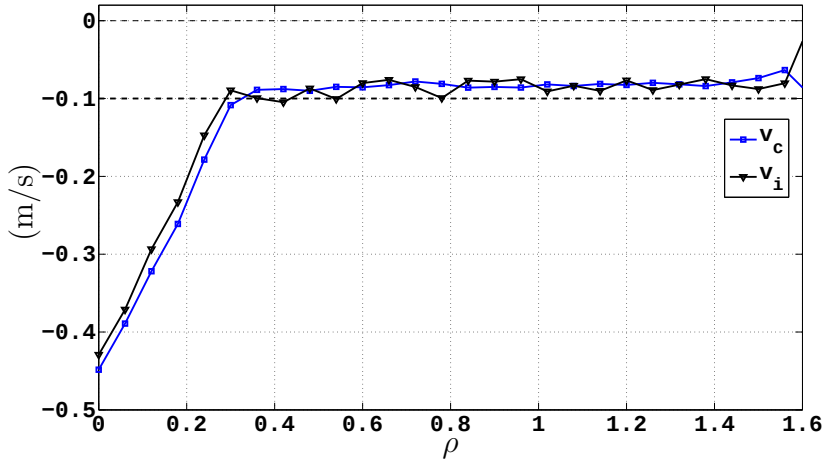

Figure 5.10.: Robustness results for feedforward controller combined with SMC based in PD sliding manifold. Parameter ρ is varied in the range $[0, 1.6]$.

allows to control the valve in a wide range, i.e. $[-70\%, 56\%]$ respect to nominal friction condition.

5.7. Discussion

We have addressed the SLC design for EMVA system subjected to input and output constraints. A controller based on the combination of feedforward and sliding mode control has been designed and successfully tested numerically in the EMVA system.

Simulation results show the potential of this control technique to be implemented in

EMVA prototype. As a result, due to the nice robustness properties of sliding mode control and the use of feedforward control action based on the knowledge of the model, we have obtained a robust and feasible control scheme that renders EMVA system a reliable solution to be used in camless engines.

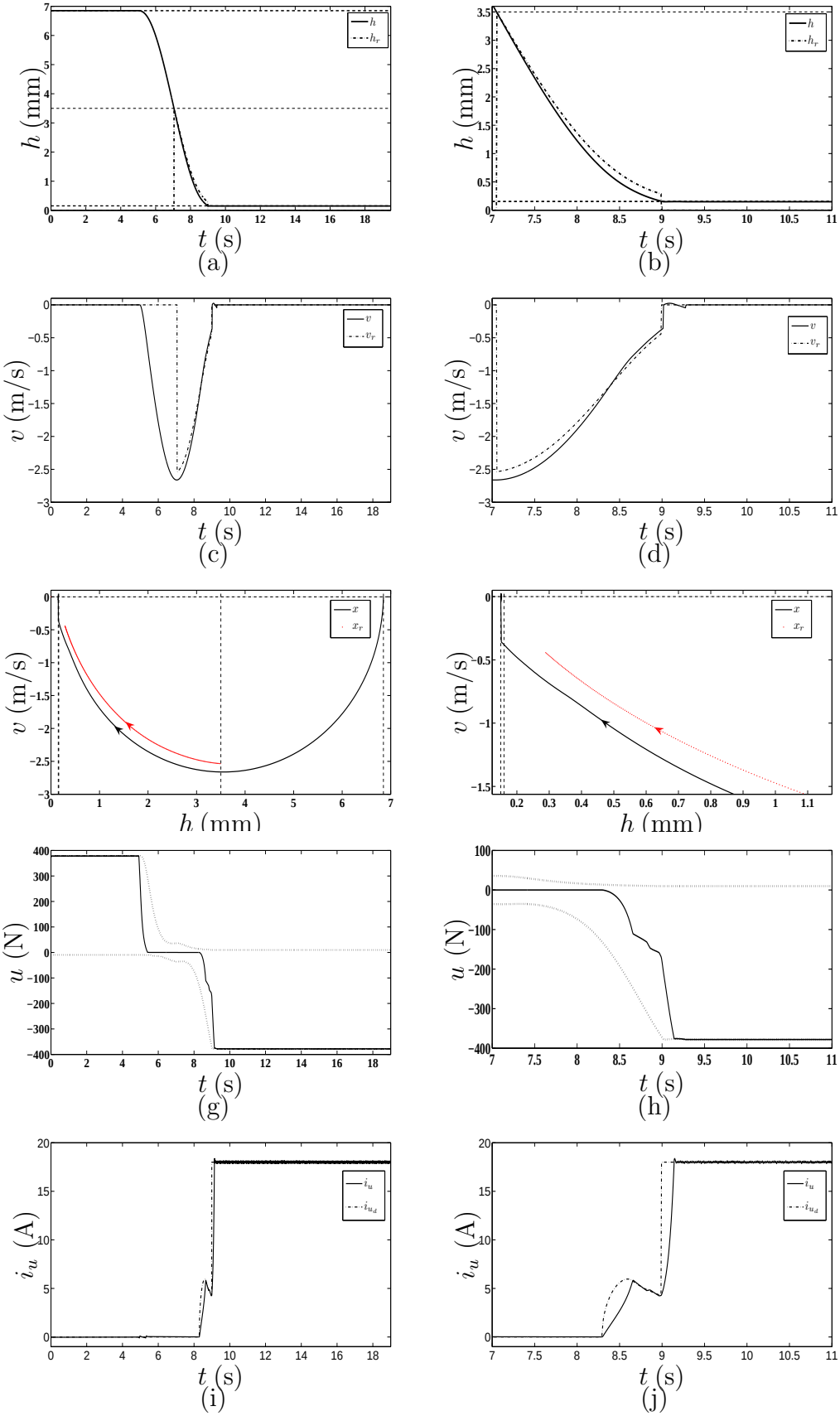

Figure 5.11.: Soft landing control in EMVA system via combined Feedforward and SMC when system presents low friction condition, e.g. $\rho = 0.2$: a)-b) valve position; c)-d) valve velocity; e)-f) phase portrait; g)-h) control action; i)-j) upper current

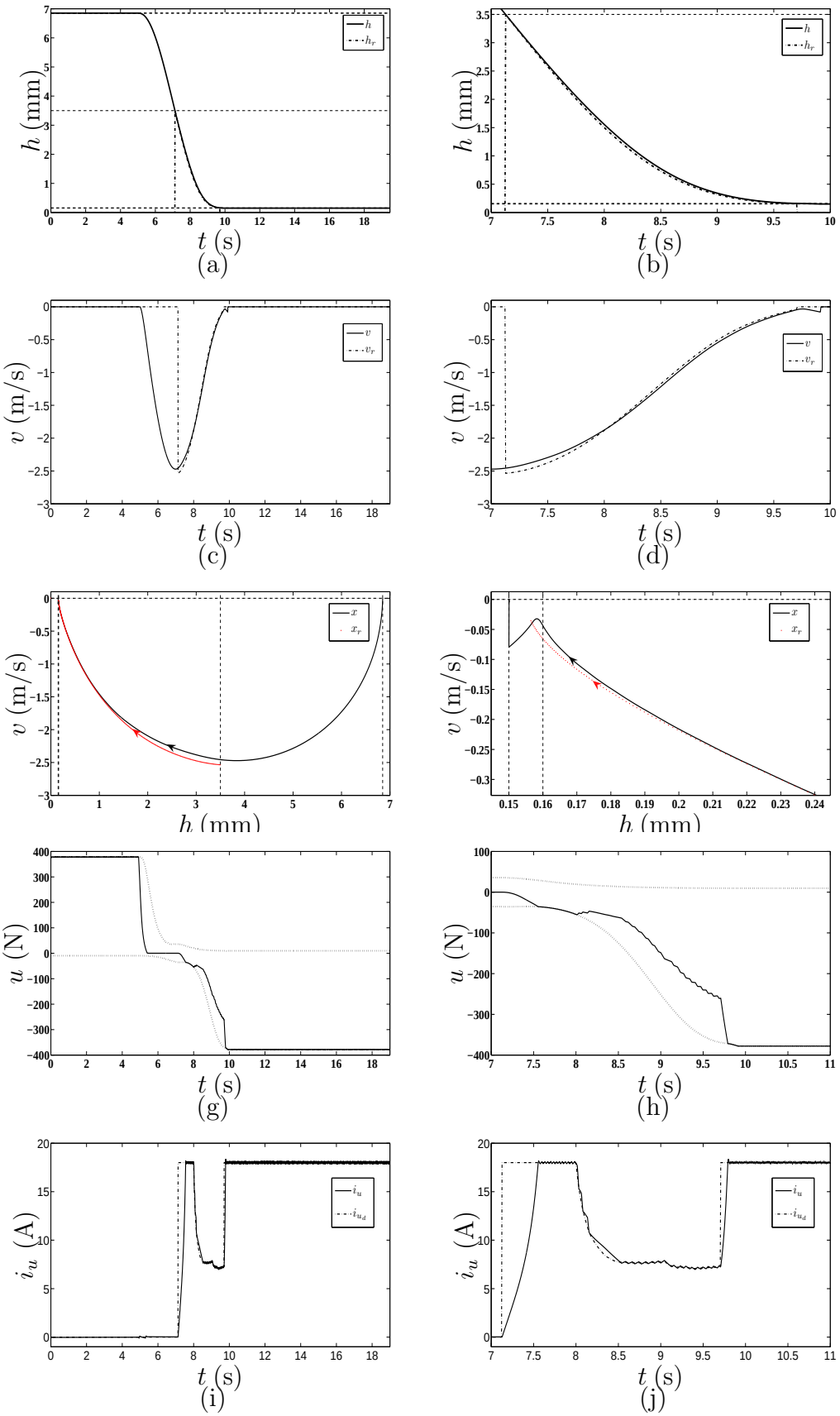

Figure 5.12.: Soft landing control in EMVA system via combined Feedforward and SMC when system presents high friction condition, e.g. $\rho = 1.5$: a)-b) valve position; c)-d) valve velocity; e)-f) phase portrait; g)-h) control action; i)-j): upper current

CHAPTER 6

CONCLUSIONS

Veni, vidi, vici.

(Gaius Iulius Caesar (2 August, 47 a.C))

We have shown that the modelling, analysis and control of novel mechatronic valve actuators for automotive system, in particular EMVA system, can be successfully addressed in the framework of non-smooth dynamical system and nonlinear control theory.

In this thesis, nonlinear control strategies to solve control problems in EMVA system have been developed. The proposed control schemes have been tested numerically and validated on an experimental setup.

A summary of contributions is presented as follows.

- In Chapter 2, we presented an introduction to EMVA system in Automotive Engineering. After a brief background on Internal Combustion (IC) engine, we motivated the use of mechatronic devices to drive the engine valves and their potential use for future camless engines. In particular we presented the main advantages, disadvantages and the control challenges in a double magnet EMVA actuators.

- The derivation of a mathematical model for EMVA system was addressed in

Chapter 3. Though different authors have used linear friction force models to describe friction effects in EMVA system, we noted that EMVA system can be modelled as a non-smooth mechanical oscillator with friction, where friction was described by a static non-smooth friction model that includes viscous, Coulomb and Stribeck effect. From experiments we clearly observed that proposed model predicts altogether, both transient and steady state response, allowing to confirm the nonlinear nature of EMVA system. Furthermore, through a sensitivity analysis, we evaluated the prediction capabilities of the mathematical model for EMVA via numerical analysis, when considering parameter variations in friction force.

- In Chapter 4, we addressed the so-called First Catching Control (FCC) problem, proposing a Novel Key-on controller. The constrained nature of the magnetic force, acting on the armature, makes classical feedback controllers ineffective, due to they produce no feasible current. In this context, the proposed Key-on controller, which is a nonlinear controller, based on Lyapunov 's direct method, aimed at friction compensation and tuned through bifurcation diagram analysis, is introduced as a viable solution to cope with FCC control specifications. Furthermore, this control allowed to perform the first lift operation in a robust way by pumping energy into the system through the proper compensation of energy losses due to friction. The Key-on controller was tested experimentally in a good agreement with theoretical predictions and the more important reaching the control goal while satisfying application requirements.

- In Chapter 5, a novel control scheme was presented to address the SLC control problem for a double magnet EMVA system subjected to input and output constraints. Due to strict SLC control specifications and the existence of physical constraints in magnetic force actuator, we proposed a force based control law, where the key elements of control scheme include the trajectory planner, which we discovered has to yield a reference trajectory to evolve in a natural shape at the system and a control law consisting on the combination of both feedforward and feedback control actions. Feedforward control action accounts for effectively compensates nominal dynamics of the system, while feedback controller, based on Sliding Mode Control, accounts for compensating large disturbance forces, while rendering the overall control system robust to bounded disturbances. SLC controller was designed and successfully tested numerically in the EMVA system. Furthermore, through a robustness analysis, we showed that soft-landing operations have been achieved while satisfying

application requirements such as: safety landing, impacts intensity reduction and the avoidance of undesired effects on system dynamics, for a wide range of friction disturbances. Due to the nice robustness properties of proposed controller, we obtained a robust and feasible control scheme that renders EMVA system a reliable solution to be used in camless engines.

- The analysis of closed-loop nonlinear dynamics and induced bifurcation phenomena at Key-on were characterized in Appendix B through analytical and numerical methods. Moreover, the predicted phenomena were tested experimentally. Saddle Node bifurcation of Cycles and Subcritical Hopf bifurcation were characterized for a nonlinearity of the type Stribeck, by deriving the describing function for such nonlinearity. Furthermore, the existence of the induced equilibrium set was characterized in the context of Fillipov systems by writing the system as a differential inclusion.

- In Appendix C we presented further research results, obtained in the laboratories from University of Naples Federico II. The developed work consisted on the experimental validation of a novel model reference switched adaptive strategy for bimodal PWA dynamical systems, where, the idea behind the control scheme is to formulate a switched extension of the original Minimal Control Synthesis (MCS) adaptive law for smooth dynamical systems in order to cope with switchings in the plant and/or reference model. Experimental results were shown on the control of a PWA electric circuit confirming the effectiveness of the switching controller even when it is implemented via a commercial inexpensive digital microcontroller. Developed research also provided a first insight into the algorithm robustness, in particular with respect to uncertainties on the switching times between one mode and the other.

BIBLIOGRAPHY

[1] Fev company. Germany. www.fev.com.

[2] Marine engineering dave. http://davidt9000.blogspot.com.

[3] M. Abramowitz and Irene A. Stegun. *Handbook of Mathematical Functions with Formulas Graphs, and Mathematical Tables*, volume 9th printing of *55*. National Bureau of Standards Applied Mathematics, New York, 1972.

[4] T. Ahmad and M. A. Theobald. A survey of variable-valve-actuation technology. In *SAE Technical Paper*, volume no. 891674, 1989.

[5] H. J. Ahn, S. Y. Kwak, J. U. Chang, and D. C. Han. A new EMV system using a PM-EM hybrid actuator. In *Proc. of IEEE International Conference on Mechatronics (ICM05)*, pages 816–821, July 2005.

[6] R. Alzate, M. di Bernardo, U. Montanaro, and S. Santini. Experimental and numerical verification of bifurcations and chaos in cam-follower impacting systems. *Nonlinear Dynamics*, 50(3):409–429, Dec. 2007.

[7] S. Andersson, A. Soderberg, and S. Bjorklund. Friction models for sliding dry, boundary and mixed lubricated contacts. *Tribology International*, 40(4):580–587, Apr. 2007.

[8] M. S. Ashhab, A. G. Stefanopoulou, J. A. Cook, and M. B. Levin. Camless engine control for a robust unthrottled operation. *SAE Technical Paper*, no. 981031, 1998.

[9] K. J. Astrom, J. Aracil, and F. Gordillo. A new family of smooth strategies for swinging up a pendulum. In *Proc. of 16th IFAC World Congress*, pages 1118–1123, Prague, Czech Republic, 2005.

[10] K.J. Astrom and K. Furuta. Swinging up a pendulum by energy control. *Automatica*, 36:287–295, 2000.

[11] N. Auffret and N. Dronniou. Control method for the intake and exhaust valves of an engine and internal combustion engine comprising such valves. U. S. Patent 7,591,244, Sep. 2009. Renault Trucks.

[12] Giorgio Bartolini, Alessandro Pisano, and Elio Usai. Second-order sliding-mode control of container cranes. *Automatica*, 7(3):1783–1790, 2002.

[13] M. Basso, R. Genesio, and A. Tesi. A frequency method for predicting limit cycle bifurcations. *Nonlinear Dynamics*, 13, 1997.

[14] M. Battistoni, L. Foschini, and L. Postrioti M. Cristiani. Development of an electro-hydraulic camless VVA system. *SAE Technical Paper*, no. 2007-24-0088, 2007.

[15] J. Büchl. Method of activating an electromagnetic positioning means and apparatus for carrying out the method. U.S. Patent 4544986, Oct. 1985.

[16] C. Boie, L. Kather, G. Schmitz, F. Van der Staay, and G. R. Feyerl. Method of starting an electromagnetic actuator operating a cylinder valve of a piston-type internal-combustion engine. U.S. Patent 6333843, Dec. 2001.

[17] C. Bruestle and D. Schwarzenthal. Variocam plus - a highlight of the porsche 911 turbo engine. In *SAE Technical Paper*, volume no. 2001-01-0245, 2001.

[18] S. Butzmann, J. Melbert, and A. Koch. Sensorless control of electromagnetic actuators for variable valve train. *SAE Technical Paper*, no. 2000-01-1225, 2000.

[19] W. S. Chang, T. A. Parlikar, M. D. Seeman, D. J. Perreault, J. G. Kassakian, and T. A. Keim. A new electromagnetic valve actuator, 2005. Massachusetts Institute of Technology-Laboratory for Electronic and Electromagnetic Systems.

[20] J. Che and D. Chen. Automatic landing control using h_∞ control and stable inversion. In *Proc. of 40th IEEE Conference on Decision and Control*, pages 241–246, Orlando, Florida, USA, Dec. 2001.

[21] Ryan R. Chladny and Charles R. Koch. Flatness-based tracking of an electromechanical variable valve timing actuator with disturbance observer feedforward compensation. *IEEE Transactions on Control Systems Technology*, 16(4):652–663, July 2008.

[22] R. E. Clark, G. W. Jewell, S. J. Forrest, J. Rens, and C. Maerky. Design features for enhancing the performance of electromagnetic valve actuation systems. *IEEE Transactions on Magnetics*, 41(3):1163–1168, March 2005.

[23] H. Dankowicz. On the modeling of dynamic friction phenomena. *ZAMM. Z. Angew. Math. Mech.*, 79(6):399–409, 1999.

[24] L. D. Davis. *Handbook of genetic algorithms*. Van Nostrand Reinhold Company, New York, 1991. ISBN 978-0442001735.

[25] C. Canudas de Wit, H. Olsson, K. J. Astrom, and P. Lischinsky. A new model for control of systems with friction. *IEEE Transactions on Automatic Control*, 40(3):419–425, Mar. 1995.

[26] M. Degner and J. Grabowski.

[27] P. Dell'Orto, M. Marchetti, E. Chiavazzo, G. Manganiello, A. di Gaeta, and G. Police. Electro-hydraulic variable valve actuator and method to control valves of internal combustione engines. EU Patent1770247, Apr. 2007.

[28] M. di Bernardo, C. Budd, A. R. Champneys, and P. Kowalczyk. *Piecewise-smooth Dynamical Systems, Theory and Applications*. Springer, 2008. ISBN 978-1-84628-039-9.

[29] M. di Bernardo, C. J. Budd, A. R. Champneys, P. Kowalczyk, A. B. Nordmark, G. Olivar, and P. T. Piiroinen. Bifurcations in nonsmooth dynamical systems. *SIAM Review*, 50(4):629–701, Nov. 2008.

[30] M. di Bernardo, A. di Gaeta, C. I. Hoyos Velasco, and S. Santini. Energy-based Key-On control of a double magnet electromechanical valve actuator. *IEEE Transactions on Control*

Systems Technology, Aug. 2011. In press.

[31] M. di Bernardo, A. di Gaeta, C. I. Hoyos Velasco, and S. Santini. Experimental nonlinear dynamics of a double magnet electro-mechanical valve actuator (EMVA). In *Proc. of the 7th European Nonlinear Dynamics Conference (ENOC 2011)*, Rome, Italy, July 2011.

[32] M. di Bernardo, V. Esposito, C. I. Hoyos Velasco, and S. Santini. Experimental control of chaos in cam-follower systems. In *Proc. of the 7th European Nonlinear Dynamics Conference (ENOC 2011)*, Rome, Italy, July 2011.

[33] M. di Bernardo, U. Montanaro, S. Santini, A. di Gaeta, and V. Giglio. Design and validation of a novel model reference adaptive algorithm to control etb for drive-by-wire applications. *SAE International Journal of Passenger Cars - Mechanical Systems*, 2(1):1268–1284, Oct. 2009.

[34] M. di Bernardo, C. I. Hoyos Velasco, U. Montanaro, and S. Santini. Experimental validation of a novel adaptive controller for piecewise affine systems. In *Proc. of IEEE International Symposium on Circuits and Systems (ISCAS 2010)*, pages 1543–1546, Paris, France, Aug. 2010.

[35] M. di Bernardo, C. I. Hoyos Velasco, U. Montanaro, and S. Santini. Experimental implementation and validation of a novel minimal control synthesis adaptive controller for continuous bimodal piecewise affine systems. *Control Engineering Practice*, Nov. 2011. In press.

[36] A. di Gaeta. *Modelling and Control of an Electromechanical Valve Actuator for Camless Engine*. PhD thesis, Department of Systems and Computer Engineering, University of Naples "Federico II", Naples, Italy, Feb. 2003.

[37] A. di Gaeta, V. Giglio, and G. Police. Model-based decoupling control of a magnet engine valve actuator. *SAE International Journal of Engines*, 2:254–271, Mar. 2010.

[38] A. di Gaeta, L. Glielmo, V. Giglio, and G. Police. Modeling of an electromechanical engine valve actuator based on a hybrid analytical-fem approach. *IEEE/ASME Transactions on Mechatronics*, 13(6):625–637, Dec. 2008.

[39] A. di Gaeta, U. Montanaro, S. Massimino, and C. I. Hoyos Velasco. Experimental investigation of a double magnet EMVA at Key-On engine: a mechanical resonance based control strategy. *SAE International Journal of Engines*, 3(2):352–372, Dec. 2010.

[40] P. Dolcini, C. Canudas de Wit, and H. Béchart. Improved optimal control of dry clutch engagement. In *Proc. of 16th IFAC Triennial World Congress*, pages 25–30, Prague-Czech Republic, 2005.

[41] T. Dresner and P. Barkan. A review of variable valve timing benefits and modes of operation. *SAE Technical Paper*, no. 891676, 1989.

[42] T. Dresner and P. Barkan. A review of variable valve timing benefits and modes of operation. *SAE Technical Paper*, no. 891676, Aug. 1989.

[43] A. C. Elrod and M. T. Nelson. Development of a variable valve timed engine to eliminate the pumping losses associated with throttled operation. *SAE Technical Paper*, no. 860537, 1986.

[44] P. Eyabi and B. Washington. Modeling and sensorless control of an electromechanical valve actuator. *Mechatronics*, 16(6):159–175, Nov. 2006.

[45] R. Flierl, D. Gollasch, A. Knecht, and W. Hannibal. Improvements to a four cylinder gasoline engine through the fully variable valve lift and timing system univalve. *SAE Technical Paper*, no. 2006-01-0223, 2006.

[46] R. Flierl and M. Kluting. The third generation of valvetrains-new fully variable valvetrains for throttle-free load control. *SAE Technical Paper*, no. 2000-01-1227, 2000.

[47] European Federation for Transport and Environment (T&E). How clean are europe's cars?: An analysis of carmaker progress towards eu co_2 targets in 2010, Sep. 2011. www.transportenvironment.org/Pages/cars-and-co2.

[48] T. Fujita, K. Onogawa, S. Kiga, Y. Mae, Y. Akasaka, and K. Tomogane. Development of innovative variable valve event and lift (VVEL) system. *SAE Technical Paper*, no. 2008-01-1349, Apr. 2008.

[49] F. Garofalo, L. Glielmo, L. Iannelli, and F. Vasca. Optimal tracking for automotive dry clutch engagement. In *Proc. of 15th IFAC Triennial World Congress*, pages 367–372, Barcelona-Spain, 2002.

[50] V. Giglio, B. Iorio, G. Police, and A. di Gaeta. Preliminary experiences in the design of an electromechanical valve actuator. *SAE Technical Paper*, no. 2001-24-0016, Sep. 2001.

[51] V. Giglio, B. Iorio, G. Police, and A. di Gaeta. Analysis of advantages and of problems of electromechanical valve actuators. *SAE 2002 Transactions Journal of Engines*, 111(3):1768–1779, Mar. 2002.

[52] A. H. Glattfelder and W. Schaufelberger. *Control Systems with Inputs and Output Constraints*. Advanced Texbooks in Control and Signal Processing. 2003.

[53] L. Glielmo, P. Gutman, L. Iannelli, and F. Vasca. Robust smooth engagement of an automotive dry clutch. In *Proc. of IFAC conference on Mechatronic Systems*, volume 4 of *1*, pages 632–637, 2006.

[54] Robert Bosch GmbH. *Automotive Electrics Automotive Electronics*. 4th Edition. Professional Engineering Publishing, 2004.

[55] T. Gobel and T. Esch. Method for affecting the mixture formation in cylinders of piston-type internal combustion engines by varying the valve strokes. U. S. Patent 5,996,539, 1999. FEV Motorentechnik GmbH, Germany.

[56] K. Graichen, M. Treuera, and M. Zeitza. Swing-up of double pendulum on a cart by feedforward and feedback control with experimental validation. *Automatica*, 43(1):63–71, 2007.

[57] C. Gunselmann and J. Melbert. Soft-landing control for sensorless electromagnetical spring-mass actuators. In *Proc. of Second International Conference on Power Electronics, Machines and Drives (PEMD)*, volume 2, pages 715–718, 2004.

[58] L. Guzzella. Automobiles of the future and the role of automatic control in those systems. *Annual Reviews in Control*, 33:1–10, 2009.

[59] M. Haas. Uniair-the first fully-variable, electro-hydraulic valve control system. In *Proc. of Schaeffler Symposium*, pages 250–263, 2010.

[60] C.K. Halse, R.E. Wilson, M. di Bernardo, and M.E. Homer. Coexisting solutions and bifurcations in mechanical oscillators with backlash. *Journal of Sound and Vibration*, 305(3):854–885, May 2007.

[61] R. H. A. Hensen, M. J. G. van de Molengraft, and M. Steinbuch. Friction induced hunting limit cycles: A comparison between the lugre and switch friction model. *Automatica*, 39(12):2131–2137, Dec. 2003.

[62] J. B. Heywood. *Internal Combustion Engine Fundamentals*. McGraw-Hill Book Company, 1988.

[63] W. Hoffmann, K. S. Peterson, and A. G. Stefanopoulou. Iterative learning control for soft landing of electromechanical valve actuator in camless engines. *IEEE Transactions on Control Systems Technology*, 11(2):174–184, 2003.

[64] Joachim Horn, Joachim Bamberger, Peter Michau, and Stephan Pindl. Flatness-based clutch control for automated manual transmissions. In *15th IFAC Triennial World Congress*, pages 361–366, Barcelona-Spain, 2002.

[65] T. Hosaka and M. Hamazaki. Development of the variable valve timing and lift (VTEC) engine for the honda NSX. *SAE Technical Paper*, no. 910008, 1991.

[66] http://www.nonoise.org. Article vii. noise and vibration control, 2001.

[67] R. Huang and Y. Zhao. A control strategy based on exact linearization for electromagnetic valve actuation. In *SAE Technical Paper*, volume no. 2007-01-1596, 2007.

[68] M. Iwashiro, K. Furuta, and K. J. Astrom. Energy based control of pendulum. In *Proc. of the IEEE International Conference on Control Applications*, page 715.720, Sep. 1996.

[69] Kim J. and D. K. Lieu. Designs for a new quick-response latching electromagnetic valve. *Proc. of the 2005 IEEE International Conference on Electric Machines and Drives*, pages 1773–1779, 2005.

[70] Jih-Gau Juang, Hao-Hsiang Chang, and Kai-Chung Cheng. Intelligent landing control using linearized inverse aircraft model. In *Proc. of the American Control Conference*, pages 3269–3274, Anchorage, AK, May 2002.

[71] Jih-Gau Juang and Jern-Zuin Chio. Aircraft landing control based on fuzzy modeling networks. In *IEEE lnternational Conference on Control Applications*, pages 144–149, Glasgow, Scotland, U.K, Sep. 18-20 2002.

[72] Jih-Gau Juang and Wen-Pin Lin. Aircraft landing control based on cmac and ga techniques. In *Proc. of the 17th World Congress The International Federation of Automatic Control*, Seoul- Korea, Jul. 6-11 2008.

[73] H. K. Khalil. *Nonlinear systems*. Third Edition. Prentice Hall. Inc., New Jersey, 2002.

[74] Chang-Sei Kim and Keum-Shik Hong. Boundary control of container cranes from the perspective of controlling an axially moving string system. *International Journal of Control, Automation and Systems*, 7(3):437–445, 2009.

[75] Seong Pil Kim, Jang Ho Lee, Bong-Ju Kim, Hyoung Jun Kwon, Eung Tai Kim, and Iee-Ki Ahn. Automatic landing control law for unmanned helicopter using lyapunov approach. In *Proc. of 25th Digital Avionics Systems Conference, 2006 IEEE/AIAA*, number ISBN: 1-4244-0377-4, pages 1–8, Portland, OR, Feb. 2007.

[76] Alexander I. Kozynchenko. Enhancing the manoeuvring capabilities of a lunar landing module using predictive guidance algorithms. *Acta Astronautica*, 67:406–416, Feb. 26 2010.

[77] Erwin Kreyszig. *Advanced Engineering Mathematics*. Jhon Wiley & and Sons, INC, New York, 8th edition, 1999.

[78] Y. A. Kuznetsov and A. Gragnani. One parameter bifurcations in planar filippov systems. *International Journal of Bifurcation and Chaos*, 13(8):2157–2188, 2003.

[79] V. Lanza, Bonnin M, and M. Gilli. On the application of the describing function technique to the bifurcation analysis of nonlinear systems. *IEEE Transactions on Circuits and Systems*, 54(4), 2007.

[80] R. I. Leine and N. van de Wouw. Dry friction induced attractivity of equilibrium sets in mechanical multibody systems. In *Proc. of the Design Engineering Technical Conferences & Computers and Information in Engineering Conference (DETC 2005), ASME Symposium on Nonlinear Dynamics In Engineering Systems*, Long Beach, California, USA, Sep. 2005.

[81] T. G. Leone, E. J. Christenson, and R. A. Stein. Comparison of variable camshaft timing strategies at part load. *SAE Technical Paper*, no. 960584, 1996.

[82] D. J. Lewis, J. D. Russell, D. John amd N. Trask, and T. Megli. Starting an engine with valves that may be deactivated. U. S. Patent 5,996,539, Mar. 2004. Ford Global TechnologiesFiled.

[83] J. J. Liu, Y. P. Yang, and J. H. Xu. Electromechanical valve actuator with hybrid mmf for camless engine. In *Proc. of the 17th IFAC World Congress*, pages 10698–10703, July 2008.

[84] L. Liu and S. Chang. A moving coil electromagnetic valve actuator for camless engines. In *Proc. of the 2009 IEEE International Conference on Mechatronics and Automation*, pages 176–180, Changchun, China, Aug. 2009.

[85] Xing-Long Liua. Optimal soft landing control for moon lander. *Automatica*, 44(3):1097–1103, Aug. 2008.

[86] B. Armstrong-He louvry, P. Dupont, and C. Canudas de Wit. A survey of models, analysis tools and compensation methods for the control of machines with friction. *Automatica*, 30(7):1083–1138, July 1994.

[87] G. Lucente, M. Montanari, and C. Rossi. Hybrid optimal control of an automated manual transmission system. In *15th IFAC Triennial World Congress*, volume 7 of *1*, CSIR International Convention Centre- South Africa, 2008.

[88] J. Ma, H. Schock, U. Carlson, A. Hoglund, and M. Hedman. Analysis and modeling of an electronically pneumatic hydraulic valve for an automotive engine. *SAE Technical Paper*, no. 2006-01-0042, 2006.

[89] K. Madsen, H.B. Nielsen, and O. Tingleff. Methods for non-linear least squares problems, 2nd edition. Informatics and Mathematical Modelling, Apr. 2004.

[90] Lorinc Marton and Bela Lantos. Control of mechanical systems with stribeck friction and backlash. *ELSEVIER, Systems and Control letter*, 58:141–147, 2008.

[91] Lorinc Marton and Bela Lantos. Control of mechanical systems with stribeck friction and backlash. *ELSEVIER, Systems and Control letter*, 58(141):147, 2009.

[92] H. Mazen and H. Mohammad. Intake valve timing in multi-valve, camless engines. U. S. Patent RE42,667, Sep. 2011. Ford Global Technologies.

[93] J. C. McCoy, L. Hiltunen, P. Caporuscio, and H. Lacher. Camless engine with crankshaft position feedback. U. S. Patent 6,523,523, Feb. 2003. Siemens VDO Automotive Corporation.

[94] P. Mercorelli. An antisaturating adaptive preaction and a slide surface to achieve soft landing control for electromagnetic actuators. *IEEE/ASME Transactions on Mechatronics*, Issue: 99:1–10, Dec. 2010.

[95] Lawrence Mianzo and Huei Peng. Output feedback h_∞ preview control of an electromechanical valve actuator. *IEEE Transactions on Control Systems Technology*, 15(3):428–437, May 2007.

[96] T. Moriya, Y. Komatsu, H. Sono, and T. Sugai. Energization control method and electromagnetic control system in electromagnetic driving device. U. S. Patent 5,363,601, June 1997. Honda Giken Kogyo Kabushiki Kaisha, Japan.

[97] K. Nagaya, H. Kobayashi, and K. Koike. Valve timing and valve lift control mechanism for engines. *Mechatronics*, 16(2):121–129, Mar. 2006.

[98] T. Nguyen, J. Leavitt, F. Jabbari, and J. E. Bobrow. Accurate sliding-mode control of pneumatic system using low-cost solenoid valves. *IEEE/ASME Transactions on Mechatronics*, 12(2):216–219, 2007.

[99] Commission of the European Communities. A competitive automotive regulatory framework for the 21st century, 2007. http://ec.europa.eu/reducing_co2_emissions_from_cars.

[100] J. P. Ordaz Oliver and O. A. Domínguez Ramírez. Control based on swing up and balancing scheme for an underactuated system, with gravity and friction compensator. In *Proc. of IEEE Fourth Congress of Electronics, Robotics and Automotive Mechanics*, pages 603–607, 2007.

[101] T. A. Parlikar, W. S. Chang, Y. H. Qiu, M. D. Seeman, D. J. Perreault, J. G. Kassakian, and T. A. Keim. Design and experimental implementation of an electromagnetic engine valve drive. *IEEE/ASME Transactions On Mechatronics*, 10(5):482–494, Oct. 2005.

[102] K. Peterson, A. G. Stefanopoulou, T. Megli, and M. Haghgooie. Output observer based feedback for soft landing of electromechanical camless valvetrain actuator. In *Proc. of American Control Conference*, 2002.

[103] K. Peterson, A. G. Stefanopoulou, Y. Wang, and T. Megl. Virtual lash adjuster for an electromechanical valve actuator through iterative learning control. In *ASME IMECE*, 2003.

[104] K. S. Peterson and A. G. Stefanopoulou. Extremum seeking control for soft landing of an electromechanical valve actuator. *Automatica*, 40:1063–1069, Jan. 2004.

[105] V. Picron, Y. Postel, E. Nicot, and D. Durrieu. Electro-magnetic valve actuation system: First steps toward mass production. *SAE Technical Paper*, no. 2008-01-1360, 2008.

[106] M. Pischinger and P. Kreuter. Electromagnetically operated actuators. U.S. Patent 4455543, 1984.

[107] M. Pischinger, F. Van Der Staay, H. Baumgarten, and H. Kemper. Benefits of the electromechanical valve train in vehicle operation. *SAE Technical Paper*, no. 2000-01-1223, 2000.

[108] Y. H. Qiu, T. A. Parlikar, W. S. Chang, M. D.Seeman, T. A. Keim, D. J.Perreault, and J. G.Kassakian. Design and experimental evaluation of an electromechanical engine valve drive. In *Proc. of 35th Annual IEEE Power Electronics Specialists Conference*, pages 4838–4843, Oct. 2004.

[109] R. H. Rassern. Single-cylinder engine test of a motor-driven variable valve actuator. *SAE Technical Paper*, no. 2001-01-0241, 2001.

[110] M. Rebbert, G. KreusenM, and S. Lauer. A new cylinder deactivation by FEV and mahle. *SAE Technical Paper*, no. 2008-01-1354, 2008.

[111] W. E. Richeson and F. L. Erickson. Pneumatic actuator with solenoid operated control valves. U.S. Patent 4873948, Oct. 1989.

[112] SAE. *Variable Valve Optimization*. SP-2174. SAE Internationl, 2008. ISBN 978-0-7680-2016-8.

[113] Y. Sakawa and Y. Shindo. Optimal control of container cranes. *Automatica*, 18(3):257–266, 1982.

[114] K. Sakurama, S. Hara, and K. Nakano. Swing-up and stabilization control of a cart pendulum

system via energy control and controlled lagrangian methods. *Electrical Engineering in Japan*, 160(4):24–31, 2007.

[115] M. M. Schechter and M. B. Levin. Camless engine. *SAE Technical Paper*, no. 960581, 1996.

[116] Sheng Shouzhaon, Ashfaq Ahmad Mian, Zhao Chao, and Jiang Bin. Autonomous takeoff and landing control for a prototype unmanned helicopter. *Control Engineering Practice*, 2010. In press.

[117] J. J. Slotine. *Applied nonlinear control*. Prentice Hall, New Jersey, 1991.

[118] R. A. Stein, K. M. Galietti, and T. G. Leone. Dual equal VCT - A variable camshaft timing strategy for improved fuel economy and emissions. *SAE Technical Paper*, no. 950975, 1995.

[119] R. Stribeck. Die wesentlichen eigenschaften der gleit-und rollenlager. *Z. Verein. Deut Ing.*, 46(38):1341–1348, 1902.

[120] S. H. Strogatz. *Nonlinear dynamics and chaos*. Westview Press, Cambridge, USA, 2001. ISBN 978-0738204536.

[121] Z. Sun. Method for valve seating control for an electro-hydraulic engine valve. U. S. Patent 7,866,286, Jan. 2011. GM Global Technology Operations.

[122] C. Tai, A. Stubbs, and T. Tsao. Modeling and controller design of an electromagnetic engine valve. In *Proc. of American Control Conference*, 2001.

[123] C. Tai and T. Tsao. Quiet seating control design of an electromagetic engine valve actuator. In *Proc. of ASME International Mechanical Engineering Congress and Exposition*, New York, Nov. 2001.

[124] C. Tai and T. C. Tsao. Control of an electromechanical camless valve actuator. In *In Proc. of the American Control Conference*, pages 262–267, Anchorage, May 2002.

[125] C. Tai and T. C. Tsao. Control of an electromechanical actuator for camless engines. In *In Proc. of the American Control Conference*, pages 3113–3118, Denver, Colorado, June 2003.

[126] C. Tai, T. C. Tsao, N. A. Schorn, and M. B. Levin. Increasing torque output from a turbodiesel with camless valvetrain. *SAE Technical Paper*, no. 2002-01-1108, 2002.

[127] T. Takahashi, K. Furuta, S. Hatakeyama, S. Suzuki, and A. Sugiki. Swing-up control of inverted pendulum by periodic input. In *Proc. of 15th IFAC World Congress*, pages 283–286, Barcelona, Spain, 2002.

[128] A. Titolo. The variable valve timing system-application on a V8 engine. *SAE Technical Paper*, no. 910009, 1991.

[129] J. Tsai, C. R. Koch, and M. Saif. Cycle adaptive feedforward approach controllers for an electromagnetic valve actuator. *IEEE Transactions on Control Systems Technology*, Jan. 2011. In press.

[130] T. Urushihara and K. Hiraya. System and method for auto-ignition of gasoline internal combustion engine. U. S. Patent 6,386,177, May 2002. Nissan Motor Co.

[131] V. I. Utkin. *Sliding Regimes in the Theory of Variable Structure Systems*. MIR, Moscow, 1978.

[132] N. van de Wouw and R. I. Leine. Attractivity of equilibrium sets of systems with dry friction. *Nonlinear Dynamics*, 35(1):19–39, 2004.

[133] C. I. Hoyos Velasco and J. M. Londoño. Nonlinear dynamics analysis of a delayed system with hysteresis. In *Proc. of the 8th International Conference on Structural Dynamics (EURODYN)*, pages 1–8, July 2011.

[134] Y. Wang, T. Megli, M. Haghgooie, K. S. Peterson, and A. G. Stefanopoulou. Modeling and control of electromechanical valve actuator. *SAE Technical Paper*, no. 2002-01-1106, 2002.

[135] J. P. Watson and R. Wakeman. Simulation of a pneumatic valve actuation system for internal combustion engine. *SAE Technical Paper*, no. 2005-01-0771, 2005.

[136] J. Zhao and R. J. Seethaler. Compensating combustion forces for automotive electromagnetic valves. *Mechatronics*, 20:433–441, 2010.

APPENDIX A

EMVA CONTROL UNIT

Si cerno longius, quia steti humeris gigantum.

(Isaac Newton, 1642-1727.)

This appendix presents the decoupling architecture to control EMVA systems.

A.1. The decoupling architecture to control EMVA systems

The decoupled control architecture for EMVA systems presented in [37] consists mainly in two nested control loops and it can be schematized as in Fig. A.1. The inner feedback controller (CCC, Coil Current Controller) regulates to demanded values the upper and lower coil currents by varying the coil voltages. Instead, the outer controller is chosen by the supervisor (Scheduler) on the basis of the control task to be performed and the EMVA operating condition. In particular the First Catching Controller (FCC) is scheduled at the engine startup to transfer the engine valve from the initial half-stroke position to opening/closing. Instead, the Soft Landing Controller (SLC) is activated to control the valve motion during the last part of the valve stroke to perform soft catching operations. We note that, the output of both these subcontrollers is the demanded magnetic force to be applied on the armature. A purposely designed algorithm is implemented into the Force - To - Currents (FTC) block in order to link the outer and the inner control loop. This block transforms the demanded magnetic force be applied to theinto a pair of feasible reference coil currents to be tracked by using the Coil Current Controller (block CCC). There exists an additional block, the Open-loop Current Pulses (OCP) block, which provides directly the reference set point for the coil currents to the inner current control loop, in order to perform other valve

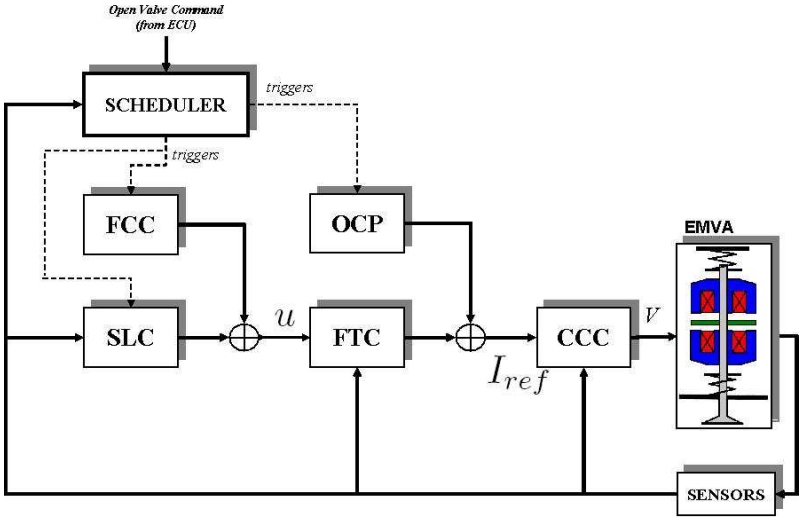

Figure A.1.: Block scheme of the EMVA control unit.

operations. Control blocks FCC, SLC and OCP are synchronized by a scheduler that is a function of the Open Valve Command signal and of the valve state.

In what a follows some details about the CCC strategy (CCC block) and the FTC inverse algorithm (FTC block) will be given. Further details on the supervisor policy, OCP block and on SLC block can be found in [37].

A.1.1. Coil Current Controller

The *Coil Current Controller* (CCC) block in Fig. A.1 regulates the currents in the coils to a desired current vector $I_{ref}(t) = [i_{u_d}(t)\ i_{l_d}(t)]^T$. To achieve this control task, the multi-hysteresis control strategy proposed in [37] has been implemented. The control algorithm is based on a double band hysteresis to reduce high switching frequencies. Schematics of the CCC block is depicted in Fig. A.2(a). The first band, termed *Fast*, controls rapid transients while the second one, termed *Slow*, controls steady state currents. Denoting with $H(e; V_{min}, V_{max}, e_{thr})$ the hysteresis function in Fig. A.2(b), where the error e is the argument, $\pm e_{thr}$ are the symmetric switching thresholds, and V_{min} and V_{max} are the minimum and maximum control voltages, respectively, the multi-hysteresis controller for each coil can be described as:

$$V = \begin{cases} H_F(e) & \text{if} \quad \dfrac{di_d}{dt} \neq 0 \text{ or } |e| > e_{thr_f} \\ H_S(e) & \text{if} \quad \dfrac{di_d}{dt} = 0 \text{ and } |e| \leqslant e_{thr_f} \end{cases}, \tag{A.1}$$

where V is the coil voltage, $e = i_{ref} - i_L$ is the current tracking error, i_{ref} is the reference coil current to be tracked and i_L is the measured load current, $H_F(e) = H(e; -V_F, V_F, e_{thr_f})$ and $H_S(e) = H(e; 0, V_S, e_{thr_s})$ are the fast and slow hysteresis functions respectively, with V_F, V_S, e_{thr_f} and e_{thr_s} being control parameters to be properly tuned.

Note that, the H_F controller uses a high bipolar control action, $V = \pm V_F$, to regulate the current, while H_S drives the coil by imposing a low control voltage, $V = V_S$ with $V_S \ll V_F$, or $V = 0$ (free

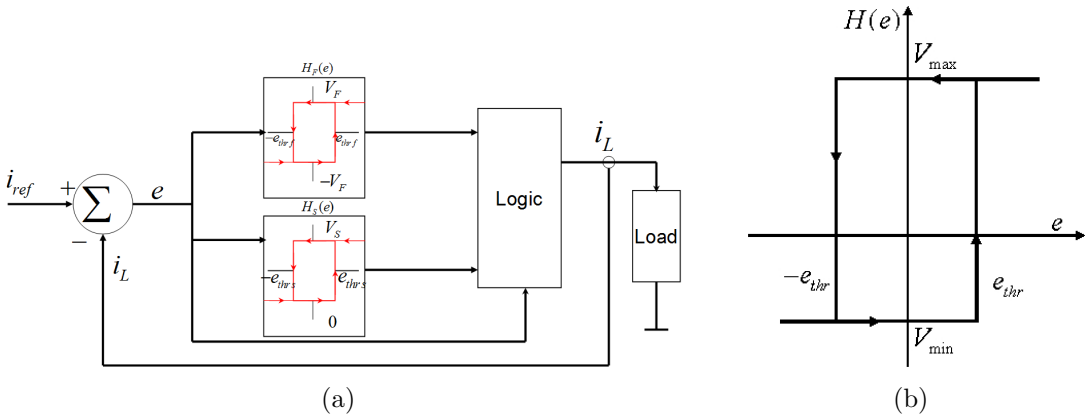

Figure A.2.: Coil currents controller: a) Multi-Hysteresis control scheme; b) Hysteresis control function.

evolution). For further details on the control logic, see [39].

Notice that, by means of this multi-hysteresis strategy, the chattering frequency of the control action, unavoidable with switching based control strategies, decreases with respect to a single hysteresis control approach. Hence, the heat produced in the power electronic circuit and in the materials (eddy-currents) reduces, increasing the efficiency of the electromagnet.

A.1.2. Force To Current algorithm

The *Force-To-Current* block in Fig. A.1 has the task to transform the output $u(t)$ of the outer controllers (SLC and FCC) in the desired current vector $I_{ref}(t) = [i_{u_d}(t)\ i_{l_d}(t)]^T$ to be fed into the CCC.

Let us $F_{M_d} = u(t)$ be the desired magnetic force. From a mathematical viewpoint, the problem consist on calculating the inverse of the magnetic force function $F_M(i_u, i_l, h)$ with respect to i_u and i_l for each h position.

Assuming that the the effect due to the mutual interaction between coils is negligible (see [37] for further details), by considering that one magnet at time is enabled (as it is in normal working conditions) and by taking into account the symmetry of the actuators, the problem is to get the current from a given desired force, say F_d and then derive the desired coil currents according to the scheme in Fig. A.3(a). More in detail, when the armature has to be attracted by the upper magnet ($F_d < 0$) then $i_{u_d} := F^{-1}(|F_d|, h)$ and $i_{l_d} := 0$. Dually, when the armature has to be attracted by the lower magnet ($F_d > 0$) then $i_{l_d} := F^{-1}(F_d, g_{\max} - h)$ and $i_{u_d} := 0$. The reader can refer [37] for further details. Here we remark that for the results of this algorithm are stored into a lookup-table for different values of the air gap g and of the required magnetic force F_d. Fig. A.3(b) shows the iso-force curves as a function of the air gap g and parameterized with respect to the required force F_d.

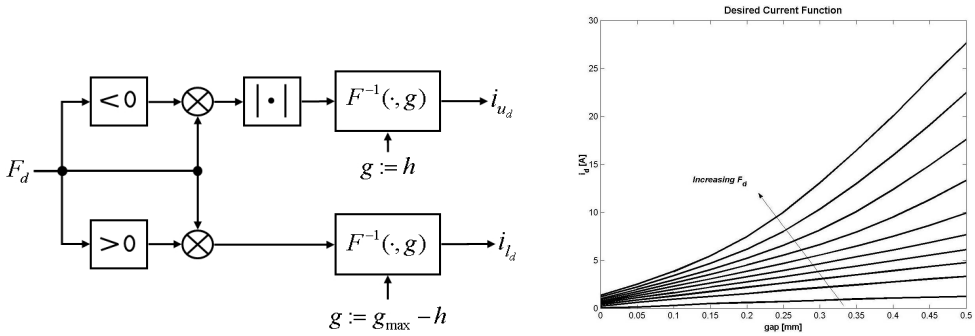

(a) (b)

Figure A.3.: Force To Current (FTC) algorithm: a) block scheme generating the two desired coil currents at a given position h from a desired Magnetic force F_d; c) Desired coil current vs air gap for different reference magnetic force

APPENDIX B

NONLINEAR DYNAMICS ANALYSIS FOR EMVA AT KEY-ON

All truths are easy to understand once they are discovered; the point is to discover them.

(Galileo Galilei, 1564–1642.)

This appendix describes the nonlinear dynamics analysis for the EMVA system at the Key-on.

B.1. Analysis of the friction-induced equilibrium set

In this section, we investigate the existence of the equilibrium set detected numerically in regions I and II of the bifurcation diagram, for $\alpha < F_s$ (see Fig. 4.4). Substituting the friction model (3.3), and the expression of the control action (4.10) into (3.1), we can describe the closed-loop dynamic behavior of the EMVA, as:

$$\dot{x} = \begin{cases} F_1(x, \alpha), & H(x) > 0, \\ F_2(x, \alpha), & H(x) < 0, \end{cases} \tag{B.1}$$

with

$$F_1(x,\alpha) = \begin{pmatrix} v \\ -\frac{k}{m}(h-h_{eq}) - \frac{F_c+(F_s-F_c)e^{-v_s v}+\sigma v}{m} + \frac{\alpha}{m} \end{pmatrix}, \tag{B.2}$$

$$F_2(x,\alpha) = \begin{pmatrix} v \\ -\frac{k}{m}(h-h_{eq}) - \frac{-(F_c+(F_s-F_c)e^{v_s v})+\sigma v}{m} - \frac{\alpha}{m} \end{pmatrix}, \tag{B.3}$$

where $x \in \mathbb{R}^2 := [h,\, v]^T$ is again the state vector; $\alpha \in \mathbb{R}^+$ is the control gain and $\Sigma := \{x \in \mathbb{R}^2 | H(x) = v = 0\}$ is the switching manifold. Furthermore, the armature is supposed to start lying on the switching surface $H(x) = 0$, namely $x(0) = [h_{eq},\, 0]^T$.

Note that each vector field F_1 and F_2 is smooth in both the state x and the parameter α, and for $\alpha \neq F_s$, they are discontinuous on the boundary Σ :

$$F_1(x,\alpha) - F_2(x,\alpha) = \begin{bmatrix} 0 \\ \frac{2}{m}(\alpha - F_s) \end{bmatrix} \neq \begin{bmatrix} 0 \\ 0 \end{bmatrix}. \tag{B.4}$$

From the above considerations, it is apparent that the analysis of the closed loop system must be carried out in the context of Filippov systems [78]. Specifically, we have to study the behavior of the system when the trajectory x is sliding on manifold Σ.

Following *Utkin 's equivalent control method* [29,131], the system can evolve according to the sliding vector field F_{12} given by:

$$F_{12} = \frac{F_1 + F_2}{2} + \frac{F_2 - F_1}{2}\beta(x). \tag{B.5}$$

where:

$$\beta(x) = -\frac{H_x F_1 + H_x F_2}{H_x F_2 - H_x F_1}, \tag{B.6}$$

with $H_x = \frac{dH}{dx}$.

From the definition of $H(x)$, we have $H_x = [0\ \ 1]$. Substituting (B.2) and (B.3) into (B.6), we have the following general expression for the equivalent control β:

$$\beta = \frac{2k(h-h_{eq}) + (F_s - F_c)(e^{-v_s v} - e^{v_s v}) + 2\sigma v}{2F_c + (F_s - F_c)(e^{-v_s v} + e^{v_s v}) - 2\alpha}. \tag{B.7}$$

Now, evaluating β on the sliding surface Σ, where $v = 0$, we easily obtain:

$$\beta(h) \triangleq \beta(h,v)|_{v=0} = \frac{k(h-h_{eq})}{(F_s - \alpha)}, \quad \forall \alpha < F_s. \tag{B.8}$$

From the above expression, since $-1 \leq \beta(h) \leq 1$, we can explicitly define the sliding region in terms of the control gain α, as:

$$\widehat{\Sigma} := \{x \in \Sigma | \quad h_{eq} - \frac{F_s - \alpha}{k} \leq h \leq h_{eq} + \frac{F_s - \alpha}{k}\}. \tag{B.9}$$

This confirms that the sliding region $\widehat{\Sigma}$ tends to shrink as the value of α increases according to the numerical observations (see Figs. 4.5, 4.7 and 4.8).

Now, we can analyze the dynamics of the system in the sliding region, by evaluating vector fields F_1 and F_2 in (B.3) and the equivalent control β in (B.8) for $x \in \widehat{\Sigma}$, and then substituting their expressions in to the definition of the sliding vector field (B.5). After simple algebraic computation, it is easy to prove that, in the domain $\widehat{\Sigma}$, F_{12} coincides with the null vector and, as a consequence, each armature position h belonging to region (B.9) is an equilibrium position for the EMVA system as expected (for $0 \leq \alpha < F_s$).

B.2. Limit cycles analysis

In this section is shown how the existence of limit cycles detected numerically can be accounted for by using a describing function approach [13, 79]. To this aim, the closed loop system, obtained when the open loop system (3.1) (see Fig. 3.5(b)) is controlled by the Key-on controller in (4.10) can be written as [31]:

$$\begin{cases} m\ddot{h} + f_f(\dot{h}) + k(h - h_{eq}) = u, \\ u = \alpha \text{sgn}(\dot{h}). \end{cases} \tag{B.10}$$

By setting $x = h - h_{eq}$, $v = \dot{h}$, $w_n = \sqrt{\frac{k}{m}}$, $\zeta = \frac{\sigma}{2\sqrt{mk}}$, $b = \frac{1}{m}$, and rearranging the control and friction terms in (3.1) and (3.3), the resulting closed loop system can be rewritten as the feedback connection (see Fig. B.1(a)) of two passive systems whose state space representation is

$$\begin{cases} \dot{\mathbf{x}} = \mathbf{A}\mathbf{x} + \mathbf{B}\hat{u} \\ y = \mathbf{C}\mathbf{x} \\ \hat{u} = -\psi(y, \alpha), \end{cases} \tag{B.11}$$

where $\mathbf{x} = [x\ v]^T$ is the state vector, $\mathbf{A} = [0\ 1; -w_n^2\ -2\zeta w_n]$ is the state matrix, $\mathbf{B} = [0\ b]^T$ is the input matrix, $\mathbf{C} = [0\ 1]$ is the output matrix and $\psi(v, \alpha) : \mathbf{R} \times \mathbf{R}^+ \to \mathbf{R}$ is a time-invariant memoryless locally Lipschitz nonlinear function with a discontinuity at $v = 0$, described by

$$\psi(v, \alpha) = \begin{cases} -\alpha + \mu_c + \mu_{sc} e^{-\mu_e v} & \text{if } v > 0, \\ \{\alpha - \mu_s, \mu_s - \alpha\} & \text{if } v = 0, \\ \alpha - \mu_c - \mu_{sc} e^{\mu_e v} & \text{if } v < 0, \end{cases} \tag{B.12}$$

where $\mu_{sc} = \mu_s - \mu_c$ being $\mu_s \geq \mu_c$, with $\mu_s = F_s$, $\mu_c = F_c$ and $\mu_e = \frac{1}{v_s}$.

The nonlinearity $\psi(v, \alpha)$ is depicted in Fig. B.1(b) for different values of the control parameter α.

B.2.1. Describing function

The key idea behind our approach is to consider the system as the feedback interconnection of a linear system with a nonlinear term $\psi(v, \alpha)$ depicted in Fig. B.1(b), which involves the control parameters, and then to study the onset of oscillations using a describing function approach [73]. The describing function method has also been suggested as a viable tool to characterize bifurcations of nonlinear systems [13, 79]. In this work we are interested in deriving the describing function for the nonlinearity (B.12) with the aim of characterizing the coexistence of periodic solutions and detecting their bifurcations points. The derivation is as follows.

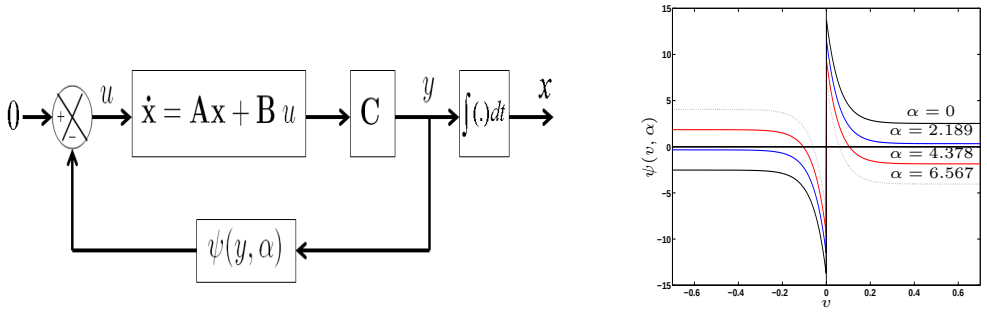

(a) (b)

Figure B.1.: Unforced system under study: (a) Feedback connection to be studied through describing function analysis; (b) Nonlinearity $\psi(v, \alpha)$ for different values of control parameter α.

Under the assumption that there exists a self-sustained oscillation of amplitude a with frequency w (rad/seg), and considering the band-pass feature of the linear system, the balance harmonic equation

$$G(jw)\Psi(a,\alpha) + 1 = 0 \tag{B.13}$$

must hold, yielding the two equations:

$$\mathrm{Re}(G(jw))\Psi(a,\alpha) + 1 = 0 \quad and \quad Im(G(jw))\Psi(a,\alpha) = 0, \tag{B.14}$$

where $G(jw)$ is the transfer function of the linear system in (B.11) and $\Psi(a,\alpha)$ is the describing function for the nonlinearity (B.12) evaluated at the first harmonic $a\sin(wt)$. As $\psi(v,\alpha)$ is an odd function, defining $\theta := wt$, $\Psi(a,\alpha)$ can be given as [73]:

$$\Psi(a,\alpha) = \frac{2}{\pi a}\int_0^{\pi} \psi(a\sin(\theta))\sin(\theta)d\theta. \tag{B.15}$$

Now, by considering the odd symmetry of the terms in (B.15) and the nonlinear expression (B.12) for $v > 0$, the integral (B.15) can be recast as:

$$\Psi(a,\alpha) = \frac{4}{\pi a}\left[\mu_c - \alpha + \mu_{sc}\int_0^{\pi/2} e^{-\mu_e a\sin(\theta)}\sin(\theta)d\theta\right], \tag{B.16}$$

that can be solved explicitly giving:

$$\Psi(a,\alpha) = \frac{4}{\pi a}\left[\mu_c - \alpha + \frac{\pi}{2}\mu_{sc}(L_{-1}(a\mu_e) - I_1(a\mu_e))\right], \tag{B.17}$$

where $L_n(z)$ is the Modified Struve function [1] of order $n = -1$, and $I_n(z)$ is the modified Bessel

[1] $L_n(z) = \frac{2\left(\frac{1}{2}z\right)^n}{\sqrt{\pi}\Gamma\left(n+\frac{1}{2}\right)}\int_0^{\pi/2}\sinh(z\cos\theta)\sin^{2n}\theta d\theta$, from page 498 in [3], where $\Gamma(n)$ is the gamma function.

function of the first kind [2] with $n = 1$. Here, $\Psi(a, \alpha) : R^+ \times R^+ \to R$ is the describing function for different values of the control parameter α, whose level curves for different values of α are depicted in Fig. B.2(b).

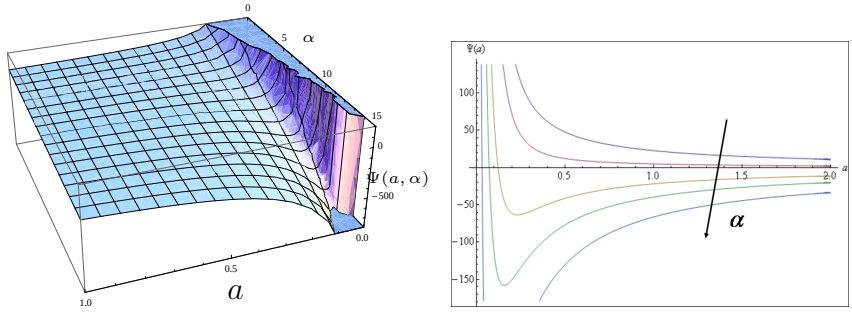

(a) (b)

Figure B.2.: Describing function graphical analysis: (a) 3D plot for function $\Psi(a, \alpha)$; (b) Level curves for function $\Psi(a, \alpha)$ for different values of parameter α.

B.2.2. Limit cycles analysis through describing function

From (B.14), the frequency of the oscillations $w = w_n$ can be found by requiring that $\text{Im}(G(j\omega)) = 0$ while the amplitude of the oscillations can be computed by looking for the pair α and a such that:

$$\text{Re}(G(jw))|_{w=w_n} \Psi(a, \alpha) + 1 = 0 \quad \Rightarrow \quad b\Psi(a, \alpha) + 2\zeta w_n = 0;\ a > 0. \tag{B.18}$$

Hence, by replacing (B.17) into (B.18), we get:

$$\eta(a, \alpha) := \frac{\Delta}{=} 4b\left[\mu_c - \alpha + \frac{\pi}{2}\mu_{sc}(L_{-1}(a\mu_e) - I_1(a\mu_e))\right] + 2\zeta w_n \pi a = 0, \quad a > 0,\ \alpha > 0. \tag{B.19}$$

Equation (B.19) is solvable for a in a given range of α with the other parameters, e.g μ_c, μ_{sc}, μ_e and ζ, fixed to their nominal values so that it is possible to obtain the velocity limit cycle amplitude a for different parameters of interest. In so doing, by varying the control parameter α, there exist two solutions, say $a^S(\alpha)$ and $a^U(\alpha)$ for stable and unstable limit cycles of valve velocity.

Finally, we remark that solutions a^S and a^U obtained through describing function analysis correspond to the amplitude of the steady state solution for velocity signal, namely $v_\infty(t)$, and here we use those results to predict the stationary behavior in the system position, namely $x_\infty(t)$. Since $v_\infty(t) = a\sin(w_n t)$, here we derive $x_\infty(t) \stackrel{\Delta}{=} \int_{-\infty}^{t} v_\infty(\tau)d\tau = -\frac{a}{w_n}\cos(w_n t)$. Hence, by considering the variable change used in Sec. B.2, the extremum oscillation points for coexisting position limit cycles are written as:

$$h_\Pi^S(\alpha) = \left\{heq \pm \frac{1}{w_n}a | a \in a^S(\alpha)\right\} \quad \text{and} \quad h_\Pi^U(\alpha) = \left\{heq \pm \frac{1}{w_n}a | a \in a^U(\alpha)\right\}. \tag{B.20}$$

[2] $I_n(z) = \frac{1}{\pi}\int_0^\pi e^{z\cos(\theta)}\cos(n\theta)d\theta$ from page 376 in [3]

B.2.3. Results

Results are obtained for system parameter values reported in table 3.1. Specifically, when α is varied, Fig. B.3(a) shows different level curves for $\eta(\alpha, a)$ (B.19) as a function of a for different values of control parameter α. Note that a solution $a = \bar{a}$ can be found only if $\alpha \geq 4.708$. Thus for $\alpha < 4.708$, the closed-loop EMVA does not exhibit periodic motion, while for $\alpha \in]4.708,\ F_s[$, the system presents two coexisting feasible solutions, $a^S(\alpha)$ and $a^U(\alpha)$. Thus the well known saddle node bifurcation of limit cycles [120] is expected to occur at $\alpha = 4.708$. Moreover, notice how the limit cycle corresponding to $a^U(\alpha)$ approaches zero as α increases, and then it becomes zero ($a^U(\alpha) = 0$) at $\alpha = F_s$. For $\alpha > F_s$, the amplitude a^S of the other limit cycle grows, while the solution a^U becomes negative and therefore not admissible. This corresponds to a potential subcritical Hopf bifurcation event [120].

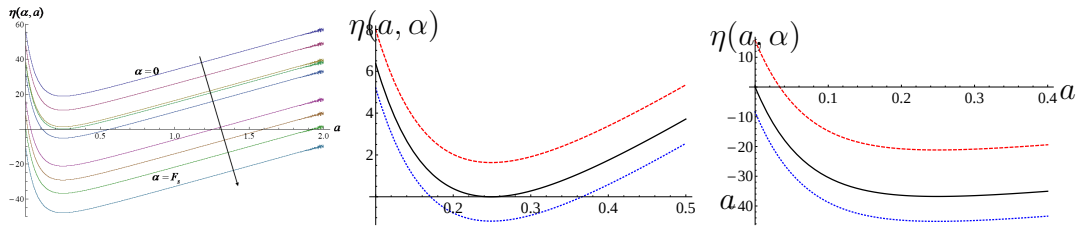

(a) (b) (c)

Figure B.3.: Analysis of limit cycles: (a) Different level curves for $\eta(a, \alpha)$ when α is varied; (b) The tangency mechanism in function $\eta(\alpha, a)$ that describes the existence of a saddle node of cycles bifurcation point; (c) The zero crossing in function $\eta(\alpha, a)$ describes the no existence of limit cycles (since $a > 0$), thus this mechanism describes the existence of subcritical Hopf bifurcation phenomena.

B.2.4. Simulation results

Our analytical prediction can now be compared (see Fig. B.4) with numerical results obtained via a closed loop bifurcation diagram computed using a brute force continuation method. At $\alpha = 4.709(\text{N})$, the oscillation amplitude of the velocity limit cycle are: $a^S = a^U = 0.248(\text{m/s})$ that was characterized as SNC bifurcation point, and at $\alpha = F_s = 13.9(N)$ a SH bifurcation was identified as expected. Also, as predicted, between these two bifurcation points there exist two coexisting solutions for equation (B.19) in the range $\alpha \in [4.709, 13.9]$.

A comparison of the numerical bifurcation diagram with the analytical expressions obtained via the describing function approach is shown in Fig. B.4, where a remarkable agreement between analysis and numerics can be observed.

Trough obtained describing function, here it is studied the effect on the limit cycle branches (B.20) and the variation of bifurcation points caused by the single variations of parameter in the nonlinear friction force (3.3). The results are depicted in Fig. B.5 where for each case of analysis three bifurcation diagrams are obtained in order to compare the bifurcation diagram for variation in the order of $\pm 50\%$ respect to the nominal one. For instance, note that stable branches for limit

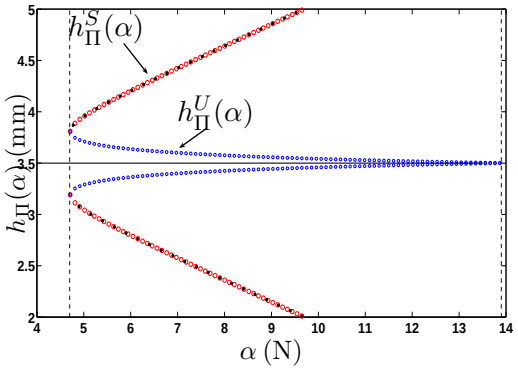

Figure B.4.: Comparison between numerical solutions and those ones obtained through describing function analysis;

cycles depends strongly on friction force shape for large velocities, being parameter σ and F_c the main responsible of limit cycle variations (see Figs. B.5(b) and); by the other hand, unstable solutions depends strictly on the nonlinearity shape for low values of velocity. Note also that, while SNC bifurcation takes place at different points when parameters vary, which corresponds to high sensitivity to parameter variation, while the SH bifurcation remains at the same point, being affected only by the discontinuity of the friction force, that is, at $\alpha = F_s$. Thus, SH bifurcation point is sensitive only to parameter F_s as Fig. B.5(f) shows.

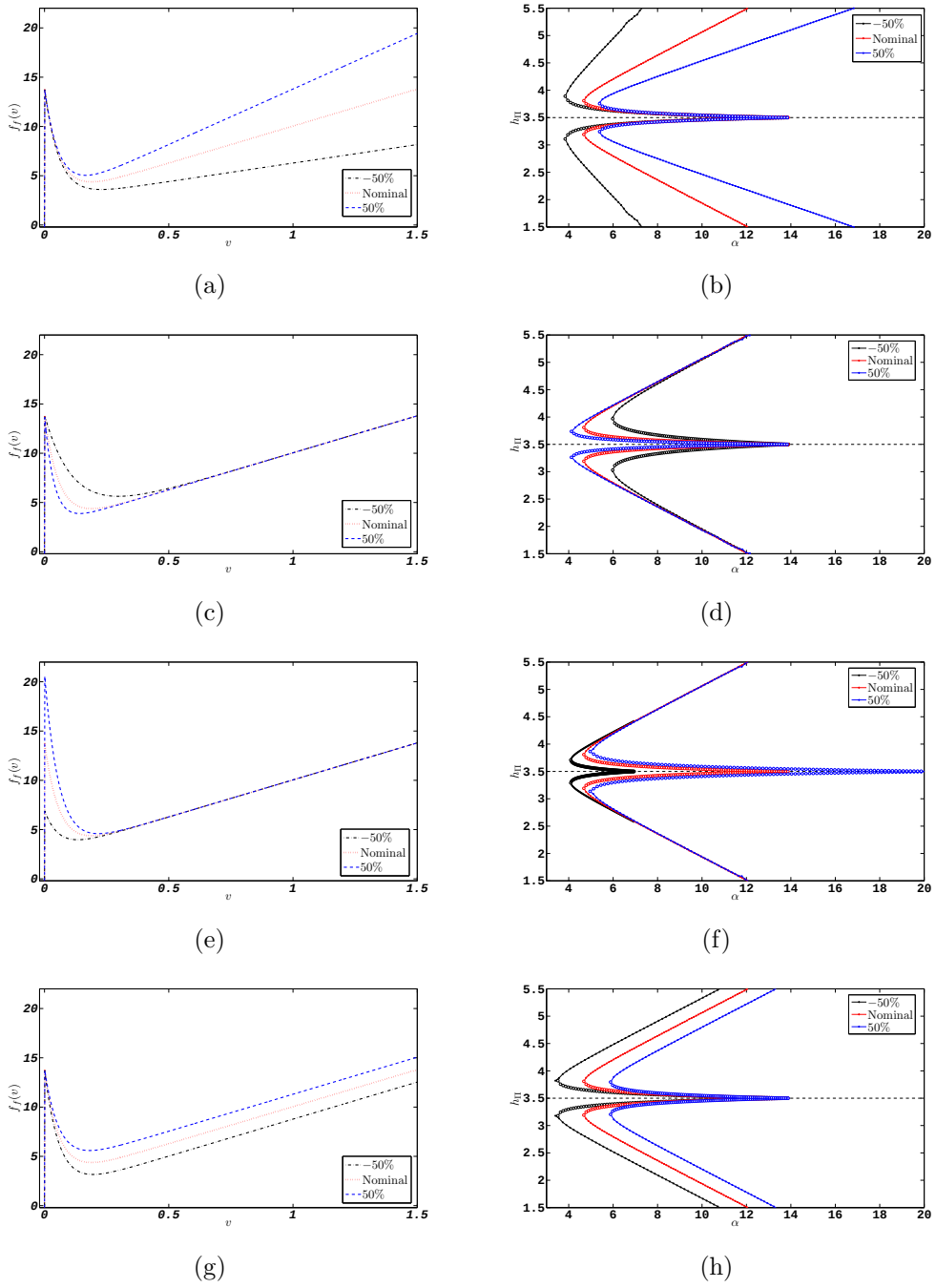

Figure B.5.: Variation of bifurcation diagrams and bifurcation points (SN) and (SH) for single parameter variation in friction model $F_f(v)$, when considering a variation range of $\pm 50\%$ respect to nominal values: a)-b) varying σ; c)-d) varying v_s: e)-f) varying F_s; g)-h) varying F_c.

APPENDIX C

FURTHER RESULTS

That's one small step for a man, one giant leap for humankind (Jul. 21 1969).

(Neil Armstrong, 1930-....)

This Appendix describes other research results obtained on the experimental validation of switched adaptive controllers for Piece-Wise Affine systems, which were obtained in the laboratories from University of Naples Federico II.

Experimental Implementation and Validation of a Novel Minimal Control Synthesis Adaptive Controller for Continuous Bimodal Piecewise Affine Systems

Mario di Bernardo[a], Carlos Ildefonso Hoyos Velasco[a], Umberto Montanaro[b], Stefania Santini[a]

[a]*Department of Systems and Computer Engineering, University of Naples Federico II, Italy*
[b]*Istituto Motori, National Research Council, Naples, Italy*

Abstract

This paper presents the first digital implementation of a novel model reference adaptive scheme for the control of continuous bimodal piecewise affine systems. The algorithm is based on the minimal control synthesis algorithm, originally developed as a MRAC for smooth systems. The resulting adaptive algorithm is a switched feedback controller able to cope with uncertain continuous PWA systems. The analogue continuous-time control law is implemented by using a digital low-cost commercial microcontroller. The aim is to control a piecewise-linear electrical circuit. The experimental validation process is made challenging by the presence of measure uncertainties, noise, quantization errors, unmodelled nonlinear dynamics and computational delays. Experiments confirm the effectiveness of the controller to cope with switching in the circuit dynamics, establishing the strategy as a viable control tool. Nevertheless, the experimental analysis provides a first insight into the robustness of the algorithm.

Keywords: piecewise linear controllers; model reference adaptive control; validation; implementation; discontinuous control

1. Introduction

Many systems and devices in a wide range of different applications can be effectively modeled by piecewise affine (PWA) sets of ODEs changing configuration according to the phase space region (or domain) visited by their trajectories. Examples include mechanical systems with friction and/or backlash (Hensen, 2002), (Vasak et al., 2004), switching power converters in Electronics (Geyer et al., 2005), (Tahami et al., 2006), genetic network (Hernandez et al., 2004) or irregular heartbeats (Keener and Sneyd, 1988) in biology, complementarity and hybrid systems (Brogliato, 2003), (Brogliato and Heemels, 2009), (Angenent et al., 2010), (Rodrigues and How, 2003).

Much research effort has been focused on synthesizing strategies for controlling PWA systems (e.g. (Rodrigues and How, 2003), (Almer et al., 2010),(Mariethoz et al., 2008), (Bemporad and Morari, 1999),(Lazar et al., 2008), (Pang and Grimble,

2010) and references therein). For example, the control of DC-DC converters using model predictive control is discussed in (Mariethoz et al., 2008), (Almer et al., 2010), while Lyapunov-based approaches are used in (Lazar et al., 2008). Surprisingly, few results are available in the literature on Model Reference Adaptive Controllers (MRAC) for this class of systems. Recently, novel hybrid model reference adaptive control strategies for piecewise affine continuous systems have been presented in the literature (di Bernardo et al., 2010b), (Tao and Sang, 2010). The approach in (di Bernardo et al., 2010b) is based on using a novel extension of passivity theory to switched systems (Zhao and Hill, 2008), to formulate a consistent proof of global asymptotic tracking. The resulting hybrid control strategy consists of a feedforward and a feedback action whose gains switch according to the phase space regions visited by the plant and reference model. The strategy allows for the reference model to be smooth or piecewise-affine and it is shown analytically to guarantee asymptotic tracking of the reference model trajectories without requiring a priori knowledge of the plant matrices. The control strategy is the first extension to switching plants of the family of Minimal Control Synthesis (MCS) adaptive controllers (Hodgson and Stoten, 1996) which is a particularly viable MRAC approach in the presence of unknown and uncertain plant matrices (Stoten and H.Benchoubane, 1990). MCS has been successfully applied to a vast number of real applications (see, for example, automotive electro-mechanical system (di Bernardo et al., 2010a) and DC motor (di Bernardo et al., 2007b)).

Despite being analyzed theoretically, the novel MRAC scheme for PWA systems has been never validated experimentally. When dealing with the synthesis of novel control strategies, this is a fundamental and crucial step of the design process to test the robustness and the performance of the closed-loop behavior (see, for example, Rupp and Guzzella (2010), Ishitobi et al. (2010)). The experimental validation process is hard because of measure uncertainties, the unavoidable presence of noise, quantization errors, unmodelled nonlinear dynamics, measurement and computation delays. Also, the challenges of implementing a fairly complex algorithm on a cost effective microcontroller must be properly investigated. Issues include the digital implementation of the overall control algorithm, limited on-chip memory and computational delays.

The aim of this paper is to discuss the technological implementation of the hybrid model reference adaptive algorithm presented in (di Bernardo et al., 2010b). The control of a piecewise smooth electrical circuit, which was presented in (Heemels et al., 2002), is taken as a representative example. The control objective is to make the hybrid circuit follow a smooth reference system.

Experimental results reported in this paper show the effectiveness of the controller when implemented via the digital microcontroller Microchip PIC24FJ128GA010 (Microchip Technology Inc., 2006) (program memory of 128 kB, SDRAM of 8 KB).

Experimental results provided here give also a first insight into the algorithm robustness, in particular with respect to unavoidable uncertainties in the switchings between one mode and the other during the tests.

The rest of the paper is outlined as follows. The specific control problem and its mathematical formulation is described in Section 2.1, while the switched control

algorithm is presented in Section 2.2. Details on the piecewise smooth electrical circuit chosen as representative testbed example are provided in Section 3, preliminary numerical analysis is illustrated in Section 4, while the description of the set-up used to perform the experimental analysis is presented in Section 5. The effectiveness of the novel adaptive switched control scheme is shown by experimental results in Section 6. Finally, conclusions are drawn in Section 7. Further mathematical details can be found in Appendix A and Appendix B.

2. MRAC for continuous bimodal piecewise affine systems

2.1. Problem statement and definitions

Suppose that the state space of the plant of interest, say $\Omega \subseteq \mathbb{R}^n$, is partitioned into two polyhedral cells

$$\begin{aligned} \Omega_0 &\triangleq \left\{ x \in \mathbb{R}^n : H^T x + h \leq 0 \right\}, \\ \Omega_1 &\triangleq \left\{ x \in \mathbb{R}^n : H^T x + h \geq 0 \right\}, \end{aligned} \tag{1}$$

defined by a generic hyperplane (or *switching manifold*) given by:

$$\Sigma : H^T x + h = 0, \tag{2}$$

with $H \in \mathbb{R}^n$ and $h \in \mathbb{R}$ being constant vectors assumed to be known.

We assume the plant to be described by an n-dimensional bimodal PWA system of the form:

$$\dot{x}(t) = A_i x(t) + Bu(t) + B_i, \quad \text{if} \quad x \in \Omega_i, \quad i = 0, 1, \tag{3}$$

where $x \in \mathbb{R}^n$ is the state vector, $u \in \mathbb{R}$ is the scalar input and the matrices A_i, B and B_i, $i = 0, 1$, are assumed to be given in control canonical form as:

$$A_i = \begin{bmatrix} 0 & 1 & \cdots & 0 \\ 0 & 0 & \ddots & \vdots \\ \vdots & \vdots & & 1 \\ a_i^{(1)} & a_i^{(2)} & \cdots & a_i^{(n)} \end{bmatrix}, \quad B = \begin{bmatrix} 0 \\ 0 \\ \vdots \\ b \end{bmatrix}, \quad B_i = \begin{bmatrix} 0 \\ 0 \\ \vdots \\ b_i \end{bmatrix}, \quad i = 0, 1, \tag{4}$$

with $b > 0$. (As shown in (di Bernardo et al., 2011) this is not too restrictive as many generic PWA Continuous (PWAC) systems can be transformed into such a form.)

The problem is to find an adaptive piecewise-smooth continuous feedback control law $u(t)$ to ensure that the state variables of the plant track with a bounded error (or asymptotically) the states, say $\widehat{x}(t)$, of a reference model, independently from their initial conditions.

Here, we assume that the reference model can be either a smooth LTI or a bimodal PWA system of the form:

$$\dot{\widehat{x}}(t) = \widehat{A}_j \widehat{x}(t) + \widehat{B} r(t) + \widehat{B}_j, \quad \text{if} \quad \widehat{x} \in \widehat{\Omega}_j, \quad j = 0, 1, \tag{5}$$

where $\widehat{x} \in \mathbb{R}^n$, $\widehat{x}(0) = \widehat{x}_0$, $r \in \mathbb{R}$ and the switching manifold $\widehat{\Sigma}$ is:

$$\widehat{\Sigma} : \widehat{H}^T \widehat{x} + \widehat{h} = 0, \tag{6}$$

for some $\widehat{H} \in I\!R^n$ and $\widehat{h} \in I\!R$, so that the state space is divided into the following polyhedral cells:

$$\begin{aligned} \widehat{\Omega}_0 &\triangleq \left\{ \widehat{x} \in I\!R^n : \widehat{H}^T \widehat{x} + \widehat{h} \leq 0 \right\}, \\ \widehat{\Omega}_1 &\triangleq \left\{ \widehat{x} \in I\!R^n : \widehat{H}^T \widehat{x} + \widehat{h} \geq 0 \right\}. \end{aligned} \tag{7}$$

Furthermore, the reference model defined in (5) is assumed to be well posed given the initial condition $\widehat{x}_0$.

We assume the matrices of the reference model are Hurwitz and in the companion form given by:

$$\widehat{A}_j = \begin{bmatrix} 0 & 1 & \cdots & 0 \\ 0 & 0 & \ddots & \vdots \\ \vdots & \vdots & & 1 \\ \widehat{a}_j^{(1)} & \widehat{a}_j^{(2)} & \cdots & \widehat{a}_j^{(n)} \end{bmatrix}, \quad \widehat{B} = \begin{bmatrix} 0 \\ 0 \\ \vdots \\ \widehat{b} \end{bmatrix}, \quad \widehat{B}_j = \begin{bmatrix} 0 \\ 0 \\ \vdots \\ \widehat{b}_j \end{bmatrix}, \quad j = 0, 1, \tag{8}$$

with $\widehat{b} > 0$.

Note that, without loss of generality it is possible to assume $\widehat{b}_0 = 0$. Since the matrix $\widehat{A}_0$ is Hurwitz, hence invertible, the affine transformation:

$$\widehat{z} = \widehat{x} + \widehat{A}_0^{-1} \widehat{B}_0, \tag{9}$$

is well-posed and can be applied to obtain a reference model equivalent to (5) without the affine term on the first equation ($\widehat{B}_0 = 0$).

Assumption 1. *The vector fields in* (3) *and* (5) *are supposed to be continuous across the phase-space boundaries, i.e. to be such that:*

$$\begin{cases} A_1 - A_0 = g B_e H^T, \\ B_1 - B_0 = g h B_e, \end{cases} \tag{10}$$

where $g \in I\!R$ is a constant and $B_e \in I\!R^n$ is defined as

$$B_e = \begin{bmatrix} 0 & \dots & 0 & 1 \end{bmatrix}^T. \tag{11}$$

Analogously, for the reference model it follows that:

$$\begin{cases} \widehat{A}_1 - \widehat{A}_0 = \widehat{g} B_e \widehat{H}^T, \\ \widehat{B}_1 - \widehat{B}_0 = \widehat{g}\widehat{h} B_e. \end{cases} \tag{12}$$

In what follows, we define the generic switching instant $t_{i,p}$ $(i = 0, 1)$ as the time instant when the i-th mode of the plant is activated at the p-th commutation and the generic switching instant $\widehat{t}_{j,q}$ $(j = 0, 1)$ as the time instant when the j-th mode of the reference model is selected at the q-th commutation.

Remarks

- Note that all entries on the last row of the plant matrices A_i, B_i, B and g are supposed to be unknown.
- The assumption of canonical form is not as restrictive as it may appear at first. For example, it is certainly satisfied by the large class of electro-mechanical systems modelled using a Lagrangian approach (Sontag, 1998).

2.2. Control Strategy

As detailed in (di Bernardo et al., 2010b) and (di Bernardo et al., 2008), the control problem described in Section 2.1 can be solved by means of the piecewise-smooth adaptive strategy described in this section.

Assumption 2. *There exist matrices $C_{ej} \in I\!R^{n\times 1}$ $(j = 0, 1)$ such that the following switching state-dependent PWL system*

$$\dot{z} = \widehat{A}_j z + B_e \xi, \qquad \text{if } z \in \widehat{\Omega}_j, \quad j = 0, 1, \tag{13}$$

$$y = C_{ej} z, \tag{14}$$

is passive according to the notion of passivity given in (Zhao and Hill, 2008).

For the sake of readability, the notion of passivity is also reported in Appendix A.

Note that the above assumption is not restrictive, since the reference model is usually chosen by designers and often corresponds to the conventional choice of an asymptotically stable LTI reference model in the case of smooth systems.

Passivity of a generic PWA can be also verified off-line according to the following Lemma.

Lemma 1. *If there exist some positive real constants ε_0, ε_1, θ_0^1, θ_1^0 and γ and two positive definite symmetric matrices P_0, $P_1 \in \mathbb{R}^{n\times n}$ that satisfy the following matrix inequalities*

$$P_0\widehat{A}_0 + \widehat{A}_0^T P_0 + 2\varepsilon_0 P_0 B_e B_e^T P_0 \leq 0, \tag{15}$$

$$P_1\widehat{A}_1 + \widehat{A}_1^T P_1 + 2\varepsilon_1 P_1 B_e B_e^T P_1 \leq 0, \tag{16}$$

$$P_1\widehat{A}_0 + \widehat{A}_0^T P_1 + \frac{2}{\gamma^2\theta_1^0} P_1 B_e B_e^T P_1 + \frac{1}{2}\theta_1^0 P_0 B_e B_e^T P_0 \leq 0, \tag{17}$$

$$P_0\widehat{A}_1 + \widehat{A}_1^T P_0 + \frac{2}{\gamma^2\theta_0^1} P_0 B_e B_e^T P_0 + \frac{1}{2}\theta_0^1 P_1 B_e B_e^T P_1 \leq 0. \tag{18}$$

where $\widehat{A}_0$ and $\widehat{A}_1$ are the matrices of the reference model (5), then system (13)-(14) is passive when matrices C_{ej} $(j = 1, 2)$ are set as $C_{ej} = B_e^T P_j$.

See Appendix B for the proof of Lemma 1.

When Assumption 2 is satisfied, the following piecewise smooth feedback control law can be defined

$$u(t) = K_0(t)x(t) + K_1(t)\left(H^T x + h\right) + \widehat{K}_1(t)\left(\widehat{H}^T x + \widehat{h}\right) + K_R(t)r(t), \tag{19}$$

where,

$$K_R(t) = \alpha \int_0^t y_e(\tau)\, r(\tau)\, d\tau + \beta y_e(t)\, r(t), \quad K_R(0) = 0, \tag{20}$$

$$K_0(t) = \alpha \int_0^t y_e(\tau)\, x^T(\tau)\, d\tau + \beta y_e(t)\, x^T(t), \quad K_0(0) = 0, \tag{21}$$

$$K_1(t) = \begin{cases} \rho \int_{t_{1,p}}^t y_e(\tau)\left(H^T x(\tau) + h\right) d\tau, & \text{if} \quad x \in \Omega_1, \\ 0 \quad \text{otherwise}, \end{cases} \tag{22}$$

$$\widehat{K}_1(t) = \begin{cases} \rho \int_{\widehat{t}_{1,q}}^t y_e(\tau)\left(\widehat{H}^T x(\tau) + \widehat{h}\right) d\tau, & \text{if} \quad \widehat{x} \in \widehat{\Omega}_1, \\ 0 \quad \text{otherwise}, \end{cases} \tag{23}$$

with α, β and ρ being positive constants and

$$x_e \triangleq (\widehat{x} - x), \quad y_e \triangleq C_{ej} x_e \quad \text{if} \quad \widehat{x} \in \widehat{\Omega}_j \tag{24}$$

where the matrices C_{ej} $(j = 1, 2)$ are defined according to Assumption 2.

We can then state the following theorem.

Theorem 1. *Given system* (3) *and a reference model of the form* (5) *such that Assumptions 1 and 2 hold, the adaptive control law* (19) *guarantees that:*

A. the closed loop system is globally asymptotically stable if $B_0^T B_1 = 0$*;*

B. the asymptotic tracking error is bounded (i.e. there exists $m > 0$ *and* $t_1 > 0$*:* $\|x_e\| < m$ *for* $t > t_1$*) if* $B_0^T B_1 \neq 0$*.*

The proof of the Theorem can be found in (di Bernardo et al., 2010b). (A different MCS approach for multimodal PWA systems can be found in (di Bernardo et al., 2008).) Note that the stability of the closed loop system is proven by using the recent theory of passivity for switched systems (Zhao and Hill, 2008). The main idea is to show that the closed-loop system is composed by the feedback loop of two passive switched systems. Note that the feed-foward path is shown to be of the form (13), hence it is passive by assumption. An alternative MRAC controller for PWA plant was independently presented in (Tao and Sang, 2010).

Remarks

- The adaptation law presented in (19) consists of two gains K_R and K_0 that remain switched on whatever the modes in which the plant and reference model are evolving in, and some gains, K_1 and $\widehat{K}_1$, that are switched on only when the trajectories of the plant or reference model enter certain phase space cells. Notice that the smooth gains K_R and K_0 have the same structure of the classical MCS gains (Hodgson and Stoten, 1996).

- In (di Bernardo et al., 2010b) it has been proven that the closed loop system has degree of smoothness equal to 2 according to the definition in (di Bernardo et al., 2007a), hence it can exhibit only a finite number of switchings over any finite time interval (see (di Bernardo et al., 2010b) for further details).

- In many practical cases, the aim of the control action can be that of compensating the hybrid nature of the plant. In these situations, the control design presented above offers a simple and viable solution for this to be achieved by simply choosing a smooth reference model. In this case, our approach does not require the solution of the inequalities in (15)-(18), but simply the solution of the classical Lyapunov inequality $P\widehat{A} + \widehat{A}^T P < 0$ (where $\widehat{A}$ is the dynamic matrix of the smooth reference model).

- At the generic p-th commutation, the adaptive gain $K_1(t_{1,p})$ is initialized at the last value it assumed when the trajectory of the plant $x(t)$ last left region Ω_1 (or zero otherwise). Analogously, the adaptive gain $\widehat{K}_1$ at the generic q-th commutation, $\widehat{K}_1(\widehat{t}_{1,q})$, is initialized with the last value assumed by that gain when the trajectory $\widehat{x}(t)$ left the cell $\widehat{\Omega}_1$ (or zero otherwise). Mathematically the initial conditions of the adaptive gains are set as follows:

$$\widehat{K}_1(\widehat{t}_{1,q}) = \widehat{K}_1(\widehat{t}_{0,q-1}), \tag{25}$$
$$K_1(t_{1,p}) = K_1(t_{0,p-1}). \tag{26}$$

  Furthermore at the first transition from $\widehat{\Omega}_0$ to $\widehat{\Omega}_1$ the adaptive gain $\widehat{K}_1$ is set to zero, *i.e.* $\widehat{K}_1(\widehat{t}_{1,1}) = 0$; analogously, at the first commutation from Ω_0 to Ω_1, $K_1(t_{1,1}) = 0$.

- The condition $B_0^T B_1 = 0$ needed for asymptotic tracking is naturally verified in one of following generic cases:

  1. the dynamics of the plant is described by a piecewise linear system, i.e., when $B_0 = B_1 = 0$.
  2. There exists at least one polyhedral cell, say Ω_0, where the dynamics of the plant is described by a LTI system. In this case, without loss of generality, the model of the plant can be rewritten as in (3) with $B_0 = 0$.

3. Plant and reference model

The adaptive law discussed in this paper extends the Minimal Control Synthesis (Stoten and H.Benchoubane, 1990) approach to PWA bimodal systems and, thus, it relies on a minimal knowledge of the plant (only precise knowledge of the switching surface is required). Hence, it can be implemented easily without requiring time consuming experiments for the precise characterization of the system nonlinear dynamics.

For this reason an accurate mathematical model of the plant is not strictly necessary for control synthesis and its digital implementation. Nevertheless, for the

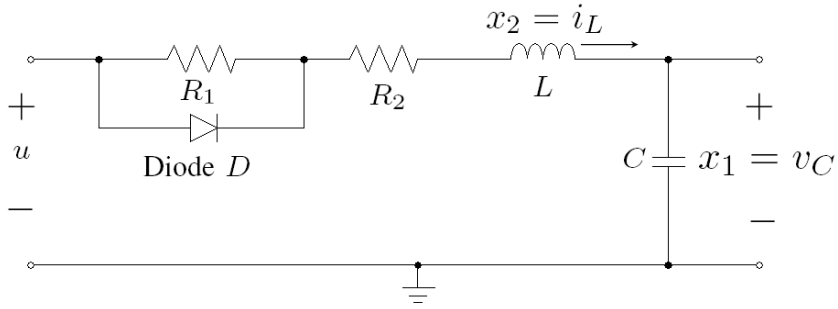

Figure 1: Plant schematic.

Table 1: System Parameter Values

Symbol	Component	Value	Unit
C	Capacitance (BSME6R3ELL102MJ20S)	$1 \cdot 10^{-3}$	F
L	Inductance (C&22R156C)	$15 \cdot 10^{-3}$	H
R1	Resistance 1 (PC5201J)	200	Ω
R2	Resistance 2	52.4	Ω
D	Schottky barrier diode (ROHM RB441Q-40)		
V_f	Forward voltage	0.2	V
r_d	approx. diode characteristic	0.25	Ω
ρ	control weight	50	-
α	control weight	1000	-
β	control weight	100	-
T_s	Sample Time	$4 \cdot 10^{-3}$	s
V_{ref}	Reference signal Amplitude	1	V
f	Reference signal frequency	1	Hz

sake of clarity and to emphasize the PWA nature of the plant and its open-loop dynamics, we present below its mathematical model.

To validate the new control scheme, a piecewise electrical circuit (Heemels et al., 2002) is used, consisting of a variable voltage source, a diode, two resistors, an inductor, and a capacitor (see Fig. 1 and Table 1 for the system schematics and parameter values). The circuit evolves through two different topologies (modes) depending on the (discrete) states of the diode characteristic ('on' or 'off'). (See Fig. 2 for the actual characteristic of the RB441Q-40 Schottky barrier diode.)

Representing the dynamic of the diode D with the common PWL modeling approach (see, for example, Sedra and Smith (2004)), where the real diode is replaced by the ideal diode in series with a voltage source V_f and resistor r_d, the circuit can be mathematically described by the following PWA model:

$$\dot{x} = \begin{cases} \begin{pmatrix} 0 & \frac{1}{C} \\ -\frac{1}{L} & -\frac{R_1+R_2}{L} \end{pmatrix} x + \begin{pmatrix} 0 \\ \frac{1}{L} \end{pmatrix} u \text{ if } x \in \Omega_0, \\ \begin{pmatrix} 0 & \frac{1}{C} \\ -\frac{1}{L} & -\frac{1}{L}\left(R_2 + \frac{R_1 r_d}{R_1+r_d}\right) \end{pmatrix} x + \begin{pmatrix} 0 \\ \frac{1}{L} \end{pmatrix} u + \begin{pmatrix} 0 \\ -\frac{R_1 V_f}{L(R_1+r_d)} \end{pmatrix} \text{ if } x \in \Omega_1, \end{cases}$$
$$y = x_1, \tag{27}$$

where C is a capacitor, L is an ideal inductor, $x_1 = v_c$ is the capacitor voltage, $x_2 = i_L$ is the inductor current, u is the input voltage, R_1 and R_2 are resistances.

The state regions Ω_0 and Ω_1 in equation (27), due to the activation and deactivation of the diode, are defined by the switching manifold $\Sigma : H^T x + h = R_1 x_2 - V_f = 0$ as:

$$\begin{aligned} \Omega_0 &= \left\{ x \in \mathbb{R}^2 : x_2 \leq \tfrac{V_f}{R_1} \right\}, \\ \Omega_1 &= \left\{ x \in \mathbb{R}^2 : x_2 \geq \tfrac{V_f}{R_1} \right\}. \end{aligned} \tag{28}$$

All parameter values are collected in Table 1. The value of g in (10) in this case can be computed as $\frac{R_1}{R_1+r_d}$.

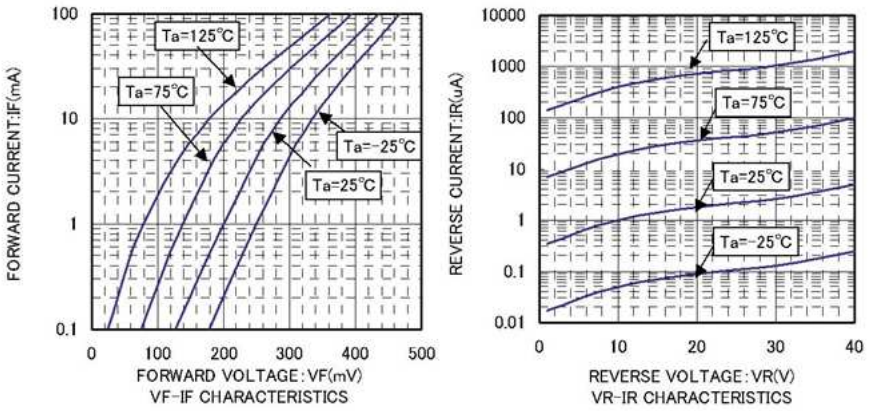

Figure 2: Characteristic of the RB441Q-40 Schottky barrier diode (ROHM Manufacturer, 2010).

To validate the hybrid adaptive control law discussed in this paper, a continuous reference model is adopted. Specifically, the control objective is to make the hybrid plant behave as a smooth RLC circuit of the form:

$$\begin{aligned} \dot{\widehat{x}} &= \begin{pmatrix} 0 & \frac{1}{\widehat{C}} \\ -\frac{1}{\widehat{L}} & -\frac{\widehat{R}}{\widehat{L}} \end{pmatrix} \widehat{x} + \begin{pmatrix} 0 \\ \frac{1}{\widehat{L}} \end{pmatrix} r, \\ \widehat{y} &= \widehat{x}_1, \end{aligned} \tag{29}$$

where $\widehat{x}_1$ is the voltage across the capacitor $\widehat{C}$, $\widehat{x}_2$ is the current through the inductor $\widehat{L}$. The parameter values have been selected as $\widehat{R} = 10$ [Ω], $\widehat{L} = 15$ [mH], $\widehat{C} = 1[mF]$, in order to have a natural frequency of $258[\frac{rad}{s}]$, settling time equal to $t_s = 34$ [ms] and rise time $t_r = 18.7$ [ms].

4. Preliminary numerical results

As a first attempt for the design and validation of the adaptive switched MCS control law, some numerical investigations have been performed by using the Matlab/Simulink platform.

Open-loop results, in the case where a sinusoidal reference input of frequency 1 [Hz] and a peak-to-peak voltage $V_{pp} = 2V$ is applied, show evidence of the differences between the open-loop behaviour of the plant and the smooth reference model as reported in Figs. 3(a) and 4(a). The hybrid nature of the plant is apparent in the time history of the inductor current (see Fig. 3(b)), where the change of the dynamics is apparent in each of the phase space regions defined by the switching manifold. Note that the system changes its dynamics according to the value assumed by the inductor current, namely, $\Sigma : i_L = x_2 = \frac{V_f}{R_1} = 1[mA]$, according to nominal values of the circuit parameters.

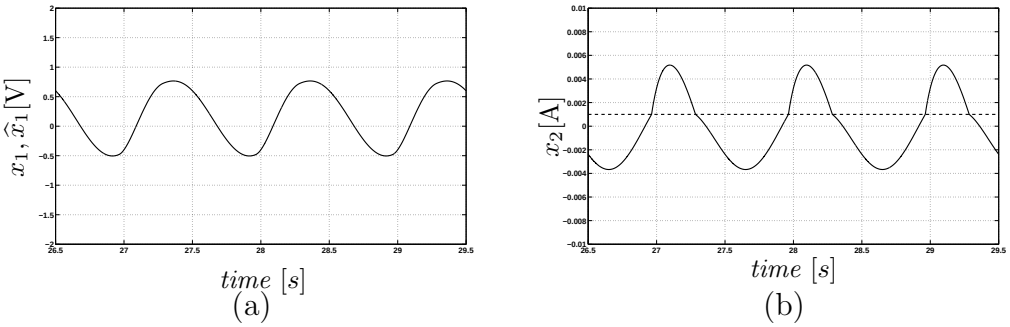

Figure 3: Open-loop simulation results: (a) Time history of the plant output $y = x_1 = v_C$(solid line); (b) Time history of the plant inductor current x_2 (black solid line) and switching manifold $x_2 = 1$[mA] (dashed line).

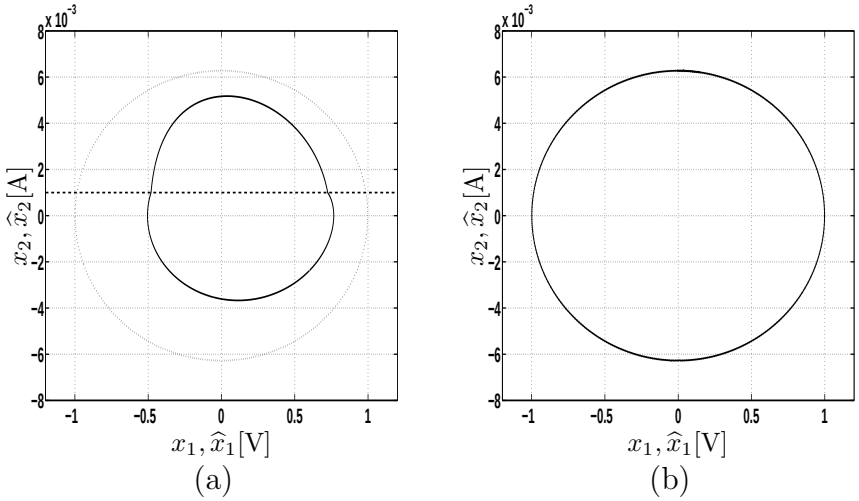

Figure 4: Simulation results. Phase portrait of the hybrid plant (solid line) and the smooth reference model (dotted line): (a) Open-loop; (b) Closed-loop.

Excellent tracking for both the state variables can instead be achieved in steady state conditions via the switching control law (19) as shown from the phase portrait in Fig. 4(b). The ability of the algorithm to adapt its gains achieving better and better performance under a smooth bounded control action is clearly shown from the transient evolution depicted in Fig. 5.

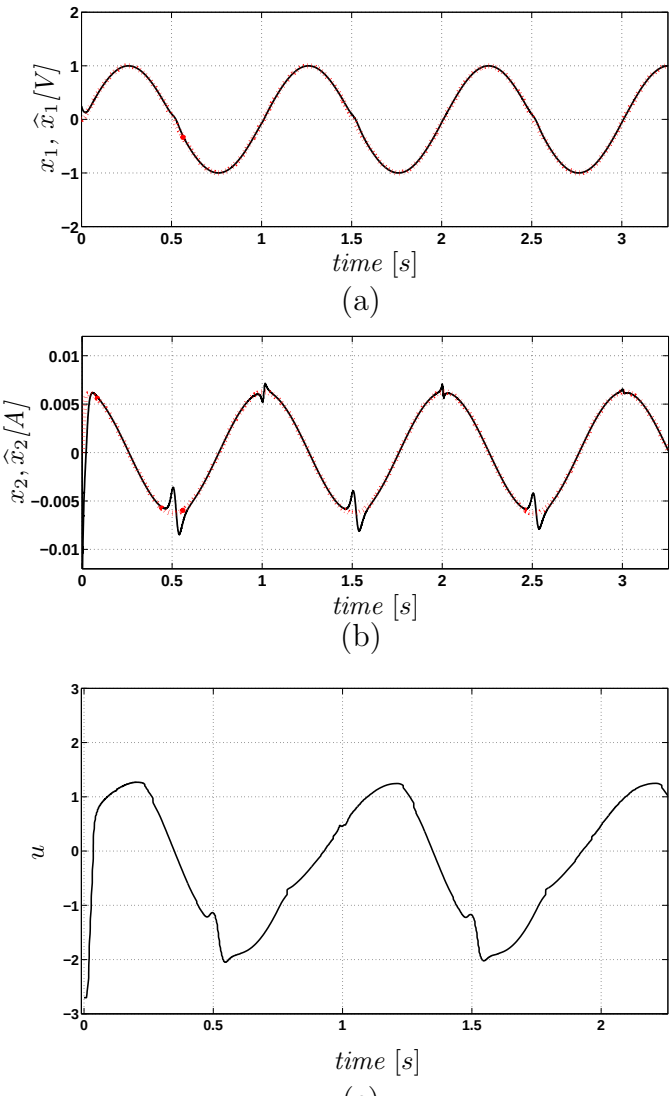

Figure 5: Closed-loop simulations results. Transient behavior: (a) Time history of the plant output ($y = x_1$, solid line) and the reference model ($\widehat{y} = \widehat{x}_1$, dotted line) ($x_1(0) = 0.5$, $\widehat{x}_1 = 0$ [V]); (b) Time history of the inductor current of the plant (x_2 solid line) and the reference model ($\hat{x}_2$, dotted line) ($x_2(0) = -4$, $\widehat{x}_2 = 0$ [mA]); (c) Time history of the control effort u.

Note that, as usual for MCS algorithms, the controller weights were chosen heuristically as a trade off between convergence time and reactivity as $\alpha = 1000$ and $\beta = 100$, while $\rho = 50$. Empirical rules for the choice of α and β are given in

(Stoten and H.Benchoubane, 1990), where it is remarked that α and β should be chosen in a $10:1$ ratio.

5. Description of the experimental set-up

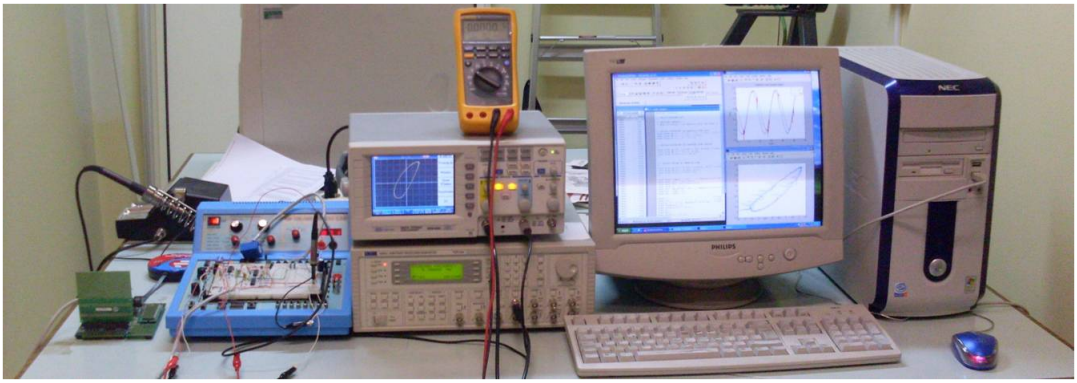

(a)

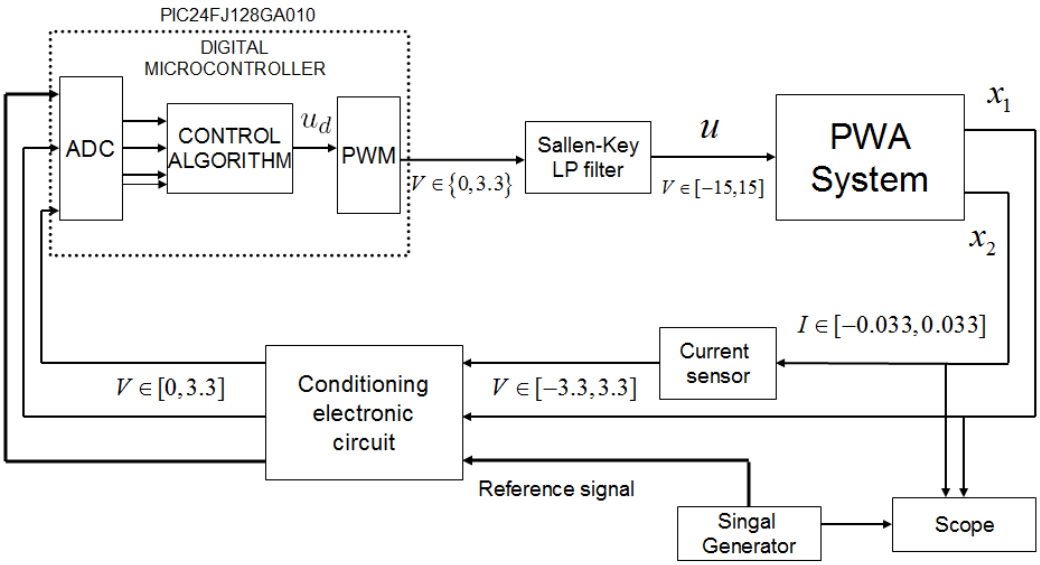

(b)

Figure 6: (a) Picture of the experimental set-up; (b) Scheme of the experimental setup.

In this section, we present the experimental set-up used for the digital implementation of the MRAC scheme described above using a cost effective, commercially available 10-bit microcontroller. The experimental set-up is shown in Fig. 6(a) and schematically depicted in Fig. 6(b).

The control law was implemented on a PIC microcontroller, namely the Microchip PIC24FJ128GA010 (Microchip Technology Inc., 2006). (Frequency of 32MHz, CPU speed up to 16 MIPS, program memory of 128kB, 8 kB SDRAM for data storing.) The control signal is digitally computed from the knowledge of the reference

voltage, the capacitor voltage and the voltage coming from a low cost inductor current sensor, namely the voltage transducer LEM LV 25-P/SP10 (LEM Manufacturer, 2011). From the measure of the inductor current, it is possible to experimentally detect the switching between one mode and another. Switchings occur when $i_L = x_2 = V_f/R_1 = 1$ [mA].

The control signal computed by the microcontroller is supplied to the plant via a PWM modulation technique. These functions are performed directly via an "on-chip" analog-to-digital (A/D) converter and PWM generator. In particular the A/D converter is a 10 bit successive approximation converter which scans sequentially the analog inputs (at most sixteen) that have to be converted. Note that the implementation of the proposed algorithms requires around 30 "add" operations, 40 "multiply" operations, 3 "divide" operations (taking 19 cycles each), 3 "compare" operations, hence the total number of cycles is around 200. According to this, the required computing time becomes about 12.5μs, while the accomplishment of the entire control task, from data acquisition to the computation of the control signal, requires a memory usage of about 0.85kB.

Since the A/D converter works properly with positive analog inputs less than 3.3 [V] (as shown in Fig. 6(b)), signal conditioning is included into the experimental set-up. Specifically, the circuit depicted in Fig. 7(a) is used to condition the voltage across the capacitor, the reference signal produced by the signal generator and the voltage generated by the current sensor. Note that, here, the aim of the Zener diode is to keep the output between the forward and reverse breakdown voltages ($V_{z,f}$ and $V_{z,r}$ respectively). Commonly, Zener diodes do not exhibit precise breakdown voltages. Hence, the saturation of the circuit characteristic (see Fig. 7(b)) is affected by uncertainty and can introduce further perturbations in the closed loop dynamics.

Finally, a low-pass active filter, namely the Sallen-Key filter (see Fig. 8 and (Texas Instruments, 2002) for further details), is adopted to remove harmonics with high frequencies from the PWM signal. We remark that the tuning of the filter parameters is a challenging task depending on the tradeoff between filter efficiency and settling time. Namely, in order to remove the unwanted harmonics the filter should have a small bandwidth, but this cannot be too small as to become insufficient to track input signal changes. On the other hand, a high bandwidth improves the settling time of the filter, but introduces ripples into the output signal. Such ripples act as additional disturbances that directly affect the plant dynamics.

The Sallen-Key filter was tuned according to the range of frequencies of the reference input and is a unity-gain low-pass filter with a 15.85[Hz] bandwidth and a quality factor of $Q = 0.5$.

To store the evolution of all systems variables, a serial connection with the UART protocol is provided. A MATLAB Graphical interface was developed to show results in real time. The GUI depicted in Fig. 9 was created for visualization and storage of the data received in the serial port rs-232. This tool works together with MPLAB IDE (a technical software used to program and embed the control algorithm into PIC microcontroller) in order to synchronize the data visualization while the experiment is running.

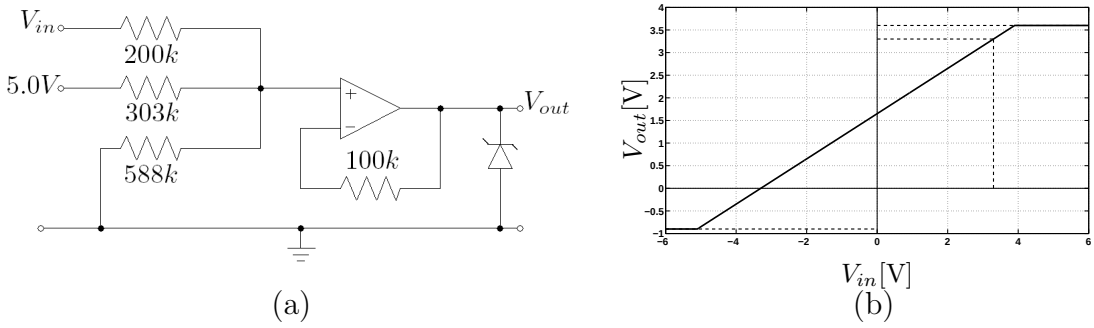

Figure 7: Conditioning circuit: (a) schematic; (b) input-output characteristic.

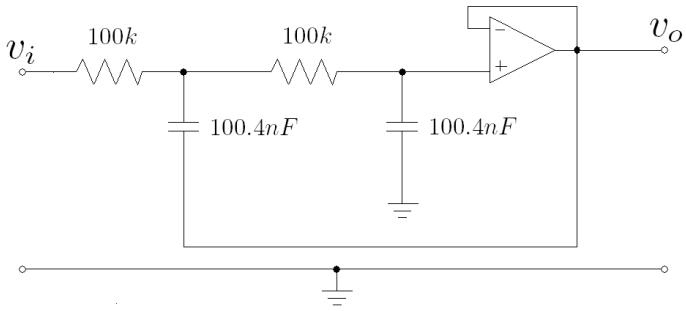

Figure 8: Schematic of the Sallen-Key filter.

6. Experimental Validation

The results of the experimental investigation confirm the ability of the algorithm to cope with the switching nature of the plant as predicted by the numerical results. All experiments were carried out with a fixed sample time period, namely $t_s = 4[ms]$ which is compatible with the estimated computing time. Integrals in the expressions of the control gains ((20)-(23)) have been computed via the well known Euler discretization method (Kreyszig, 1999) .

6.1. Open-loop behavior

The experimental open loop-behavior of the plant output, $y = x_1$ is shown in Fig. 10(a) in the case when a sinusoidal reference input of frequency 1[Hz] and a peak-to-peak voltage $V_{pp} = 2V$ is applied. Note that experimental behavior of the inductor current (see Fig. 10(b)) confirms that the switching manifold is $\Sigma := \{x_2 = 1[mA]\}$.

A further comparison of the open-loop behavior of the hybrid plant with respect to the smooth reference model can be found in the phase portrait depicted in Fig. 11 which shows a close resemblance with the numerical one given in Fig. 4.

6.2. Closed-loop behavior

The control loop has been closed choosing the control input as in (19) with the switching action of the controller depending only on the commutations of the plant (the reference model is smooth). The controller weights have been here chosen as in Section 4 and set to $\alpha = 1000$ and $\beta = 100$, while $\rho = 50$.

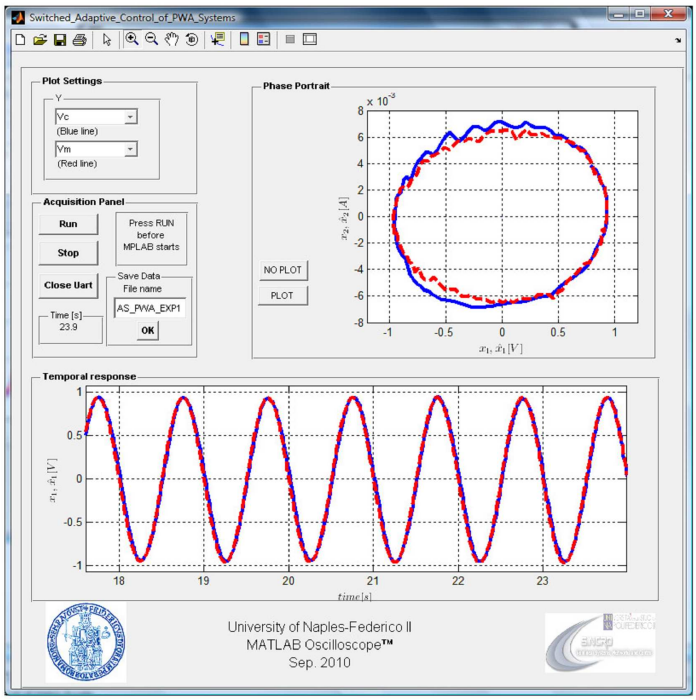

Figure 9: GUI of the set-up for visualization and storage of the data while the experiment is running.

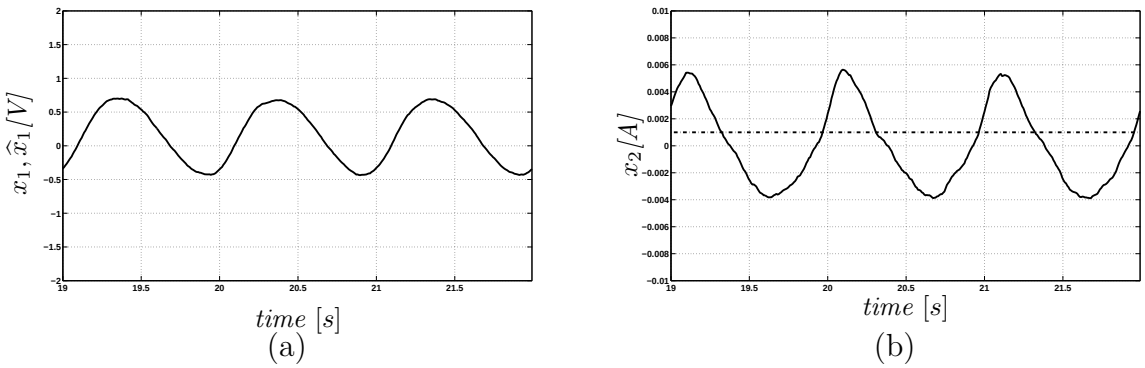

Figure 10: Open-loop experimental results: (a) Time history of the plant output $y = x_1$ (solid line); (b) Time history of the plant inductor current x_2 (black solid line). Switching manifold (red dotted line).

In excellent agreement with the numerical predictions, when the hybrid adaptive control algorithm is active, the plant tracks efficiently the reference model behavior (see Fig. 12). As expected, differently from simulations, a slight residual mismatch is still observed in the current evolution of the closed-loop system (see Fig. 12(b)). This is due to some uncertainty on the digital switching between different controller configurations, that depends on the measured current levels, the unavoidable presence of delays in the experimental implementation and the unmodelled nonlinear

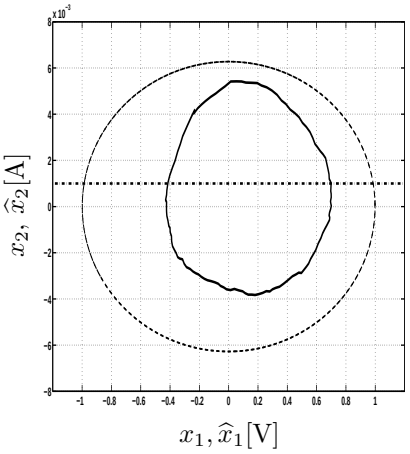

Figure 11: Open-loop experimental results: phase portrait of the hybrid plant (solid line) and the smooth reference model (dotted line).

dynamics. Moreover, the presence of oscillations on the current signal in Fig. 12(b) is also due to the inability of the Sallen-Key filter to remove all the unwanted harmonics from the PWM signal. Again, the ability of the algorithm to adapt achieving better and better performances is apparent from the transient evolution shown in Fig. 13.

A further source of uncertainty is due to the presence of quantization noise in the reference model (29) that is digitally computed by the microcontroller using the Tustin transformation (Franklin et al., 1997). This is apparent from the model reference phase portrait computed in real-time by the microcontroller and depicted in Fig. 14. Furthermore, comparison with the plant phase space evolution shown in Fig. 14 confirms the good performance of the hybrid control algorithm in tracking the reference orbit.

As predicted by the numerical investigation, the overall control input $u(t)$ required to compensate the discontinuity of the plant is continuous and bounded during both transient and steady state, as shown in Fig. 13(c). The evolution of the adaptive gains is shown in Fig. 15.

Note that, as always happens in the practical implementation of adaptive strategies, unavoidable presence of the residual mismatch and the persistent excitation of the sinusoidal reference signal $r(t)$ prevent the convergence of the adaptive gains towards a final steady state value. For this reason, following common practice (Sebusang and Stoten, 1998), gain locking was implemented in the microcontroller. In particular, the adaptive gains dynamics are locked (see Fig. 16) when the tracking error becomes lower than 5%. As shown in Figs. 17 and 18, the use of gain locking does not alter the control performance both in steady state and transient conditions.

7. Conclusions

The experimental validation of a novel model reference switched adaptive strategy for bimodal PWA dynamical systems has been presented. The idea behind the

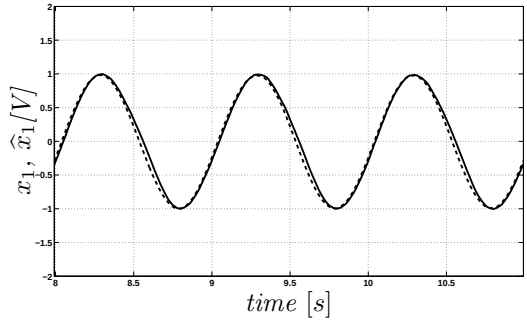

(a)

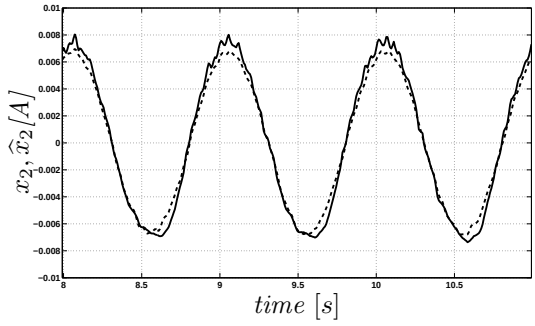

(b)

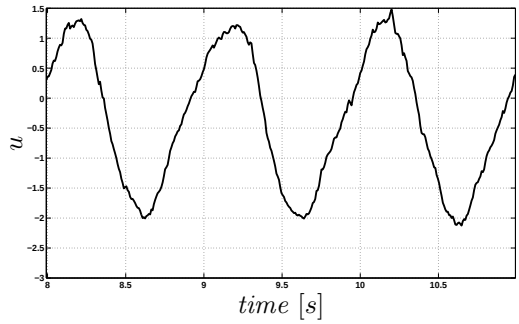

(c)

Figure 12: Closed-loop experimental results (without gain locking). Steady state behavior: (a) Time history of the plant output ($y = x_1$, solid line) compared to the reference model ($\widehat{y} = \widehat{x}_1$, dotted line); (b) Time history of the measured inductor current (x_2, solid line) compared to the reference model ($\widehat{x}_2$, dotted line); (c) Time history of the control effort u.

control is to formulate a switched extension of the original MCS adaptive law for smooth dynamical systems in order to cope with switchings in the plant and/or reference model. Experimental results were shown on the control of a PWA electric circuit confirming the effectiveness of the switching controller even when it is implemented via a commercial inexpensive digital microcontroller. This also provides a first insight into the algorithm robustness, in particular with respect to uncertainties on the switching times between one mode and the other.

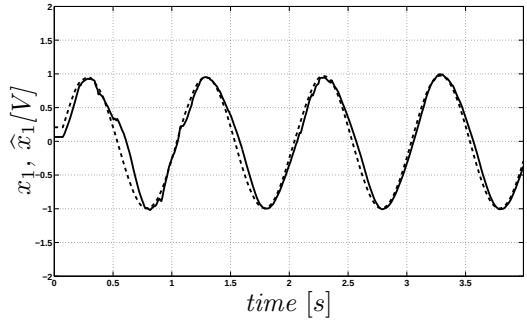

(a)

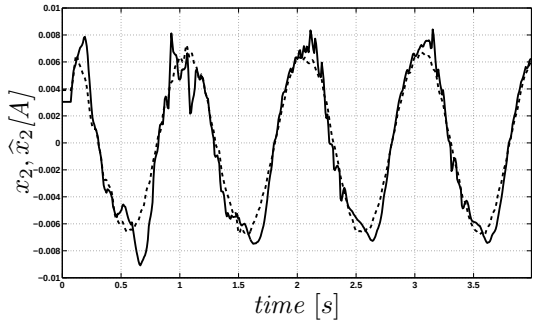

(b)

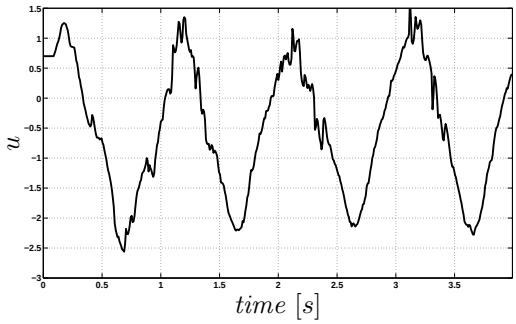

(c)

Figure 13: Closed-loop experimental results (without gain locking). Transient behavior: (a) Time history of the plant output ($y = x_1$, solid line) compared to the reference model ($\widehat{y} = \widehat{x}_1$, dotted line); (b) Time history of the measured inductor current (x_2, solid line) compared to the reference model ($\widehat{x}_2$, dotted line); (c) Time history of the control effort u.

References

Almer, S., Marithoz, S., Morari, M., 2010. Piecewise affine modeling and control of a step-up dc-dc converter. Proc. of the American Control Conference (ACC), 3299–3304.

Angenent, W., Witvoet, G., Heemels, W., van de Molengraft, M., Steinbuch, M.,

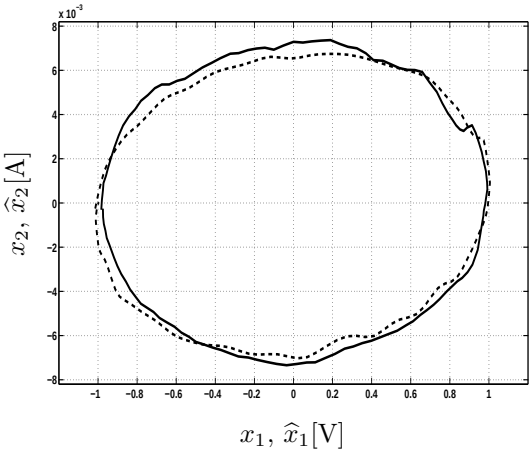

Figure 14: Closed-loop experimental results. Phase portrait of the closed-loop system (solid line) compared to the behavior of the smooth reference model computed in real-time by the microcontroller (dotted line).

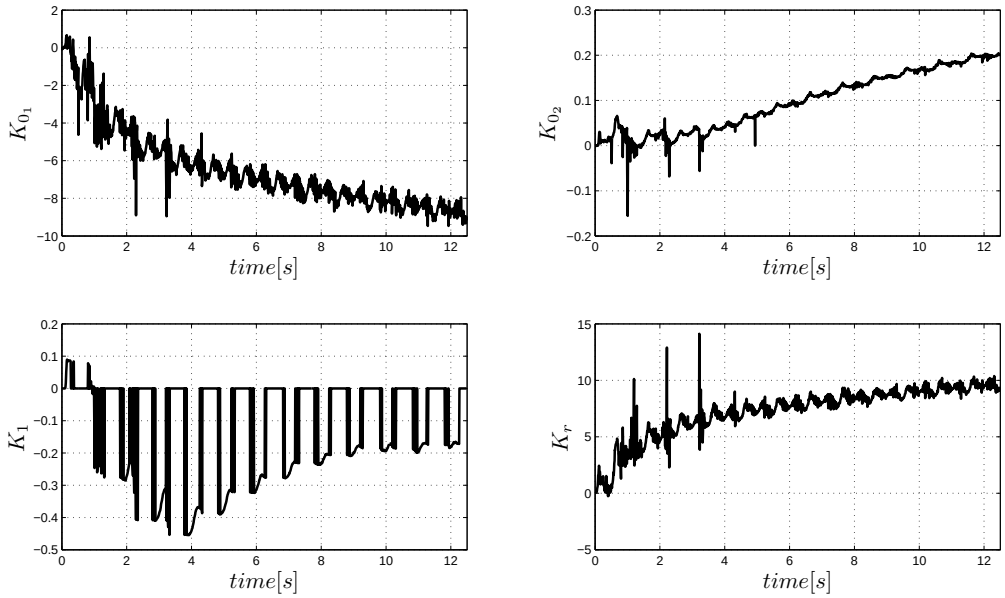

Figure 15: Closed-loop experimental results. Time evolution of the adaptive control gains (without gain locking).

2010. Performance analysis of reset control systems. International Journal of Robust and Nonlinear Control 20 (11), 1213–1233.

Bemporad, A., Morari, M., 1999. Control of systems integrating logic, dynamics, and constraints. Automatica 35 (3), 407–427.

Brogliato, B., 2003. Some perspectives on the analysis and control of complementarity systems. IEEE Transactions on Automatic Control 48 (6), 918–935.

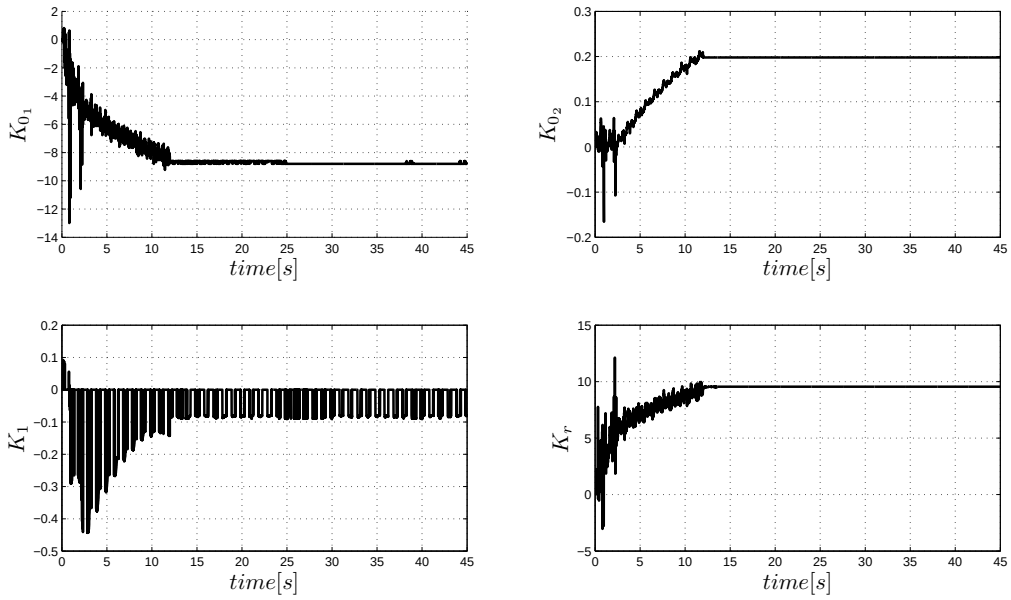

Figure 16: Evolution of the adaptive gains (with gain locking).

Brogliato, B., Heemels, W., 2009. Observer design for Lur'e systems with multivalued mappings: A passivity approach. IEEE Transactions on Automatic Control 54 (8), 1996 – 2001.

di Bernardo, M., Budd, C., Champneys, A., Kowalczyk, P., 2007a. Piecewise-Smooth Dynamical Systems: Theory and Applications. Springer-Verlag.

di Bernardo, M., di Gaeta, A., Montanaro, U., Santini, S., 2010a. Synthesis and experimental validation of the novel LQ-NEMCSI adaptive strategy on an electronic throttle valve. IEEE Transactions on Control Systems Technology 99, 1–13.

di Bernardo, M., Montanaro, U., Santini, S., February 2007b. On a novel hybrid LQ-MCS control strategy and its application to a dc motor. ISCAS, Proc. of the IEEE International Symposium on Circuits and Systems, 2459–2462.

di Bernardo, M., Montanaro, U., Santini, S., December 2008. Novel switched model reference adaptive control for continuous piecewise affine systems. IEEE Conference on Decision and Control, 1925–1930.

di Bernardo, M., Montanaro, U., Santini, S., 2010b. Minimal control synthesis adaptive control of bimodal piecewise affine systems. SIAM Journal on Control and Optimization 48 (7), 4242–4261.

di Bernardo, M., Montanaro, U., Santini, S., 2011. Piecewise linear observer and controller canonical forms of generic piecewise linear continuous systems. IEEE Transaction on Automatic Control 56 (8), 1911 –1915.

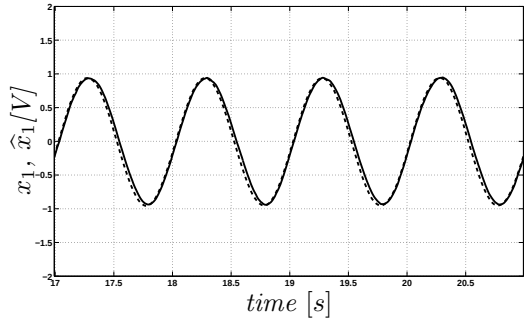

(a)

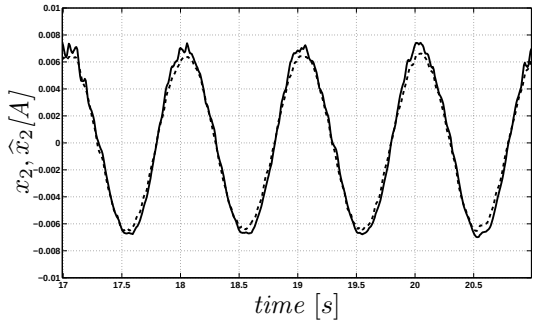

(b)

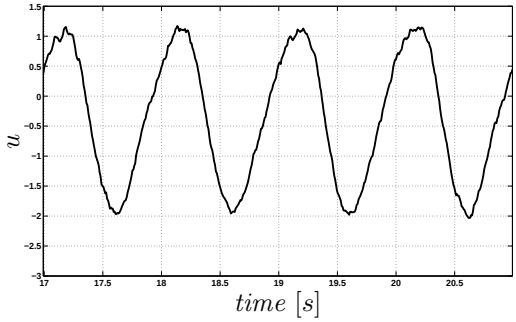

(c)

Figure 17: Closed-loop experimental results when the locking of the adaptive gains is implemented. Steady state behavior: (a) Time history of the plant output ($y = x_1$, solid line) compared to the reference model ($\widehat{y} = \widehat{x}_1$, dotted line). (b) Time history of the measured inductor current (x_2, solid line) compared to the reference model ($\widehat{x}_2$, dotted line). (c) Time history of the control effort u.

Franklin, G. F., Powell, J. D., Workman, M. L., 1997. Digital Control of Dynamic Systems. Prentice Hall.

Geyer, T., Papafotiou, G., Morari, M., December 2005. Model predictive control in power electronics: A hybrid systems approach. Proc. of the IEEE Conference on Decision and Control, and the European Control Conference, 5606–5611.

Heemels, W. P. M. H., Camlibel, M. K., Schumacher, J. M. H., 2002. On the dynamic

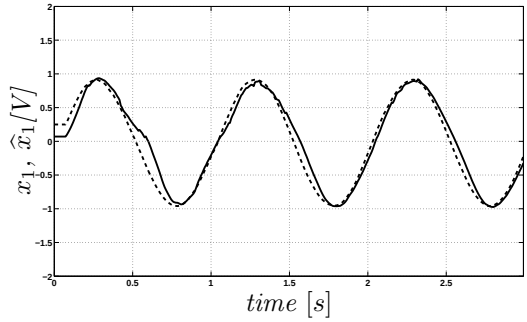

(a)

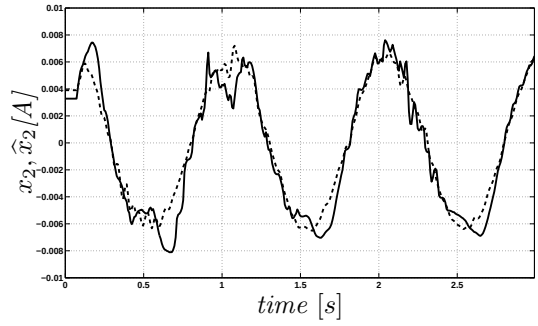

(b)

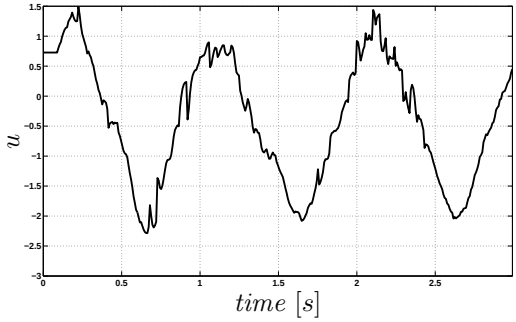

(c)

Figure 18: Closed-loop experimental results when the locking of the adaptive gains is implemented. Transient behavior: (a) Time history of the plant output ($y = x_1$, solid line) compared to the reference model ($\widehat{y} = \widehat{x}_1$, dotted line). (b) Time history of the measured inductor current (x_2, solid line) compared to the reference model ($\widehat{x}_2$, dotted line). (c) Time history of the control effort u.

analysis of piecewise-linear networks. IEEE Transactions on Circuits and Systems - I: Fundamental Theory and Applications 49 (3), 315–327.

Hensen, R. H., February 2002. Controlled mechanical systems with friction. Ph.D. thesis, Eindhoven University of Technology, Eindhoven, The Netherlands.

Hernandez, C., Page, M., Sari, T., de Jong, H., Gouz, J. L., Geiselmann, J., 2004. Qualitative simulation of genetic regulatory networks using piecewise-linear models. Bull. Math. Biol. 66, 301–340.

Hodgson, S., Stoten, D., 1996. Passivity-based analysis of the minimal control synthesis algorithm. International Journal of Control vol. 63 (1), 67–84.

Ishitobi, M., Nishi, M., Nakasaki, K., 2010. Nonlinear adaptive model following control for a 3-dof tandem-rotor model helicopter. Control Engineering Practice vol. 18 (8), 936–943.

Keener, J., Sneyd, J., 1988. Mathematical Physiology. Springer-Verlag.

Kreyszig, E., 1999. Advanced Engineering Mathematics. Jhon Wiley & and Sons inc.

Lazar, M., Heemels, W. P. M. H., Rosel, B. J. P., Nijmeijer, H., van den Bosch, P. P. J., 2008. Input-to-state stabilizing sub-optimal NMPC with an application to dc-dc converters. International Journal of Robust and Nonlinear Control 18, 890–904.

LEM Manufacturer, 2011. Data sheet of the voltage transducer LV 25-P. http://www.datasheetcatalog.com.

Mariethoz, M., Beccuti, A., Papafotiou, G., Morari, M., 2008. Sensorless explicit model predictive control of the dc-dc buck converter with inductor current limitation. APEC 2008, Proc. of Applied Power Electronics Conference and Exposition, 1710–1715.

Microchip Technology Inc., 2006. PIC24F family reference manual. http://www.microchip.com.

Pang, Y., Grimble, M. J., 2010. NGMV control of delayed piecewise affine systems. IEEE Transactions on Automatic Control 55 (12), 2817–2821.

Rodrigues, L., How, J. P., 2003. Observer-based control of piecewise-affine systems. International Journal of Control 76, 459–477.

ROHM Manufacturer, 2010. Data sheet of the schottky barrier diode RB441Q-40T-77. http://uk.farnell.com.

Rupp, D., Guzzella, L., 2010. Adaptive internal model control with application to fueling control. Control Engineering Practice vol. 18 (8), 873–881.

Sebusang, S. E., Stoten, D., 1998. Controller gain bounding in the minimal control synthesis algorithm. Proceedings of Thirtieth SouthEastern Symposium on System Theory, 141–145.

Sedra, A., Smith, K., 2004. Microelectronic Circuits (Fifth ed.). Oxford Univ. Press.

Sontag, E., 1998. Mathematical Control Theory: Deterministic Finite Dimensional Systems. Springer.

Stoten, D., H.Benchoubane, 1990. Robustness of minimal controller synthesis algorithm. International Journal of Control 51 (4), 851–861.

Tahami, F., Mobed, M., Molayee, B., 2006. On piecewise affined large-signal modeling of pwm converters. IEEE International Conference on Industrial Technology (ICIT), 1419–1423.

Tao, G., Sang, Q., 2010. Adaptive control of piecewise linear systems: the state tracking case. Proc. of the IEEE American Control Conference (ACC), 4040 – 4045.

Texas Instruments, 2002. Analysis of the sallen-key architecture. http://focus.ti.com/lit/an/sloa024b/sloa024b.pdf.

Vasak, M., Baotic, M., Petrivic, I., Peric, N., 2004. Electronic throttle state estimation and hybrid theory based optimal control. IEEE International Symposium on Industrial Electronics 1, 323– 328.

Zhao, J., Hill, D. J., 2008. Dissipativity theory for switched systems. IEEE Transactions on Automatic Control 53, 941–953.

Appendix A. Mathematical preliminaries

In what follows, the definition of passivity for switched systems is given (Zhao and Hill, 2008).

A system of the form

$$\dot{x} = \begin{cases} f_0(x) + g_0(x)\,u_0 & \text{if} \quad x \in \mathcal{D}_0, \\ f_1(x) + g_1(x)\,u_1 & \text{if} \quad x \in \mathcal{D}_1, \end{cases} \tag{A.1}$$

$$y = \begin{cases} h_0(x) & \text{if} \quad x \in \mathcal{D}_0, \\ h_1(x) & \text{if} \quad x \in \mathcal{D}_1 \end{cases} \tag{A.2}$$

is passive if there exist two positive functions (called *multiple storage functions*) $S_0(x)$ and $S_1(x)$ that satisfy the following three properties:

1. There exist two functions (called supply rates) $\omega_0^0(u_0, h_0)$ and $\omega_1^1(u_1, h_1) \in \mathrm{L}_{loc}^2]0, +\infty[$ of the form

$$\omega_i^i(u_i, h_i) = u_i^T h_i - \varepsilon_i h_i^T h_i, \quad \varepsilon_i > 0, \qquad i = 0, 1, \tag{A.3}$$

such that, for two generic time instants t and s $(t > s)$ when the ith subsystem is active, it holds that

$$S_i(x(t)) - S_i(x(s)) \leq \int_s^t \omega_i^i(u_i(\tau), h_i(\tau))\,d\tau, \qquad i = 0, 1. \tag{A.4}$$

2. There exist two functions (called *cross supply rates*) $\omega_1^0(x, u_0, h_0, t)$, $\omega_0^1(x, u_1, h_1, t) \in \text{Ł}_{loc}^1]0, +\infty[$ such that, when $x \in \mathcal{D}_0$, we have

$$S_1(x(t)) - S_1(x(s)) \leq \int_s^t \omega_1^0(x, u_0(\tau), h_0(\tau), \tau)\, d\tau, \tag{A.5}$$

whereas when $x \in \mathcal{D}_1$,

$$S_0(x(t)) - S_0(x(s)) \leq \int_s^t \omega_0^1(x, u_1(\tau), h_1(\tau), \tau)\, d\tau. \tag{A.6}$$

3. Given two positive functions $\phi_1^0(t)$ and $\phi_0^1(t) \in L_{loc}^1]0, +\infty[$, there exist two functions

$$u_0(t) = \varphi_0(x(t), t), \qquad u_1(t) = \varphi_1(x(t), t) \tag{A.7}$$

such that the following conditions hold for $i, j \in \{0, 1\}$ with $i \neq j$:

$$f_i(0) + g_i(0)\, u_i(0, t) \equiv 0 \quad \forall t \in]0, +\infty[, \tag{A.8}$$
$$\omega_i^i(u_i(t), h_i(t)) \leq 0, \tag{A.9}$$
$$\omega_j^i(x(t), \varphi_i(t), h_i(t), t) - \phi_j^i(t) \leq 0. \tag{A.10}$$

Note that if the following choice for the cross supply rates is made:

$$\omega_1^0(x, u_0, h_0, t) = \frac{1}{2}\theta_1^0\left(\gamma^2 u_0^T u_0 - h_0^T h_0\right), \tag{A.11}$$
$$\omega_0^1(x, u_1, h_1, t) = \frac{1}{2}\theta_0^1\left(\gamma^2 u_1^T u_1 - h_1^T h_1\right), \tag{A.12}$$

then the first condition given by (A.4) and the second condition in (A.5)–(A.6) can be rewritten in the following differential form:

$$\mathcal{L}_{f_0} S_0 \leq -\varepsilon_0 h_0^T h_0 \quad \text{if} \quad x \in \mathcal{D}_0, \tag{A.13}$$
$$\mathcal{L}_{f_1} S_1 \leq -\varepsilon_1 h_1^T h_1 \quad \text{if} \quad x \in \mathcal{D}_1, \tag{A.14}$$
$$\mathcal{L}_{f_0} S_1 + \frac{1}{2\gamma^2\theta_1^0}\left(\mathcal{L}_{g_0} S_1\right)\left(\mathcal{L}_{g_0} S_1\right) + \frac{1}{2}\theta_1^0 h_0^T h_0 \leq 0 \quad \text{if} \quad x \in \mathcal{D}_0, \tag{A.15}$$
$$\mathcal{L}_{f_1} S_0 + \frac{1}{2\gamma^2\theta_0^1}\left(\mathcal{L}_{g_1} S_0\right)\left(\mathcal{L}_{g_1} S_0\right) + \frac{1}{2}\theta_0^1 h_1^T h_1 \leq 0 \quad \text{if} \quad x \in \mathcal{D}_1, \tag{A.16}$$

where $\mathcal{L}_\nu$ is the Lie derivative along the vector ν.

Appendix B. Proof of Lemma 1

In this section Lemma 1 is proven.

Consider the system given in (13) - (14). This is a switched system of the form (A.1)–(A.2), where the state vector is $z \in I\!R^n$ and $f_0(z) = \widehat{A}_0 z$, $f_1(z) = \widehat{A}_1 z$, $g_0(z) = g_1(z) = B_e$, $h_0(z) = C_{e0} z$, $h_1(z) = C_{e1} z$, and $u_0 = u_1 = \xi$.

Note explicitly that, choosing the cross supply rates as in (A.11) - (A.12), the third dissipative condition of equations (A.8)-(A.10) is trivially satisfied by selecting $\phi_j^i(t) = 0$ and

$$\varphi_j(z) = \rho_j C_{ej} z \quad j = 0, 1, \tag{B.1}$$

with $\rho_j < \min\left\{\varepsilon_j, \sqrt{\gamma^{-1}}\right\}$, $j = 0, 1$. Indeed in this case we have, for all i and j, $i \neq j$, $(i, j = 0, 1)$, that:

$$f_i(z, \varphi_i(z))|_{z=0} = \left(\widehat{A}_i + B_e C_{ei}\right) z = 0, \tag{B.2}$$

$$\omega_i^i(\varphi_i(z), h_i(z)) = (\rho_i - \varepsilon_i)\, z^T C_{ei}^T C_{ei} z \leq 0, \tag{B.3}$$

$$\omega_j^i(\varphi_i(z), h_i(z)) = \frac{1}{2}\left(\gamma\rho_i^2 - 1\right) z^T C_{ei}^T C_{ei} z \leq 0. \tag{B.4}$$

Now, passivity is guaranteed simply by satisfying inequalities (A.13)–(A.16), where S_0, S_1 must be appropriately chosen. Then, let us choose S_0 and S_1 as

$$S_j(z) = z^T P_j z \quad \text{with} \quad P_j = P_j^T > 0, \quad j = 0, 1. \tag{B.5}$$

According to this choice, after some algebraic manipulations, (A.13)–(A.16) can be rewritten as

$$z^T\left(P_0\widehat{A}_0 + \widehat{A}_0^T P_0\right) z \leq -2\varepsilon_0 z^T\left(P_0 B_e C_{e0}\right) z, \tag{B.6}$$

$$z^T\left(P_1\widehat{A}_1 + \widehat{A}_1^T P_1\right) z \leq -2\varepsilon_1 z^T\left(P_1 B_e C_{e1}\right) z, \tag{B.7}$$

$$z^T\left(P_1\widehat{A}_0 + \widehat{A}_0^T P_1\right) z + \frac{2}{\gamma^2\theta_1^0} z^T P_1 B_e B_e^T P_1 z + \frac{1}{2}\theta_1^0 z^T C_{e0}^T C_{e0} z \leq 0, \tag{B.8}$$

$$z^T\left(P_0\widehat{A}_1 + \widehat{A}_1^T P_0\right) z + \frac{2}{\gamma^2\theta_0^1} z^T P_0 B_e B_e^T P_0 z + \frac{1}{2}\theta_0^1 z^T C_{e1}^T C_{e1} z \leq 0. \tag{B.9}$$

Selecting $C_{ej} = B_e^T P_j$, $j \in \{0, 1\}$, (B.6)–(B.9) become

$$z^T\left(P_0\widehat{A}_0 + \widehat{A}_0^T P_0 + 2\varepsilon_0 P_0 B_e B_e^T P_0\right) z \leq 0, \tag{B.10}$$

$$z^T\left(P_1\widehat{A}_1 + \widehat{A}_1^T P_1 + 2\varepsilon_1 P_1 B_e B_e^T P_1\right) z \leq 0, \tag{B.11}$$

$$z^T\left(P_1\widehat{A}_0 + \widehat{A}_0^T P_1 + \frac{2}{\gamma^2\theta_1^0} P_1 B_e B_e^T P_1 + \frac{1}{2}\theta_1^0 P_0 B_e B_e^T P_0\right) z \leq 0, \tag{B.12}$$

$$z^T\left(P_0\widehat{A}_1 + \widehat{A}_1^T P_0 + \frac{2}{\gamma^2\theta_0^1} P_0 B_e B_e^T P_0 + \frac{1}{2}\theta_0^1 P_1 B_e B_e^T P_1\right) z \leq 0. \tag{B.13}$$

The left-hand side of (B.10)–(B.13) is negative for all values of z if the inequalities (15)–(18) are satisfied. In so doing conditions (A.4), (A.5) and (A.6) are verified and passivity of system (13) - (14) is guaranteed.